THE LEIDENFROST PHENOMENON FOR EXTENDED LIQUID MASSES

By

BHAILALBHAI MATHURBHAI PATEL

Bachelor of Science
The Maharaja Sayajirao University
Baroda, India
1956

Bachelor of Science in Technology
University of Bombay
Bombay, India
1958

Bachelor of Science
University of Michigan
Ann Arbor, Michigan
1960

Master of Science
School of Mines and Metallurgy
University of Missouri
Rolla, Missouri
1961

Submitted to the Faculty of the Graduate School of the
Oklahoma State University
in partial fulfillment of the requirements
for the degree of
DOCTOR OF PHILOSOPHY
May, 1965

THE LEIDENFROST PHENOMENON FOR EXTENDED LIQUID MASSES

Thesis Approved:

Kenneth J. Bell
Thesis Adviser

John B. West

Jerald D. Parker

Wayne C. Edmister

Dean of the Graduate School

PREFACE

In the Leidenfrost phenomenon regime experimental vaporization data of liquids on a flat plate as a function of initial liquid volume and plate temperature were obtained for water, ethanol, benzene, and carbon tetrachloride. Initial liquid volumes from 0.05 ml to 10 ml were employed at plate temperatures varying from 150°C to 540°C. Also, high-speed motion pictures at a nominal 2750 frames per second were taken from which inter-bubble distances, bubble periods, break-off diameters, and geometric arrangement of bubbles were determined.

I am deeply indebted to Dr. Kenneth J. Bell for his counseling, guidance and inspiration supplied during this study. I would like to express my gratitude to the members of my Advisory Committee and to the entire staff of the School of Chemical Engineering for the help I have received in my graduate work. The assistance from Messrs. Eugene McCroskey, C. J. Lee, and D. E. Bush with various phases of the work is acknowledged.

Financial aid for these past three years has been gratefully received from the Oklahoma State University and from the United States Army Research Office (Durham). Financial assistance from the National Science Foundation for the purchase of the high-speed movie camera is also appreciated.

By far the greatest thanks is due to my mother and brothers, whose unfailing encouragement, aid, and patience have made my graduate studies possible.

TABLE OF CONTENTS

LIST OF TABLES

LIST OF FIGURES

CHAPTER I

INTRODUCTION

The first observations of so-called film boiling are attributed to J. G. Leidenfrost, a German doctor, in 1756 (29). He observed the behavior of small drops of water on a heated, well-polished iron spoon. He noted that the droplet was spherical at the instant when the drop touched the hot spoon and that the vaporization time of a droplet was long on a very hot spoon. The droplet vaporization time is the total elapsed time for a liquid droplet to vaporize completely on a hot surface. Such behavior of small droplets on a very hot surface is now known as the Leidenfrost phenomenon.

The problem of heat transfer from a hot surface to a pool of liquid at boiling point is complex because four different heat transfer mechanisms can exist: nonboiling convection, nucleate, transition and film boiling. The change from one region to another is accompanied by marked changes in the hydrodynamics and surface temperature of the system. These regions are shown in Figure 1.

Nonboiling Convection (region AB): This is a single phase phenomenon. There is no generation of vapor at the solid-liquid interface due to lack of sufficient superheat of the surface.

Stable Nucleate Boiling (region BC): In this region there is generation of vapor at the solid-liquid interface. The vapor takes the form of bubbles rising from various favored spots on

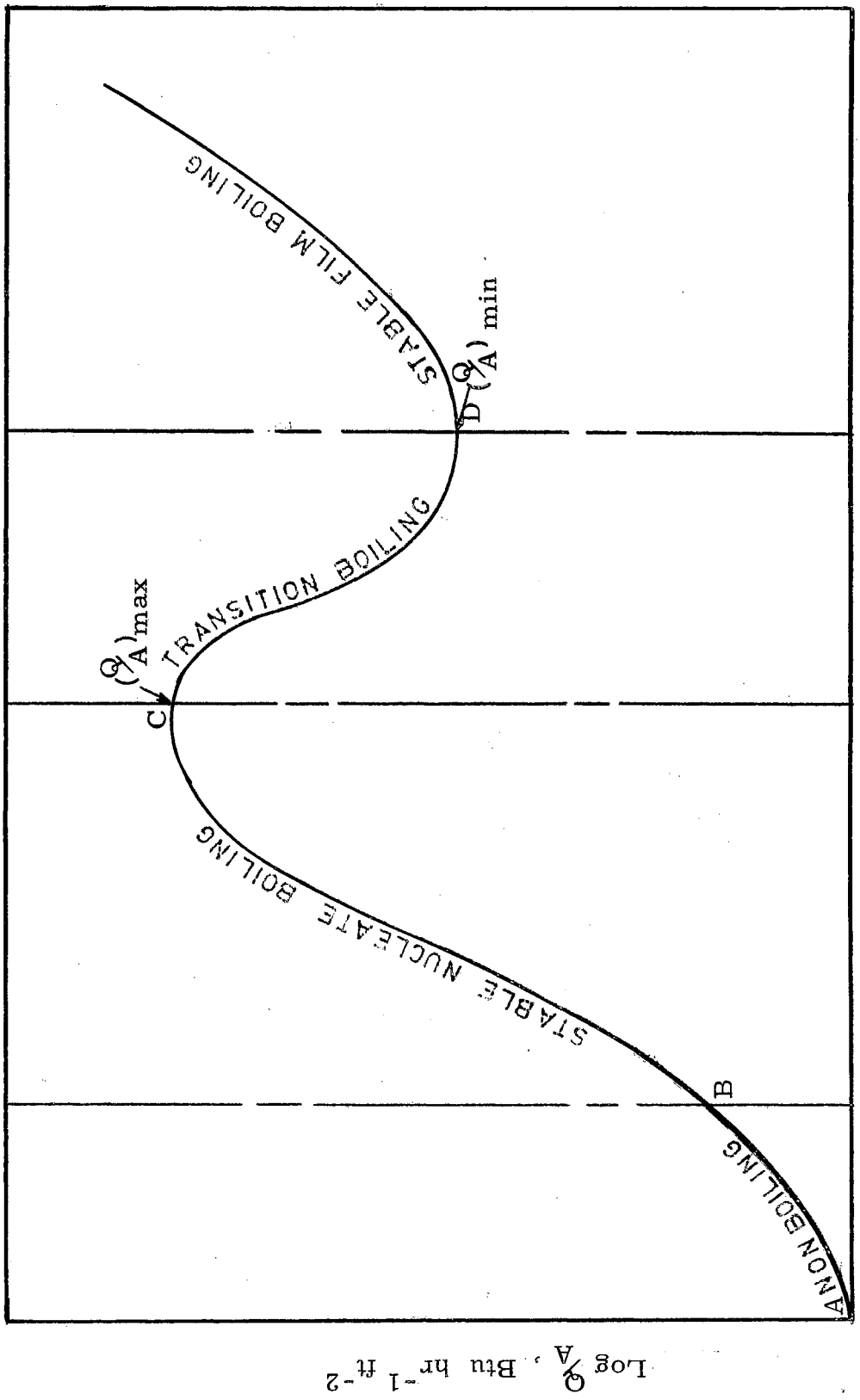

Figure 1. Typical Boiling Curve

the heated surface. When there is formation of vapor at the hot surface, a condition known as boiling is said to exist. Since the boiling in region BC occurs from favored spots or nuclei on the heater surface, this process is called nucleate boiling. An increase of the heat flux causes in turn a sharp increase of the bubble population. However, as the temperature increases, bubbles become so numerous that their motions interact. Under these conditions, the heat flux reaches its peak.

Transition Boiling (region CD): Increasing the temperature difference beyond point C results in a decrease in the heat transfer rate in region CD. This effect is probably the result of the formation of a partial vapor blanket of low thermal conductivity, which effectively insulates a part of the surface. Westwater and Santangelo (43) have found in region CD that the surface is blanketed by an unstable, irregular film of vapor which is in violent motion. CD is known as the transition boiling region.

Film Boiling (region DE): In transition boiling an increase of temperature is followed by a decrease of heat flux until the so-called "film boiling" or "spheroidal state" or "Leidenfrost state" is reached. Drew and Mueller (14) pointed out that the Leidenfrost state is related to film boiling, that is, boiling which takes place when the heating surface is covered completely with an insulating layer of vapor. The point of minimum heat flux, point D in Figure 1, is called the "Leidenfrost point". This minimum point of region DE is the beginning of film

boiling. In the film boiling region DE the heat flux increases with an increase of surface temperature but at a much slower rate than in nucleate boiling.

The above discussion usually arises in the description of pool boiling in which the surface is completely covered with liquid. Similar phenomena occur in the case that the liquid exists as discontinuous masses on the surface. If these masses are large enough that they spread out and are not spheroidal, they are termed "extended masses".

Film boiling gives lower heat transfer coefficients than nucleate boiling and should be avoided, if possible in practical applications. When, for some reason, equipment must be operated in film boiling, a knowledge of the heat transfer rate at high temperature differences in film boiling is very important to the designer. The operation of jets or rockets frequently involves the contact of a liquid with very hot surfaces, causing film boiling. Film boiling usually occurs in the boiling of mercury; attempts to use the mercury-steam cycle to obtain better thermodynamic efficiency for power plants have been hampered by a lack of knowledge of this phenomenon.

Most film boiling experimental work has been with wires and tubes (7, 14, 33, 46) in a pool of boiling liquid. However, Borishansky (6) worked with extended masses of water in film boiling, where he reported data regarding evaporation time of water. Recently Gottfried (16) presented results of analytical and experimental work for small droplets of liquid in film boiling. From hydrodynamic considerations, Chang (10), Zuber (48), and Berenson (4) derived several semi-theoretical relations pertaining to the bubble dynamics

for submerged surfaces in film boiling.

The work of this thesis was designed to obtain more information about total vaporization time and instability criteria for extended liquid masses in the film boiling regime. Also, the Leidenfrost point for different liquids was to be accurately determined. The major goals may be stated.

1. Determination of the total vaporization time for extended liquid masses to check Borishansky's data and correlation.
2. Determination of the accurate Leidenfrost point for extended masses.
3. Evaluation of the stability characteristics with regard to either vapor breakthrough or liquid breakup for extended masses.
4. A review of Zuber's equations on bubble dynamics and their applicability to extended masses.
5. Study of a semi-theoretical model for the vaporization time of extended masses and application of dimensional analysis to correlate experimental vaporization data of extended masses.
6. Comparison of quantitative data from motion pictures with the work of Hosler and Westwater for submerged surfaces in film boiling.

CHAPTER II

A SURVEY OF THE LITERATURE

There exist today excellent surveys of the field of boiling by Jakob (23), McAdams (31), Asch (1), Rohsenow (38) and Westwater (43). This survey will cover only those papers directly concerning film boiling.

The Leidenfrost Phenomenon for Small Drops

The first adequately recorded experimental work on the film boiling of small droplets dates from a tract by Leidenfrost, published in 1756 (in Latin); hence, the phenomenon is commonly given his name. Most of his work consisted of observing the behavior of liquid deposited on a well-polished iron spoon which was heated over hot coals until the spoon was glowing. Recently the English translation of Leidenfrost's treatise was prepared by Mrs. Carolyn Wares of Oklahoma University. In this treatise, under the subtitle "ON THE FIXATION OF WATER IN DIVERSE FIRE", Leidenfrost (29) describes the behavior of small droplets as follows:

> "This drop which first fell upon the glowing iron is divided into a few little globes, which after a little while are collected in one big globe again. At the instant when the drop touches the growing iron, it is spherical. It does not adhere to the spoon, as water which touches colder iron is accustomed to do.
>
> If then the spoon remains motionless, this water globule will lie quiet and without any visible motion, without any bubbling, very clear like a crystalline globe, always spherical, adhering nowhere to the spoon, but to be near it in one point. However, although motion is not visible in the pure drop,

> nevertheless it delights in a very swift motion of turning. ... Moreover, this drop evaporates only very slowly. Which drop at last exceedingly diminished so that it can hardly anymore be seen, finishes its existence with an audible crack which one easily hears with the ears, and it leaves a small particle of earth in the spoon. ... ..."

Since these early studies of the behavior of small droplets on a very hot surface, the desire for more knowledge along these lines has grown. Pleteneva and Rebinder (36) studied water, benzene, chloroform, methyl alcohol and several other similar liquids, on a stainless steel plate. They concluded that water droplets show the spheroidal state at a plate temperature of 250°C, and the droplet evaporation time rises sharply to a maximum value at 275°C plate temperature. Similar phenomena were also observed with the other liquids tested.

Kistemaker (26) performed experiments to determine heat-flow, drop to surface distance and droplet vaporization time on a brass block at temperatures from 100 to 500°C.

From the study of droplet evaporation of nitric acid and aniline, Gross-Gronomski (17) concluded that the evaporation times were exponential functions of the temperature of the hot surface.

In 1961, Gottfried (16) studied stable film boiling for small droplets of water, carbon tetrachloride, ethanol and benzene ranging in volume from 0.0058 to 0.0415 ml. He proposed a semi-analytical model with several assumptions to predict evaporation rate. One assumption was that the liquid droplets were spheres.

Recently, Lee and Bell (28) modified and extended the approach suggested by Gottfried to predict the evaporation rate of droplets. They made a series of physical and mathematical assumptions along

with postulated mechanisms of heat, mass and momentum transfer. The first assumption was that the droplet was a perfect sphere throughout the process of evaporation, and the droplet at its saturation temperature was fully supported by the vapor which was continuously being generated on the bottom of the droplet by evaporation. Also, they assumed that the heat transfer is due to conduction and radiation. They used a simplified one-dimensional equation obtained from the Navier-Stokes equations for flow between parallel plane surfaces for the vapor stream between the plate and the bottom of the droplet. Furthermore, they assumed that the upper portion of the droplet, more or less hidden from the heat source, lost mass by molecular diffusion. Lee studied vaporization times of benzene, carbon tetrachloride, water, ethanol and n-octane droplets ranging from 0.001 to 0.03 ml in initial volume. The theoretically predicted evaporation times were in fair agreement with experiment.

Borishansky (6) studied small droplets of benzene, water, ethanol and carbon tetrachloride on hot plates (600°C) of copper, stainless steel or brass. The experimental results of Gottfried, of Lee and of Borishansky were very similar for small droplets.

The Leidenfrost Phenomenon for Extended Masses

Apparently, Borishansky (6) was the first investigator to study film boiling of extended masses. He used 1 to 5 ml of water to measure total vaporization time on a brass plate at two plate temperatures, 350 and 275°C. The experimental data of Borishansky and of this work for vaporization times of extended water masses are shown in Table I of Chapter III.

Borishansky's objective was to determine heat transfer coefficients rather than total vaporization time for liquids. Therefore, for larger volumes (5 to 34 ml), the decrease of volume with time was used to estimate the heat transfer coefficient. He poured the larger quantities of liquids on steel plate directly from burettes and graduated cylinders. After a certain interval of time had elapsed a specially designed pipette was used to collect the remaining liquid from the plate surface. Dimensional analysis applied to the data for water, carbon tetrachloride, ethanol and benzene gave Equation II-1.

$$\frac{h}{k_v}\left[\frac{g_c\,\sigma_s}{g(\rho_\ell - \rho_v)}\right]^{0.5} = 7.9\left[\frac{L'}{C_v\Delta T}\right]^{0.6} \quad \text{.....} \quad \text{II-1}$$

In Equation II-1, the physical properties σ_s, ρ_ℓ and L' were taken at the saturation temperature; k_v, ρ_v, and C_v were taken at the mean vapor temperature.

Submerged Surfaces in Film Boiling

The whole field of pool boiling heat transfer was first subjected to critical examination by Nukiyama (33). He introduced the technique of observing the boiling process taking place on the surface of an immersed, electrically-heated resistance wire. He was able to get heater temperatures in water under atmospheric pressure ranging from 100 to 1100°C. He observed a maximum point in the curve of heat flux versus temperature difference. Also, he observed that at higher temperature differences a stable film of vapor was found.

A knowledge of the work of Nukiyama (33) and Scott (40) led

Drew and Mueller (14) to investigate the behavior of boiling organic liquids. Drew and Mueller (14) used a steam-heated loop of one-fourth inch copper tubing suspended in an Erlenmeyer flask which was connected by a side arm to a reflux condenser. They reported that, at large temperature differences of 80 to 100°C or more, the steam-heated tube was covered by a smooth film of vapor and the heat transfer across the vapor film was largely by conduction and convection. Also, they pointed out that the "spheroidal state" is related to film boiling.

In 1950, Bromley (6) modified an idea by Castle (8) (who credited Colburn) that the heat transfer mechanism for film pool boiling outside a horizontal tube can be analyzed similarly to the film condensation model of Nusselt. Bromley presented a derivation for pool film boiling outside a horizontal tube. The derivation is based on the fact that the liquid is separated from the tube by a continuous film of vapor. It is assumes that 1), the vapor film is smooth and is in laminar flow, 2), the temperature drop across the vapor film is constant, and 3), heat transfer across the vapor film is by conduction and radiation but not by convection.

Recently, Hosler and Westwater (20) studied water and Freon-11 on an 8 inch square horizontal aluminum surface. They presented high speed photographic results of bubble dynamics for submerged surfaces in film boiling.

Analytical Treatments of Film Boiling on Flat Plates

Film boiling on flat plates is characterized by the existence of a continuous vapor film coating the heat transfer surface and

therefore, its analysis is more susceptible to theoretical effort than the transition or nucleate regimes. Many workers (42, 30) have paid attention to the behavior of an interface separating two fluids of different density, such as the liquid-vapor interface in film boiling, when subjected to disturbances.

Taylor (42) considered the problem of two fluids having a common interface and acceleration in a direction perpendicular to the plane of the interface. He showed that the interface is conditionally unstable; that is, a disturbance will grow with time if the acceleration is directed from the lighter to the heavier fluid. An example of this is vapor beneath liquid in a gravitational field.

Taylor's analysis (42) of the problem assumes potential flow. The form of the vapor-liquid interface disturbance introduced into the first-order perturbation analysis is given by Equation II-2:

$$\eta = \eta_o e^{-ist} \cos jx \quad \text{II-2}$$

The wave number j can be expressed in terms of the wavelength λ, thus,

$$j = \frac{2\pi}{\lambda} \quad \text{II-3}$$

The wavelength or distance, is the shortest distance between consecutive similar points on the wave train. Thus it is the distance between consecutive peaks.

The result of the above analysis is an expression for s (complex value of wave frequency) as a function of fluid properties. From Equation II-2 it is seen that if s is real, the disturbance is periodic

in time and therefore stable. However, if s is imaginary, the disturbance grows exponentially with time. Also, under the usual pertubation approximation the frequency equation of the interface becomes (reference 27, page 459, Equation 2):

$$s^2 = \frac{g_c \sigma_s j^3}{\rho_\ell + \rho_v} - \frac{g(\rho_\ell - \rho_v)j}{\rho_\ell + \rho_v} \quad \ldots\ldots\ldots\ldots \quad \text{II-4}$$

Equation II-4 indicates that the disturbances of the interface can be stable or unstable according to whether the wavelength is shorter or longer than a critical value. This critical value is obtained by equating Equation II-4 to zero, thus

$$\lambda_c = 2\pi \left[\frac{g_c \sigma_s}{g(\rho_\ell - \rho_v)}\right]^{0.5} \quad \ldots\ldots\ldots\ldots \quad \text{II-5}$$

In film boiling, the first attempt to apply instability theory was made by Chang (9, 10) who pointed out that the vapor-liquid interface might exhibit waves with wavelengths equal to the critical value (32, 5) predicted by Equation II-5.

The larger the value of s, the greater the growth rate of the disturbance. Thus, the wavelength which maximizes s will be the "most dangerous" wavelength; that is, it will result in the disturbance which has the most rapid growth rate. Differentiating s^2 in Equation II-4 with respect to the wave number j, the "most dangerous" wavelength then becomes (27)

$$\lambda_d = 2\pi \left[\frac{3 g_c \sigma_s}{g(\rho_\ell - \rho_v)} \right]^{0.5} \quad \text{II-6}$$

It has become conventional to refer to those instabilities of the above type which occur in the absence of relative velocity effect (vapor velocity and motion of interface) as Taylor Instability. When relative velocity is important, the instability is called a Helmholtz Instability.

In a subsequent paper Chang (10) used the above wave approach and derived Equation II-7 for the heat transfer coefficient:

$$h = \left[\frac{k_v^3 (\rho_\ell - \rho_v) g}{8\pi^2 \mu_v \left(\frac{k_v \Delta T}{2 L \rho_v} \right)} \right]^{1/3} \quad \text{II-7}$$

In the above equation the group $k_v \frac{\Delta T}{2 L \rho_v}$ may be thought of as the "Thermal diffusivity" of the vapor-liquid interface as a result of phase change at the saturation temperature of the bulk liquid.

Chang (10) considers the bubble period also and he derived Equation II-8.

$$B_6 = \frac{(4\pi^2)^{3/2}}{2} \left[\frac{\mu_v}{g(\rho_\ell - \rho_v)} \right]^{2/3} \left[\frac{\rho_\ell L'}{k_v \Delta T} \right]^{1/3} \quad \text{II-8}$$

Zuber (47, 49) modified and extended the approach suggested by Chang. Zuber noted that the phenomenon of boiling bears similarity to a release of bubbles with variable frequency from a set of regularly spaced orifices of fixed geometry. Assuming Taylor instability Zuber postulated that the vapor columns were of width $\frac{\lambda_o}{2}$ (λ_o is a wavelength

longer than the critical wavelength), spaced λ_o units apart. Based on these assumptions, Zuber hypothesized a model to predict bubble dynamics. He assumed that the initial perturbation was in the form of cos jx, with an amplitude small compared to the wavelength. It is important to note that the Equations II-5 and II-6 were derived from two-dimensional considerations by several researchers (32, 9, 4, 5). For two-dimensional systems, all perturbations with wavelengths longer than the critical one, λ_c, are unstable. From an interface which has random initial perturbations it is expected that, because of the exponential growth, wavelengths near the "most dangerous" one, that is, near λ_d, will be the first to achieve finite (observable) amplitude. Therefore, for a two-dimensional system Zuber assumed that the geometry is characterized by disturbances with wavelengths in the spectrum

$$\lambda_c < \lambda_o < \lambda_d \quad \ldots\ldots\ldots\ldots\ldots\ldots \quad \text{II-9}$$

Because of the spectrum of unstable disturbances, the wavelength should be estimated between the limits given by Equation II-9, that is, by Equations II-5 and II-6.

Zuber derived equations predicting bubble dynamics and obtained the equations of growth rate and wavelengths which were governed by a Taylor-type two-dimensional instability, that is, the effect of velocity is negligible. In wave theory, the significant property of a wave is its frequency, or number of vibrations per second. Frequency is really to be associated with the source of the disturbance which is the interface waves. But it is assumed that bubbles are

released from the peaks of the waves. The reciprocal of frequency (or the time of one vibration) is known as the period, denoted by the letter B. Bubble periods B_1 (Equation II-10) and B_4 (Equation II-13) are related to the critical wavelength. Bubble periods B_3 (Equation II-11) and B_5 (Equation II-14) are related to the most dangerous wavelength. Zuber's equations for bubble period are listed below:

$$\frac{3}{2}\left[\frac{2\pi\rho_\ell}{g(\rho_\ell - \rho_v)}\right]^{\frac{1}{2}}\left[\frac{g_c(\sigma_s)}{g(\rho_\ell - \rho_v)}\right]^{\frac{1}{4}} < B < \frac{3}{2}\left[\frac{2\pi\rho_\ell}{g(\rho_\ell - \rho_v)}\right]^{\frac{1}{2}}\left[\frac{3g_c\sigma_s}{g(\rho_\ell - \rho_v)}\right]^{\frac{1}{4}}$$

Let $$B_1 = \frac{3}{2}\left[\frac{2\pi\rho_\ell}{g(\rho_\ell - \rho_v)}\right]^{\frac{1}{2}}\left[\frac{g_c\sigma_s}{g(\rho_\ell - \rho_v)}\right]^{\frac{1}{4}} \quad \text{II-10}$$

$$B_2 = \frac{3}{2}\left[\frac{2\pi\rho_\ell}{g(\rho_\ell - \rho_v)}\right]^{\frac{1}{2}}\left[\frac{3\,g_c\sigma_s}{g(\rho_\ell - \rho_v)}\right]^{\frac{1}{4}} = 3^{0.25}B_1 \quad \text{II-11}$$

Lewis (30) conducted experiments on the instability of liquid surfaces when accelerated in a direction perpendicular to their planes. He concluded that the amplitude of the surface waves increased at an exponential rate (as required by Taylor's first order theory (42)) until the amplitude reached about 0.4λ.

From the experimental knowledge of Lewis (30) and theoretical work on Taylor instability by Birkhoff (5), Zuber derived another series of equations and obtained an equation for bubble period which is shown below:

$$B_3 = 0.4\left[\frac{\rho_\ell + \rho_v}{3\pi\rho_\ell}\right]^{\frac{1}{2}}\left\{\frac{3}{2}\left(\frac{2\pi\rho_\ell}{g(\rho_\ell - \rho_v)}\right)^{\frac{1}{2}}\left[\frac{3g_c\sigma_s}{g(\rho_\ell - \rho_v)}\right]^{\frac{1}{4}}\right\}$$

$$B_3 = 0.4 \left[\frac{\rho_\ell + \rho_v}{3\pi\rho_\ell}\right]^{\frac{1}{2}} B_2 \quad \text{II-12}$$

In a subsequent report, Zuber and Tribus (48) obtained the equations of growth rate and wavelength which were governed by a Helmholtz-type two-dimensional instability, that is, assuming the effect of velocity is not negligible. They derived Equations II-13 and II-14 for bubble period:

$$2\pi \left[\frac{g_c(\sigma_s)}{g(\rho_\ell - \rho_v)}\right]^{\frac{1}{4}} \left[\frac{\rho_\ell + \rho_v}{g(\rho_\ell - \rho_v)}\right]^{\frac{1}{2}} < B < 2\pi \left[\frac{3g_c\sigma_s}{g(\rho_\ell - \rho_v)}\right]^{\frac{1}{4}} \left[\frac{3(\rho_\ell + \rho_v)}{g(\rho_\ell - \rho_v)}\right]^{\frac{1}{2}}$$

Let $$B_4 = 2\pi \left[\frac{g_c\sigma_s}{g(\rho_\ell - \rho_v)}\right]^{\frac{1}{4}} \left[\frac{\rho_\ell + \rho_v}{g(\rho_\ell - \rho_v)}\right]^{\frac{1}{2}} \quad \text{II-13}$$

and $$B_5 = 2\pi \left[\frac{3g_c\sigma_s}{g(\rho_\ell - \rho_v)}\right]^{\frac{1}{4}} \left[\frac{3(\rho_\ell + \rho_v)}{g(\rho_\ell - \rho_v)}\right]^{\frac{1}{2}}$$

$$B_5 = 3^{0.75} B_4 \quad \text{II-14}$$

In summary, Zuber and Tribus, and later Zuber derived Equations II-10 to II-14. Equations II-10 to II-12 are based on Taylor-type two-dimensional instability model, whereas Equations II-13 and II-14 are based on Helmholtz-type two-dimensional instability.

Berenson (4) modified and extended the method suggested by Zuber. He used the Taylor instability model and succeeded in predicting a functionality between the heat transfer coefficient and ΔT (temperature difference between plate temperature and saturated liquid temperature) for submerged surfaces on flat plates. This was achieved by analyzing the effect of vapor velocity on the instability.

He showed that the values of λ_c and λ_d given by Equations II-5 and II-6 must be modified when one considers vapor velocity. He derived also the ΔT corresponding to the minimum heat flux. The minimum heat flux is related to the Leidenfrost point (lowest temperature for stable film boiling). Berenson's equations are as follows:

$$h = \left[\frac{k_v^3 \rho_v (\rho_\ell - \rho_v) L' g}{\mu_v \Delta T \left(g_c \sigma_s / g(\rho_\ell - \rho_v)\right)^{1/2}}\right]^{1/4} \quad \text{II-15}$$

$$(\Delta T)_{min} = 0.127 \frac{\rho_\ell L'}{k} \left[\frac{g(\rho_\ell - \rho_v)}{\rho_\ell - \rho_v}\right]^{2/3} \left[\frac{g_c \sigma_s}{g(\rho_\ell - \rho_v)}\right]^{1/2} \left[\frac{\mu_v}{g(\rho_\ell - \rho_v)}\right]^{1/3} \quad \text{II-16}$$

Equation II-15 is similar to Bromley's (7) equation for film boiling on horizontal cylinder. The only differences are in the constant coefficient and the substitution of $\left(g_c \sigma_s / g(\rho_\ell - \rho_v)\right)^{1/2}$ for the tube diameter D. $\left(g_c \sigma_s / g(\rho_\ell - \rho_v)\right)^{1/2}$ and D are the geometrical scale factors for horizontal plates and tubes, respectively.

In this chapter of the dissertation we have discussed the analytical and experimental investigations which pertain to the heat transfer coefficient and to the bubble dynamics for submerged surfaces in film boiling. We shall compare bubble dynamics correlations with the experimental results from motion pictures of the Leidenfrost phenomenon in Chapter IV.

CHAPTER III

EXPERIMENTAL STUDY OF VAPORIZATION TIME

This chapter deals with the experimental study of total vaporization times of extended masses on a flat plate. The total vaporization time is reported as a function of initial liquid volume and plate temperature. The experimental data cover the size range upwards from the spheroidal state asymptotically approaching submerged surfaces in film boiling. Also, data of liquid mass thickness from still photographic measurements of projected area are included. The experimental apparatus and procedure are discussed below.

Apparatus

The plate used in this investigation was of 304 stainless steel. This metal forms a thin smooth surface coating of its oxide at temperatures of film boiling. In this respect, stainless steel is almost ideal compared to other metals such as copper. Also, stainless steel was selected since it was used by Gottfried (16) and Borishansky (6), both of whom reported success with its use.

The test surface shown schematically in Figure 2 consisted of an 8 inch diameter circular plate, with a highly polished circular indentation machined 1/8 inch deep into the center of the plate. This center test area had a 6 inch diameter and was 1/8 inch thick.

Chromel-alumel thermocouples were used for temperature measurements. These particular metals were selected for their high

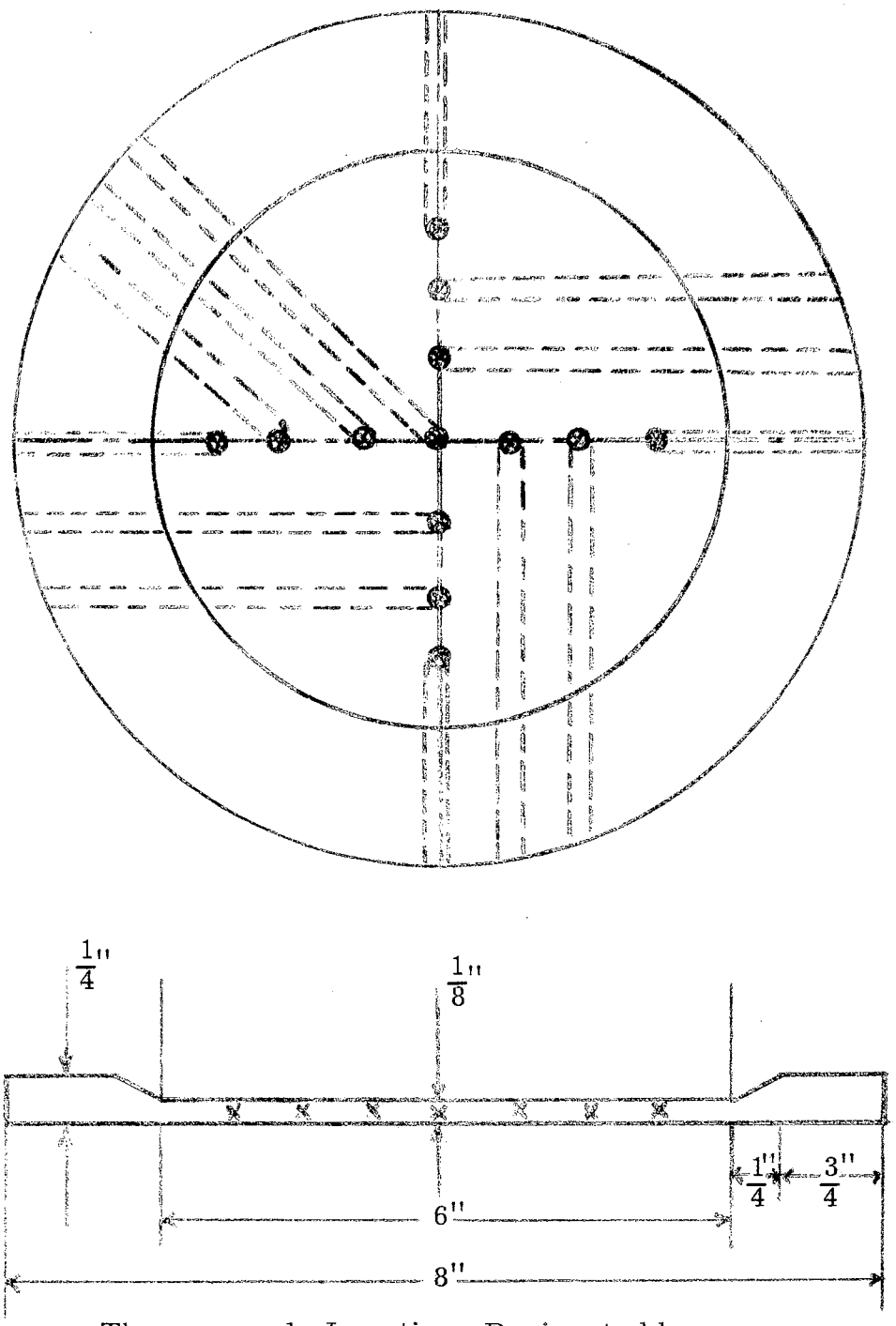

Thermocouple Locations Designated by x.

Figure 2. Schematic Top View and Cross Section of Stainless Steel Plate Showing Location of Chromel-alumel Thermocouples.

thermal e. m. f. output per degree of temperature difference and stability over the temperature range anticipated. The thermocouples were calibrated by boiling water at atmospheric pressure; calibration data of thermocouples are given in Appendix A.

Thirteen 28 gauge, calibrated chromel-alumel thermocouples were installed equidistant along two diameters of the center area, 1/8 inch from the surface of the plate. The bare thermocouple junctions were covered with a very thin sheet of insulating asbestos to prevent short circuiting between the plate and thermocouples. Each thermocouple was fastened to the plate with sauereisen high-temperature cement in order to prevent movement of the junctions during use. The thermocouple wires were covered with small pieces of ceramic tubing. The free ends of the thermocouple wires were connected to a selector switch and then to a potentiometer. The thermocouple e. m. f. was measured on a No. 8690 Leeds and Northrup milivolt potentiometer, by using an ice bath cold junction.

Figure 3 is a diagram of the apparatus used in these experiments and Figure 4 is a photograph of the same apparatus. The test area was centered upon a one-foot-square electrical heating surface. This surface was formed by placing three Hevi-Duty # 54-KSS flat-type electric heating units next to each other. Each unit had ten grooves containing coiled nichrome wire, designed to operate at a maximum of 115 volts and 650 watts. Since the entire heating surface contained 30 rows of coiled wire, a nearly uniform heat flux was obtained at the surface. The three heating units were connected in parallel to an alternating current transformer (a Variac), which was in turn connected to a 115 volt, 20 amp outlet. The heating units were supported by two

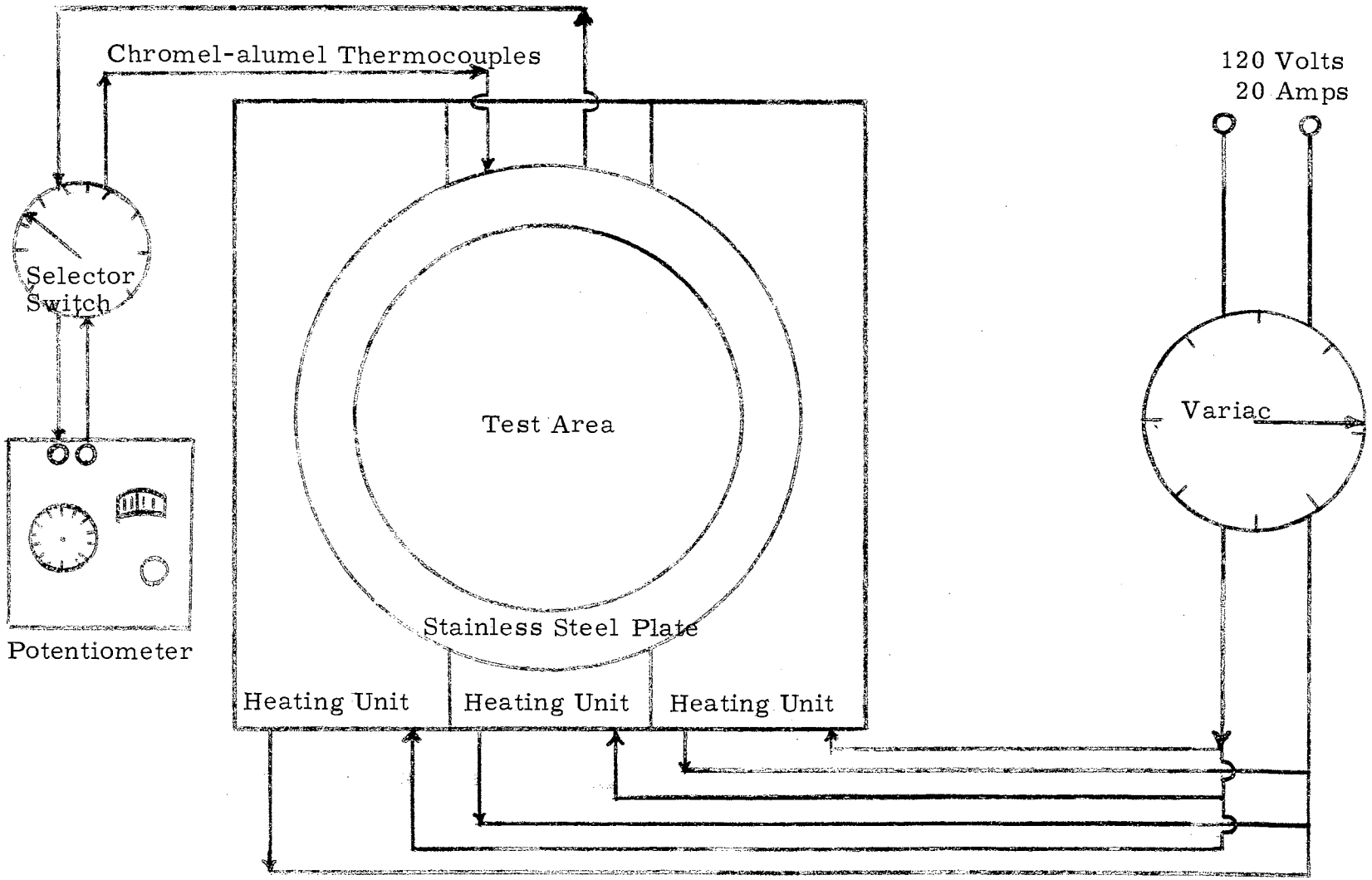

Figure 3. Schematic Drawing of Apparatus.

Figure 4. Arrangement of the Experimental Apparatus.

asbestos insulating plates which were constructed so that the level of the plate could be adjusted.

A $3\frac{1}{4}$ inch-high aluminum fence was built around the perimeter of the heating surface in order to minimize convection currents across the plate. This fence was insulated by a thick coating of asbestos cement.

Procedure

The order of investigation for the experimental vaporization time for different volumes of each liquid at constant plate temperature was 0.05, 0.1, 0.15, 1, 3, 5, 8 and 10 ml. Masses of larger initial volume (1, 3, 5, 8 and 10 ml) were produced by a calibrated 10 ml pipette and masses of smaller initial volume (0.05, 0.1 and 0.15 ml) were produced by a calibrated microliter syringe. The top of the pipette was connected to a propipette which drew the liquid to the desired level and would deliver all of the liquid to the hot plate on release. The pipette was bent at a 45° angle about one inch from the bottom to deliver large liquid masses in a short time on the plate. The pipette was gravimetrically calibrated using all four liquids. The initial liquid volumes produced in this manner were reproducible to within an average $\pm$ 4 percent, as is shown by the pipette and microliter syringe calibration data given in Appendix B.

Prior to experimental work, the surface of the test area was polished with a piece of No. 0 emery paper. In gathering data, the Variac was set at a fixed value, and about two hours were allowed for the test area to heat up to a steady-state temperature. Upon reaching steady-state, the plate temperature across the test area was constant

to within a variation of $\pm 5^{\circ}C$ which occurred at the maximum plate temperature of $539^{\circ}C$. The variation in plate temperature decreased as the temperature was lowered. The plate temperatures recorded were averaged over the time required for vaporization for these thermocouples directly below the liquid mass.

The pipette end was held about one-half inch above the test area, and a small liquid mass was placed on the plate; then the remaining liquid volume was gently delivered into the bulk of the liquid mass on the plate. The maximum time needed to place 10 ml of liuqid on the plate was less than 20 seconds at low temperature. Occasionally, the liquid masses would fragment upon impact, or stick to a speck of dirt on the plate. The data obtained under such conditions were disregarded. Three observations were recorded for each liquid at each temperature. The time required for the liquid to completely evaporate (starting from the process of placing the first drop of liquid on a plate) was measured with a stop watch (Meylan #218) which can be read to one-hundredth of a second.

Test Liquids

The water that was used in these experiments was demineralized water from the School of Chemical Engineering. The demineralized water was prepared from tap water passing through Penfield Model R-M-8 cation and anion resin beds. The pH value of the demineralized water was 6.8 instead of 7.

The ethanol used was reagent quality pure absolute ethyl alcohol, manufactured by U. S. Industrial Chemical Company, New York. Benzene

and carbon tetrachloride were analytical reagents, manufactured by Baker Chemicals Company, Phillipsburg. The manufacturer's specifications were:

Liquid	Purity, Mole %
Carbon Tetrachloride	99.96
Ethanol	99.99
Benzene	99.97

All liquids were checked for purity in a gas chromatograph and found to have less than one percent impurities. No further purification of liquids was attempted.

Still Photographic Work

For the purpose of studying the liquid thickness, a Konica FS 35 mm still camera was mounted on a photographic copying stand. The camera was fitted with an Ednalite +3 series close-up lens so that the boiling liquid could be magnified and clearly focused.

The still photographs were taken at 10^{-3} second exposure at f 2.9 using Kodak Super XX black-and-white film (ASA 100). The lens-to-object distance was about seventeen inches. Lighting was achieved by two General Electric Photoflood lamps. The distance between plate and photoflood lamp was about twenty-three inches. All photographs were taken within two seconds after delivering the last drop of liquid on a hot plate. In these experiments the volume was varied from 0.05 to 10.0 ml at constant plate temperature. The mean thickness of the liquid masses was calculated from the known volume divided by the projected area. A planimeter was used to measure the projected

area of the liquid mass from the photograph.

Results and Discussion

The experimental vaporization data of water, carbon tetrachloride, benzene and ethanol are presented in Figures 5, 6, 7 and 8, respectively. Also, the experimental vaporization data of liquids are tabulated in Appendix D.

From Figures 5 through 8, it is evident that the vaporization data are reproducible. Also, in Figures 5 through 8, the vaporization times for a given volume of each liquid are higher at low temperature (above the Leidenfrost point) than at high temperature difference. Some experimental data for liquids in the transition and nucleate regimes are shown on the left side of the Leidenfrost point in Figures 5 through 8. The temperature difference at which vaporization of the extended masses takes the longest time is known as the "Leidenfrost Point". The Leidenfrost point is the beginning of film boiling regime. From Figures 5 through 8, the Leidenfrost point occurs at about $\Delta T = 207^{\circ}C$ for water, $\Delta T = 107^{\circ}C$ for carbon tetrachloride, $\Delta T = 105^{\circ}C$ for benzene and $\Delta T = 104^{\circ}C$ for ethanol. The comparison of the Leidenfrost points among small droplets, extended liquid masses and a pool of liquid will be included in Chapter IV. Although the data points show occasional variations in vaporization time as great as $\pm$ 11 percent, particularly in the vicinity of the Leidenfrost point, most of the data points are clustered within $\pm$ 7 percent. Figure 5 shows that the experimental vaporization time of a 10 ml water mass at a plate temperature of $307^{\circ}C$ is about 16.5 minutes.

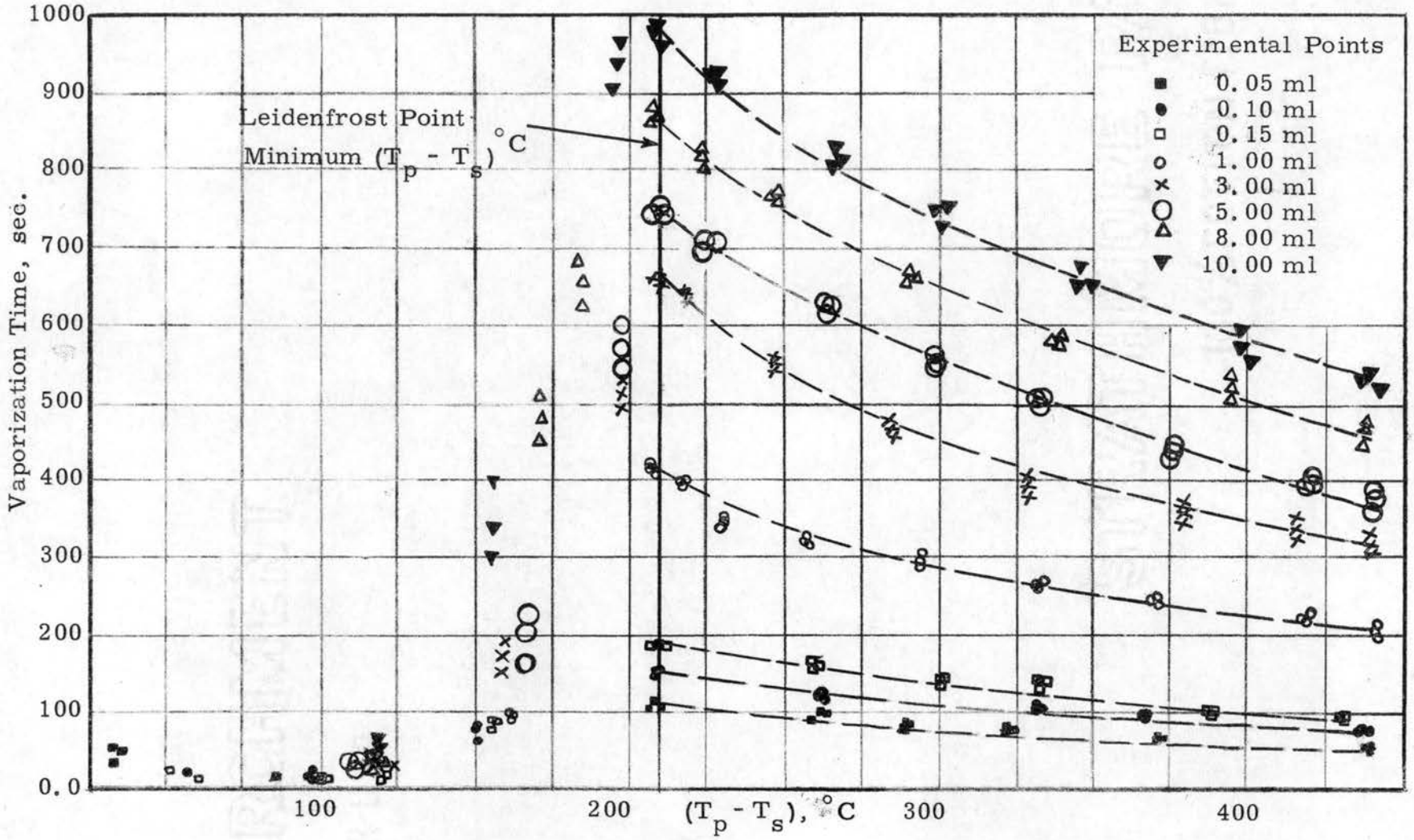

Figure 5. Liquid Vaporization Time Vs Temperature Difference. Water

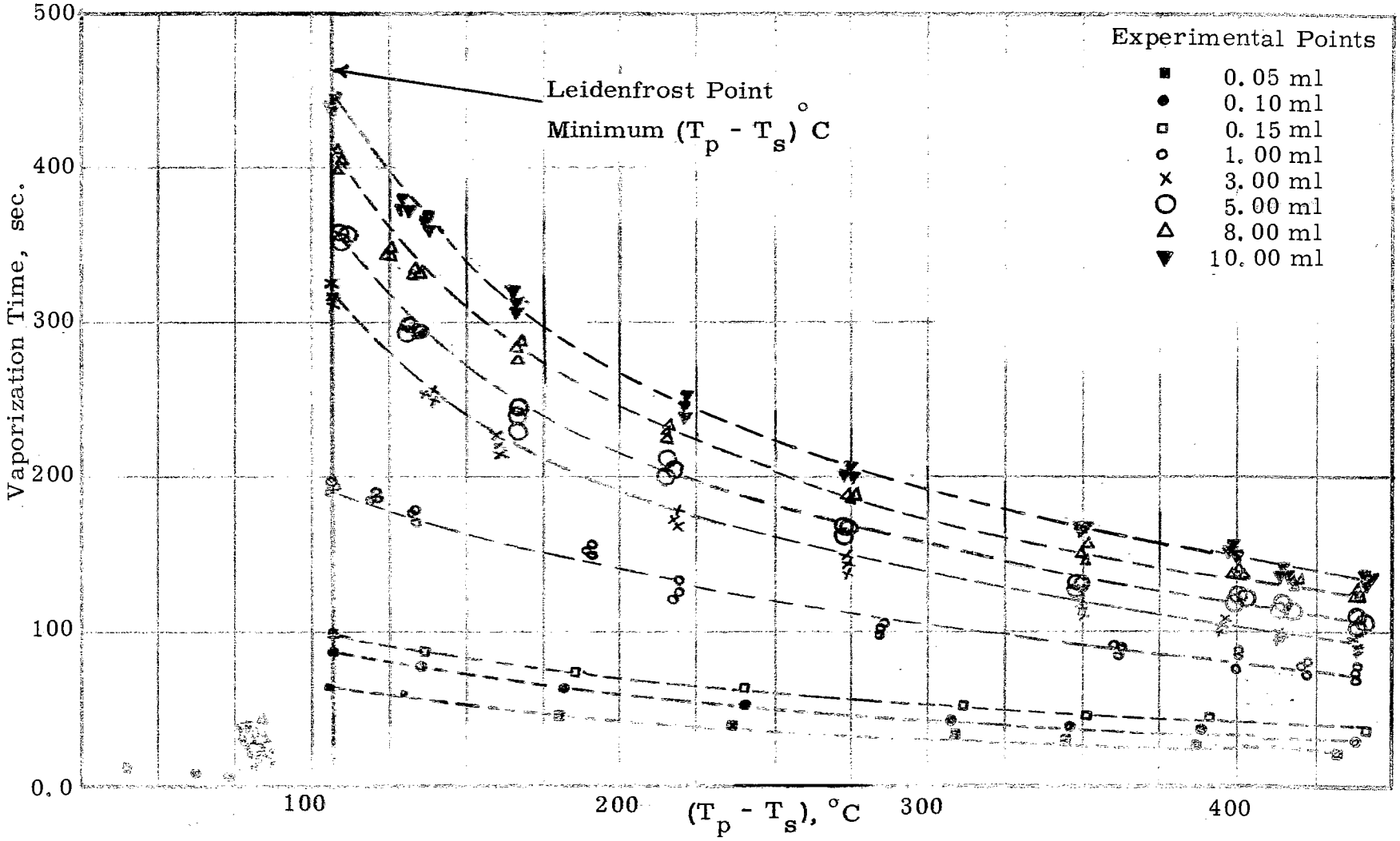

Figure 6. Liquid Vaporization Time Vs Temperature Difference. Ethanol

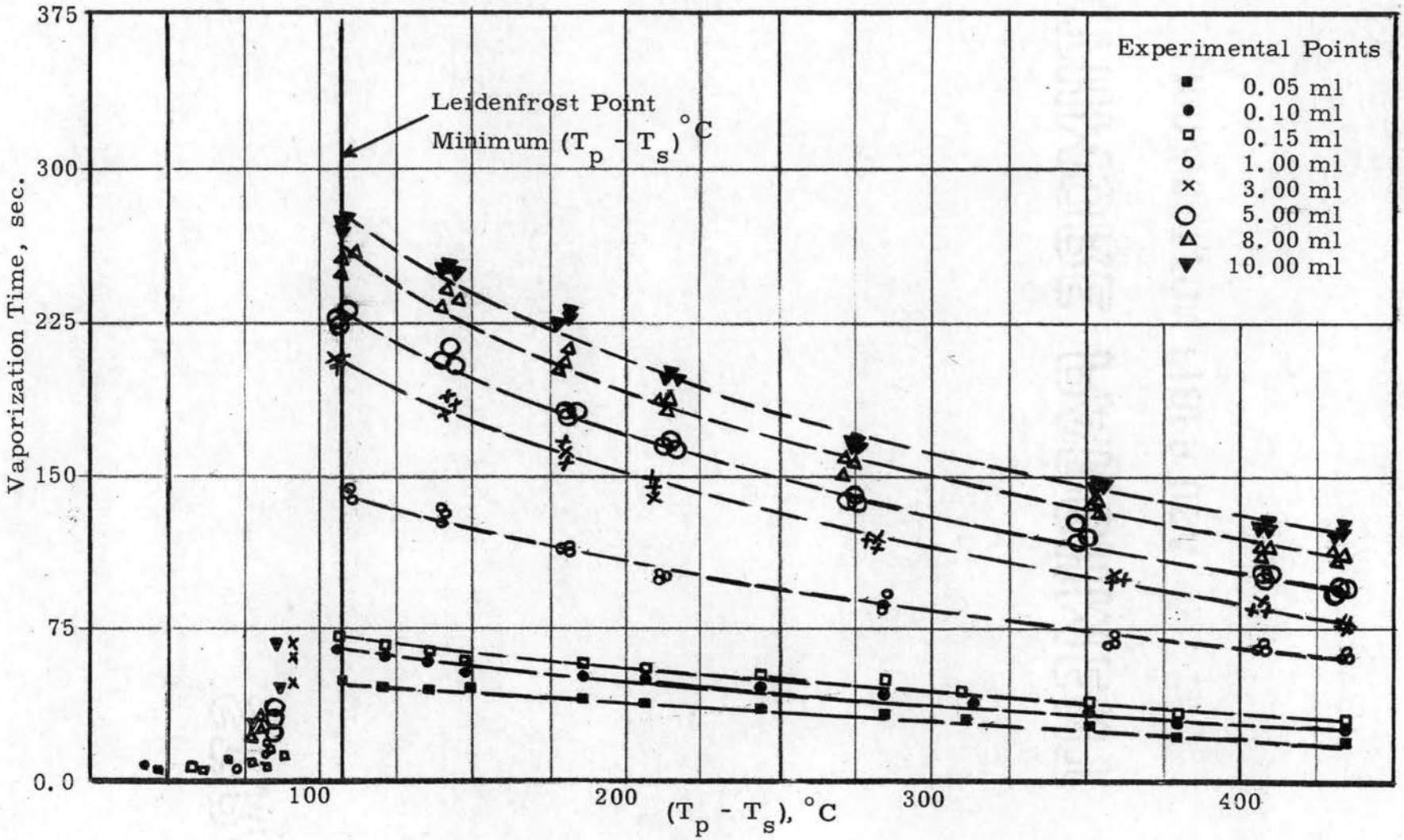

Figure 7. Liquid Vaporization Time Vs Temperature Difference. Carbon Tetrachloride

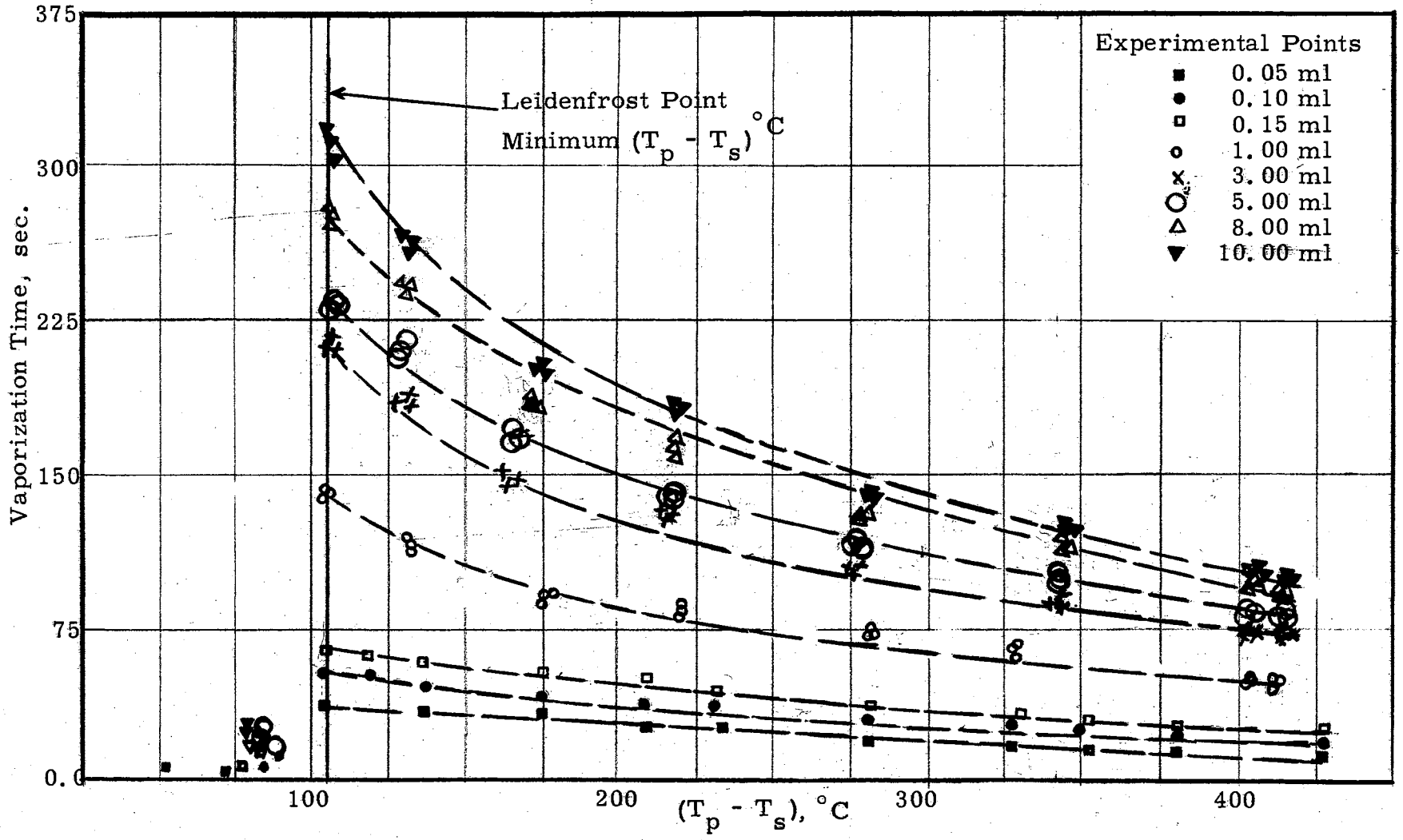

Figure 8. Liquid Vaporization Time Vs Temperature Difference. Benzene

In Figure 9, the average plate temperatures were recorded at one minute intervals for those thermocouples below the liquid mass on a plate. The curve in Figure 9 shows that the temperature suddenly decreases and then slowly returns to the steady state value during the course of vaporization of an initial 10 ml water mass. For the larger masses (8 and 10 ml) the temperature variation was always less than 12°C at the Leidenfrost point. From Figure 9, the Leidenfrost point for 10 ml of water is seen to be about 300°C (plate temperature) instead of the time average of 307°C. However, the variation in plate temperature during evaporation of 0.05, 0.10 and 0.15 ml liquid masses was less than 1°C; the Leidenfrost point of 0.05, 0.10 and 0.15 ml water masses was observed to be 307°C plate temperature. The variation in temperature during evaporation of 1, 3, and 5 ml masses was less than 7°C; the Leidenfrost point for 1, 3, and 5 ml water masses was observed to be about 305°C instead of the time average value of 307°C. For water, the Leidenfrost point is uncertain due to the wide transition regime compared to those of organic liquids. In this thesis, the author has reported the averaged lowest temperature in stable film boiling as the Leidenfrost point for extended liquid masses.

Figure 10 shows the temperature variation with time for 10 ml of water at high temperature. The average temperatures were recorded at half-minute intervals for those thermocouples below the liquid mass on a plate. The behavior in variation of temperature with time of Figure 10 is similar to that of Figure 9. For 8 and 10 ml of water masses the plate temperature variation was always less than 7°C at the highest plate temperature. The variation in temperature for 1, 3 and 5 ml masses was about 4°C and the variation for 0.05, 0.1 and

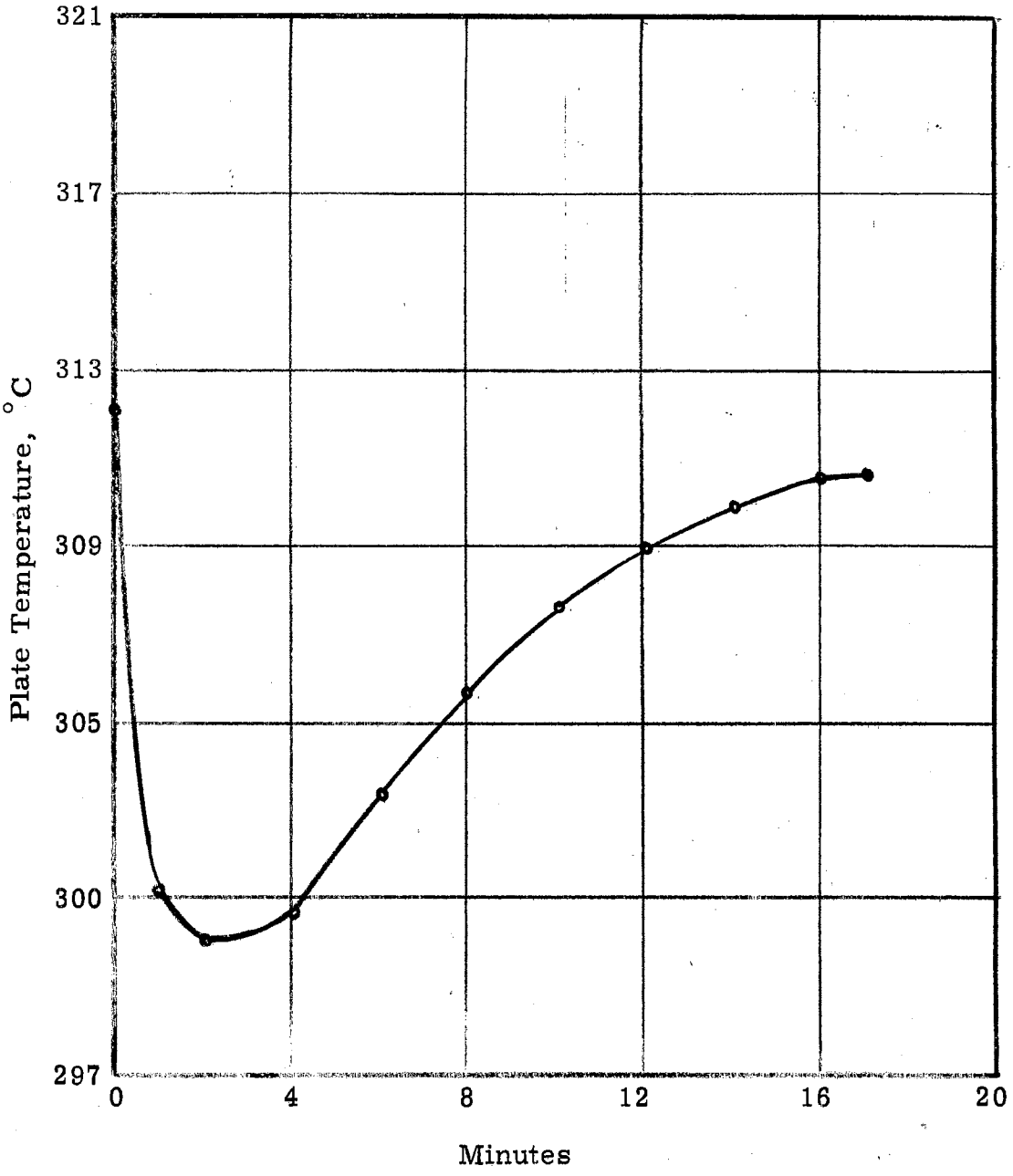

Figure 9. Temperature Variation with Time for 10 ml of Water to Evaporate Completely at Low Temperature.

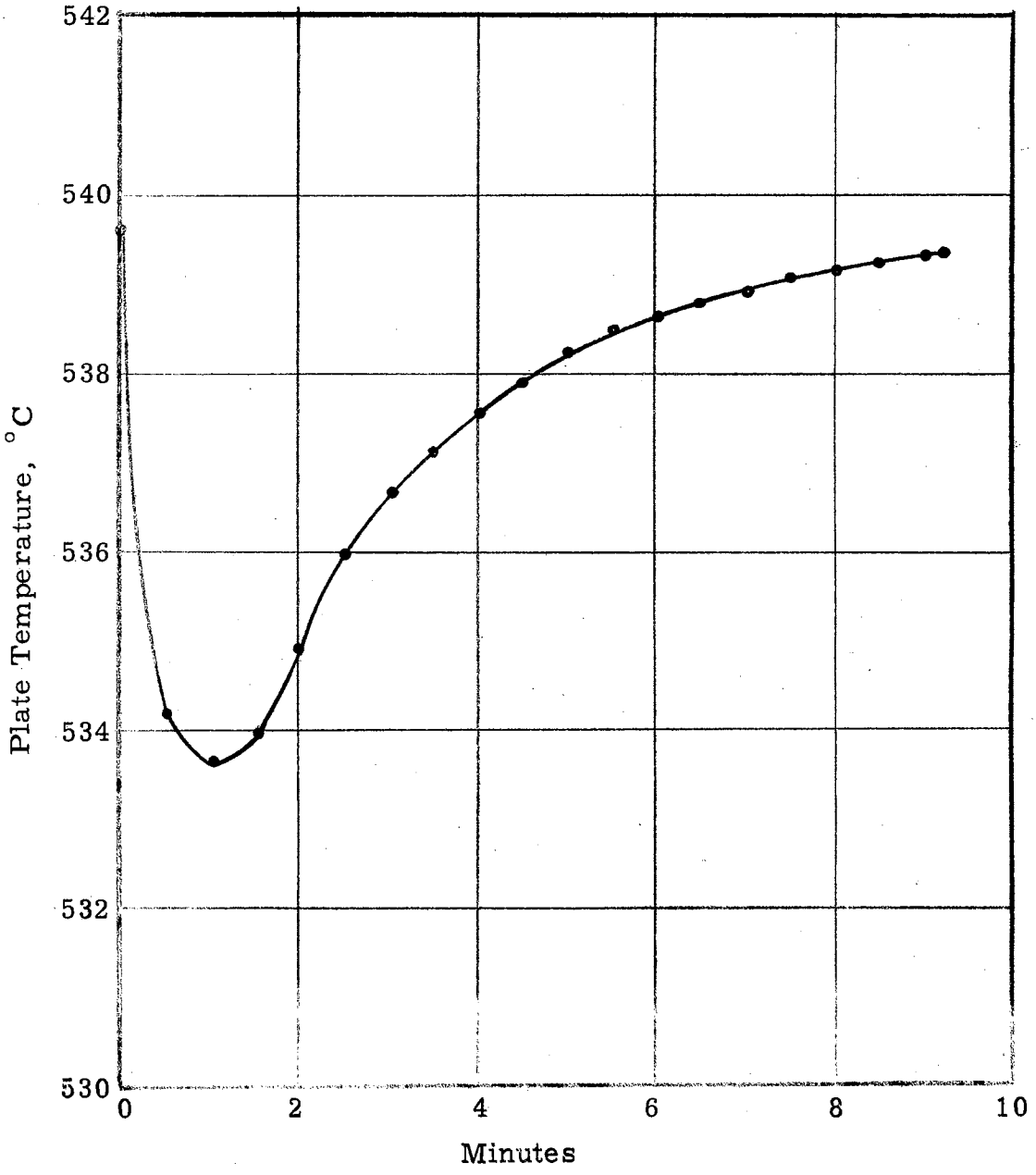

Figure 10. Temperature Vaporization with Time for 10 ml of Water to Evaporate Completely at High Temperature.

0.15 ml masses was less than 1°C.

Figure 11 shows the various characteristic shapes of extended liquid masses. The shape of the masses changes as the initial quantity of liquid is increased; the spheroids become first elliptical and then essentially flat. As the size of the mass is further increased, the vapor formed on its surface is unable to flow off to the periphery and begins to break through the thickness of the liquid as systematically formed bubbles of vapor. In experiments using water, the appearance of a vapor bubble was observed as a rule in spheroids whose volume was 2.7 ml or more. Also, in experiments using organic liquids (ethanol, benzene and carbon tetrachloride), the appearance of bubbles was observed as a rule in spheroids whose volumes were 1.2 ml or more. As the volume of liquid is increased, the number of simultaneous vapor bubbles in the liquid increases. The frequency of their formation is affected by the temperature of the heating surface. However, as the temperature of the plate increases, bubbles become so numerous that their motions interact. An attempt was made to count the number of bubbles by direct visual observations, but it was physically impossible due to the high frequency of bubble breakthrough. In these experiments at the higher plate temperature, when the masses of the organic liquid are large, the appearance of vapor bubbles is equiprobable over the entire surface of the liquid except at the extreme outer edge.

For water, Table 1 shows that the vaporization data of Borishansky and of this work agree at 350°C plate temperature. The maximum variation is about three percent at 350°C plate temperature. However, the experimental data from these two studies do not agree at 275°C

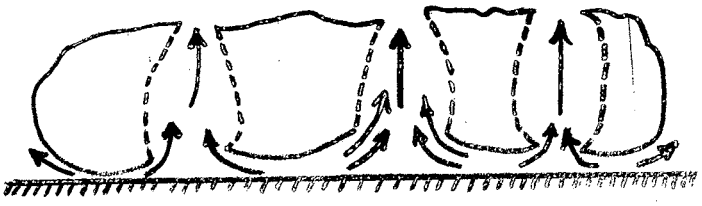

Large Liquid Volume (about 10 ml).

Liquid Volume ≥ Intermediate Liquid Volume

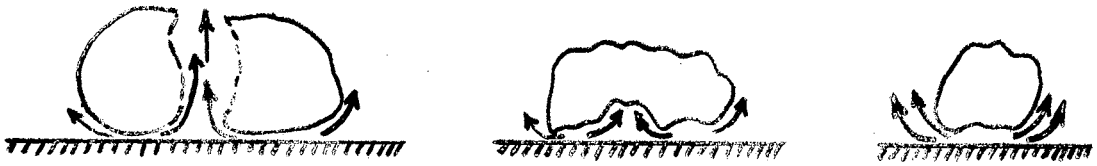

Intermediate Liquid Volume

Intermediate Liquid Volume ≥ x Liquid Volume

x = 2.7 ml of Water or 1.2 ml of Benzene, Ethanol, or Carbon Tetrachloride

Small Liquid Volume

x ≤ Small Volume ≥ 0.05 ml 0.05 ml ≤ Small Volume ≥ 10^{-4} ml

Figure 11. Characteristic Shapes of Extended Masses.

TABLE I

A Comparison of Borishansky's Data and Author's Data for the Vaporization of Water Masses

Volume of Water ml	Average Vaporization Time, sec (Borishansky)	Average Vaporization Time, sec (Author)
	Plate Temperature, 350°C	
2	482	471
3	540	535
4	614	608
5	666	663
	Plate Temperature, 275°C	
1	442	287
2	574	408
3	714	481
4	770	501

plate temperature. The experimental data of this work at 275°C seem to indicate that the masses were in the transition regime. Borishansky's data at 275°C seem to indicate that the masses were in the film boiling regime. A possible explanation could be the thermal behavior of the plate itself. A stainless steel plate was used for this entire study. Stainless steel has a thermal diffusivity of 0.62 cm^2/sec at 275°C. The thermal diffusivity of a metal is the ratio of thermal conductivity to the product of specific heat and density. Borishansky used a brass plate to study 1 to 5 ml masses of water and a carbon steel plate to study 5 to 34 ml masses of water. Brass has a thermal diffusivity of 7.3 cm^2/sec at 275°C. Carbon steel has a thermal diffusivity of 2.1 cm^2/sec at 275°C (25). It is important to remember that the vaporization times of liquid masses in the transition regime increase as the temperature of plate increases and the vaporization times of liquid masses in the film boiling regime decrease as the temperature of plate increases. A plate temperature of 275°C is near the upper end of the transition regime for water. In gathering vaporization data, temperatures are recorded from the thermocouples below the liquid mass on the plate. The thermocouple junctions are at fixed positions under the test area of plates.

When liquid is placed on the plate, heat removal is enhanced over the natural convection process to the atmosphere. Therefore, the plate cools locally as noted in Figures 9 and 10. It is probable moreover that the maximum cooling takes place at the point where the liquid first approached the plate and this point may be somewhat removed from the thermocouples. Temperature differences within

the plate will be equilibrated more slowly with a plate material of lower thermal diffusivity. Further, the Leidenfrost point is a lower bound to a stable boiling configuration, and transition boiling once established will tend to persist or even move towards the nucleate boiling regime rather than reestablishing film boiling.

In conclusion, it seems possible that the difference in the Leidenfrost temperature between the present study and those implied by Borishansky is due to the different transient thermal behavior of the test surface when the liquid mass is deposited.

Figures 12, 13, and 14 show the curves for thickness of liquid masses. The thickness remains practically constant after a certain volume has been achieved.

Borishansky's thickness curve of water in Figure 12 is higher than the curve found in this work. The source of error might be in the photographic measurement technique. Borishansky used both rings and a planimeter to measure the projected area of liquids. He did not specify the base of time for photographic technique. If he took the pictures some time after placing the last drop of liquid on the hot plate, then it is possible to get a small value of the projected area, which increases the apparent thickness liquid masses, since the thickness of liquid was obtained from the original liquid volume which was divided by projected area. Also, he did not mention any temperature for the results shown in Figure 12. Hence, it is not possible to arrive at any meaningful conclusion regarding the correctness of the thickness measurements. The average thickness of large water masses is 0.48 cm in our study whereas Borishansky's data show 0.64 cm. In this work

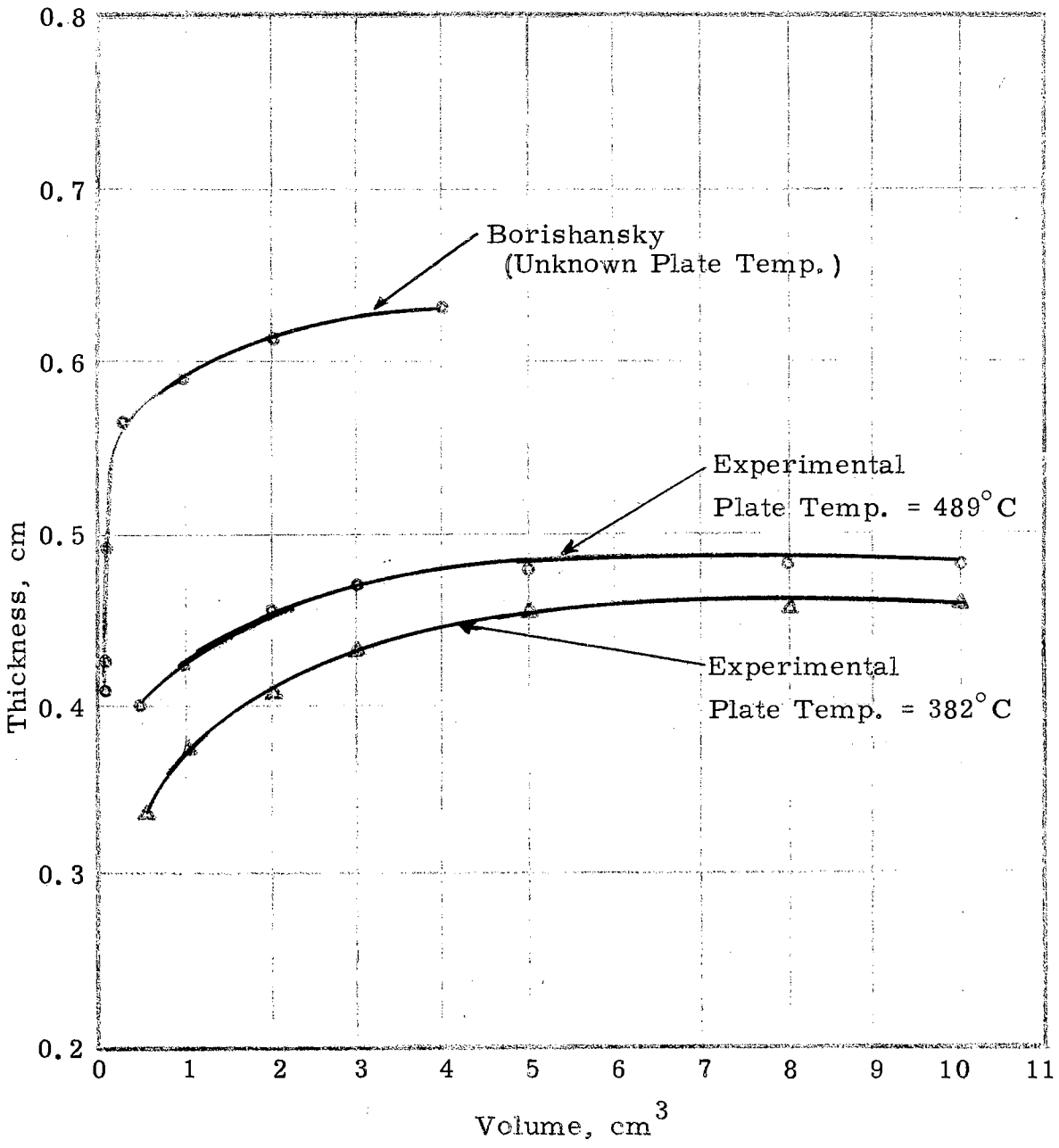

Figure 12. Thickness of Extended Masses as a Function of Volume Water

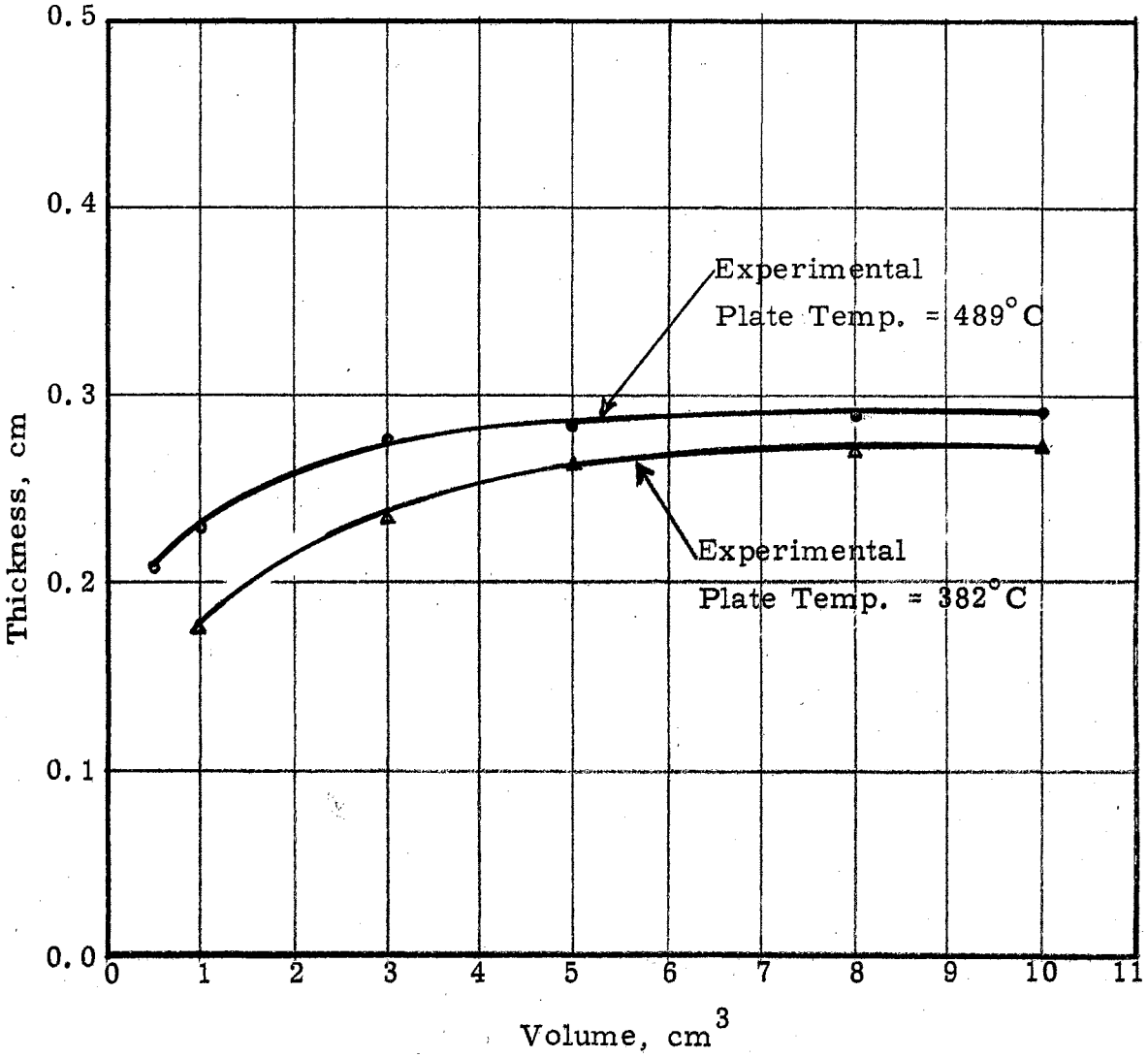

Figure 13. Thickness of Extended Masses as a Function of Volume Carbon Tetrachloride

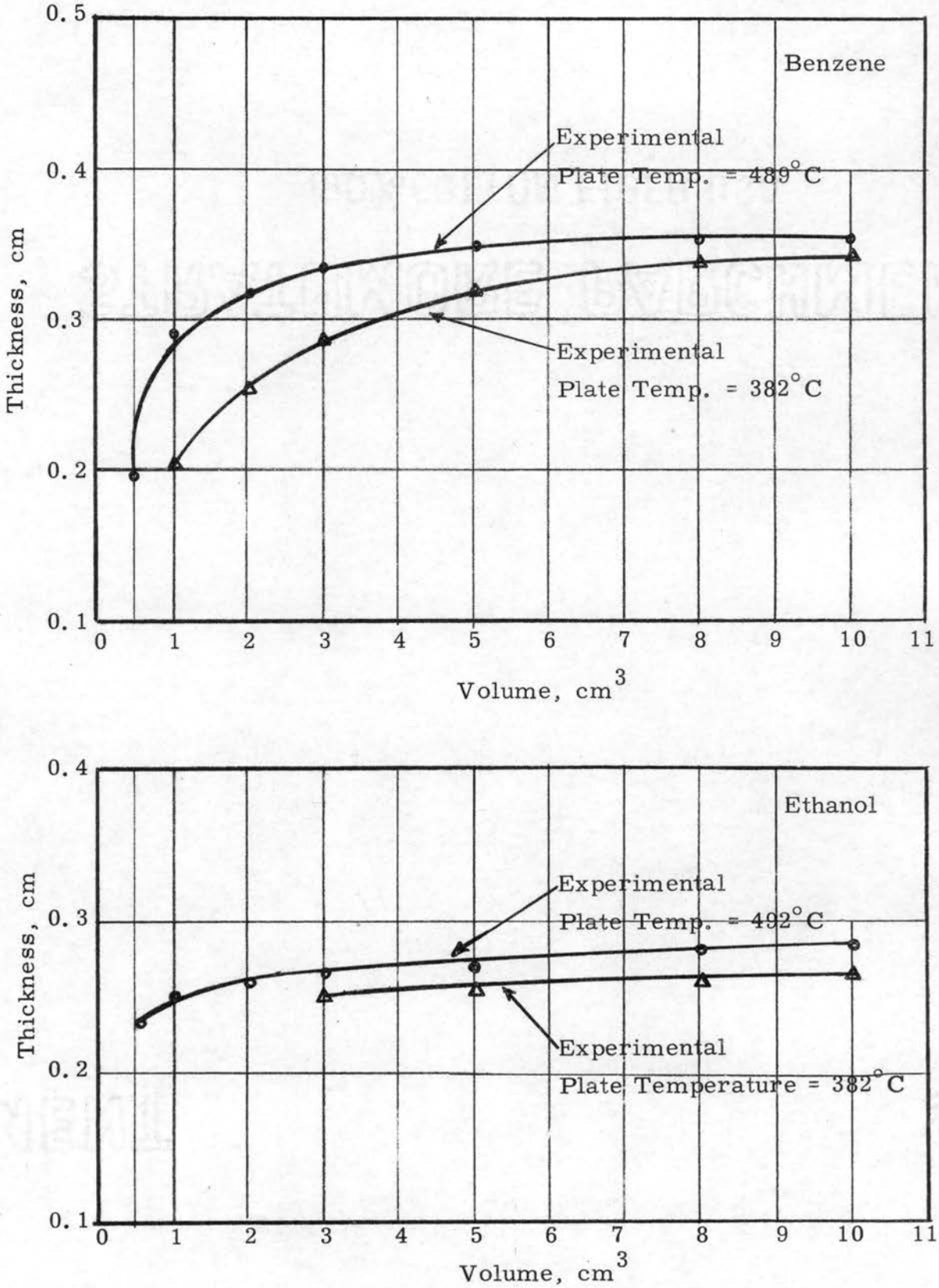

Figure 14. Thickness of Extended Masses as a Function of Volume
Benzene, Ethanol

the average thickness for benzene is about 0.35 cm, average thickness for ethanol is 0.28 cm and average thickness for carbon tetrachloride is about 0.29 cm as shown in Figures 13 and 14.

The calculated thicknesses of liquid masses shown in Figures 12, 13, and 14 are lower than the true value since only the volume of the liquid is used in calculating thickness. Actually, the combined volume of liquid and vapor bubbles should be used to get a true thickness.

The curves in Figures 15 through 18 represent the specific vaporization rate of extended liquid masses. The specific vaporization rate is the ratio of mass of liquid evaporated in unit time to the liquid mass present. The curves of Figures 15 through 18 are calculated from Figures 5 through 8 for liquid volume differences of (10-8 ml), (8-5 ml), (5-3 ml), (3-1 ml), (1-.15 ml), (.15-.1 ml), (.1-.05 ml) and Lee's work for small droplets of liquids at constant temperature. In Figures 15 to 18, the abcissa is obtained by using the formula $\left[\rho_\ell (V_{z\ell} - V_z') / (\tau_{z\ell} - \tau_z')\right] / \frac{1}{2}\rho_\ell (V_{z\ell} - V_z')$ and the ordinate is obtained by using the formula $\frac{1}{2}\rho_\ell (V_{z\ell} + V_z')$ where

τ is the vaporization time

V is the liquid volume

ρ_ℓ is the liquid density

$z\ell$ indicates value for the larger liquid volume

z' indicates value for the smaller liquid volume

In Figure 15, the upper curve is at 425°C plate temperature. The lower curve is at 320°C plate temperature. In Figures 16 through 18, the upper curves are at 451°C plate temperature. The lower curves are at Tp = 314°C. These curves of Figures 15 through 18 point

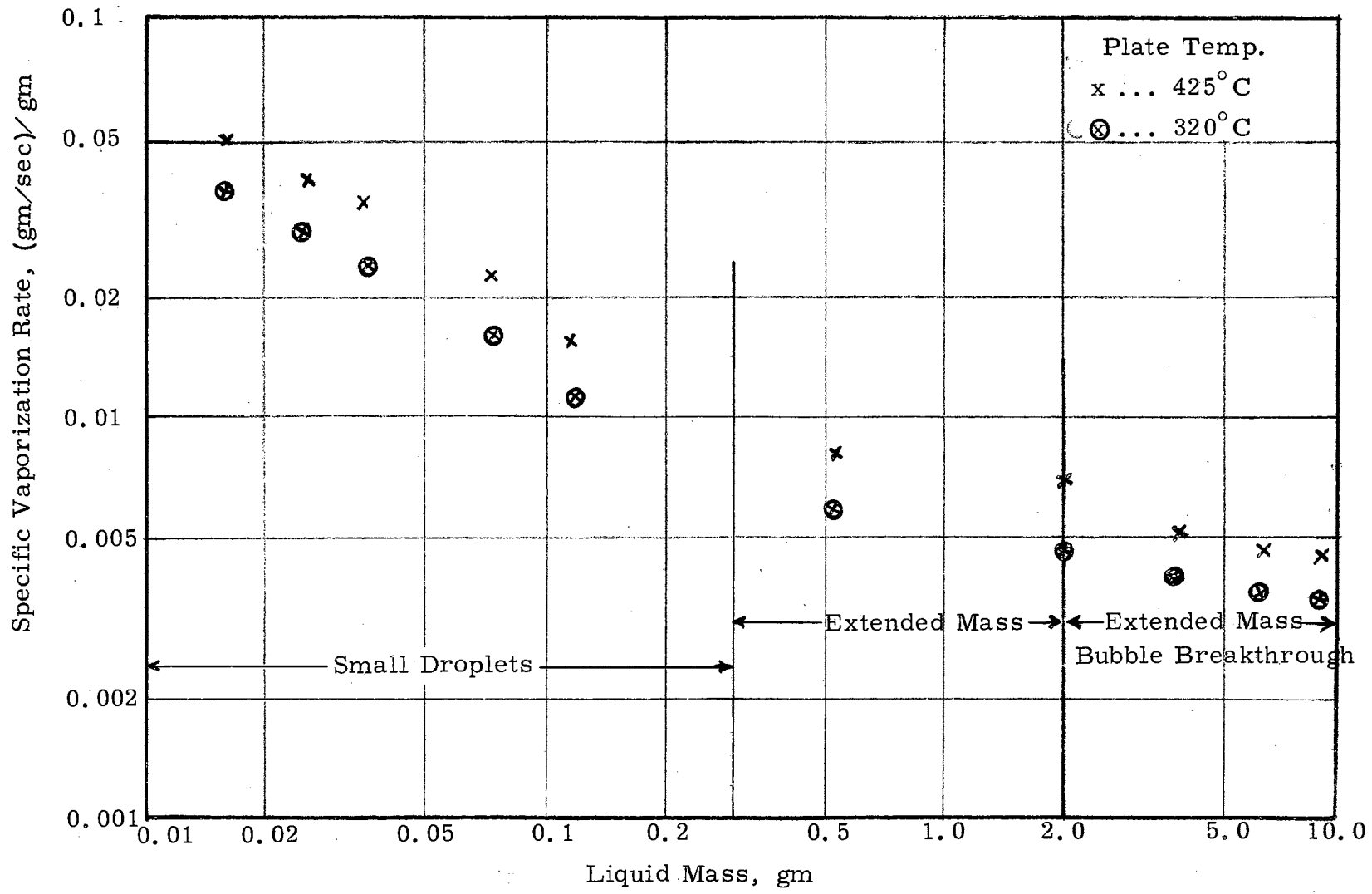

Figure 15. Specific Vaporization Rate Vs Liquid Mass
Water

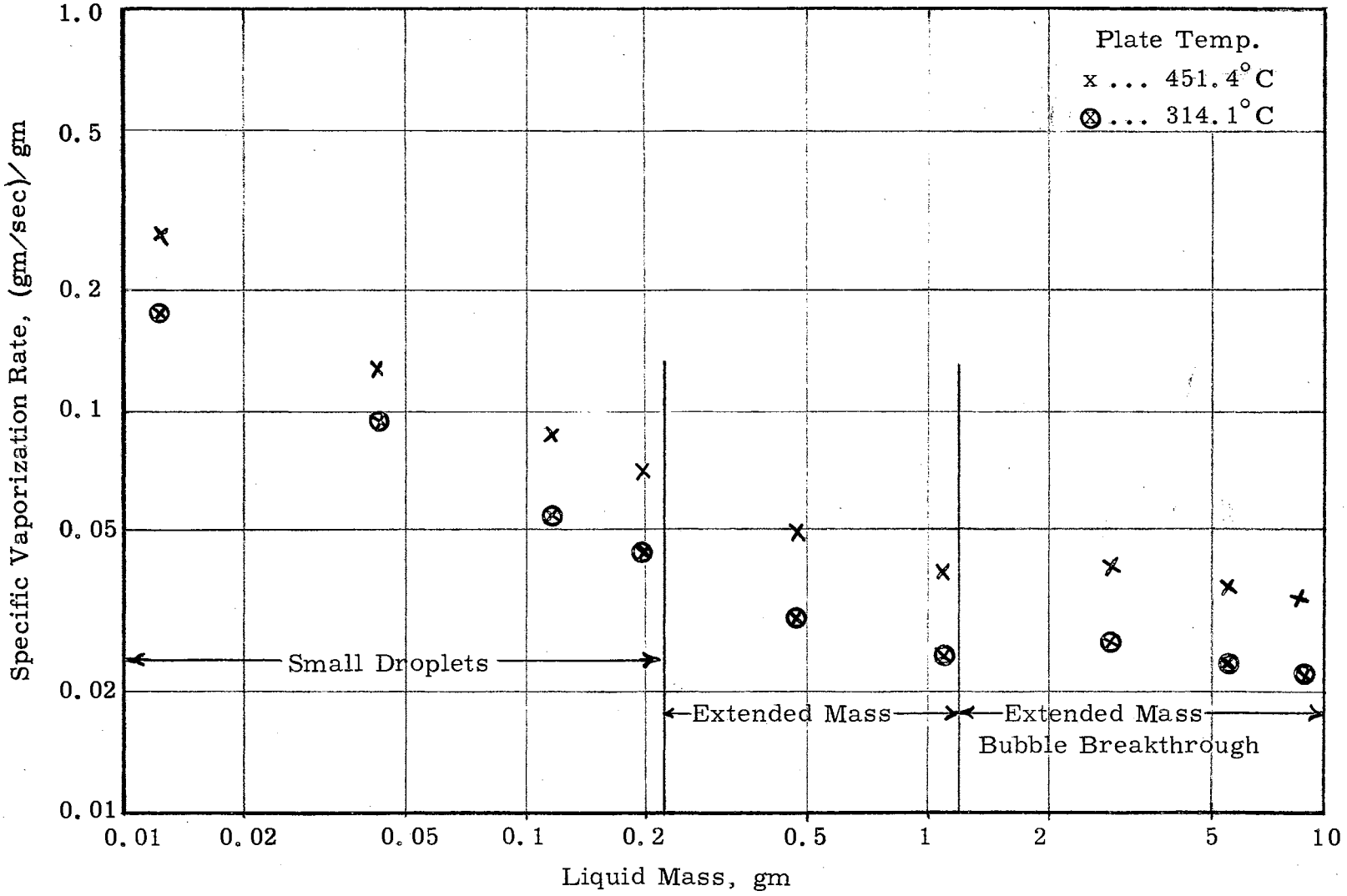

Figure 16. Specific Vaporization Rate Vs Liquid Mass
Carbon Tetrachloride

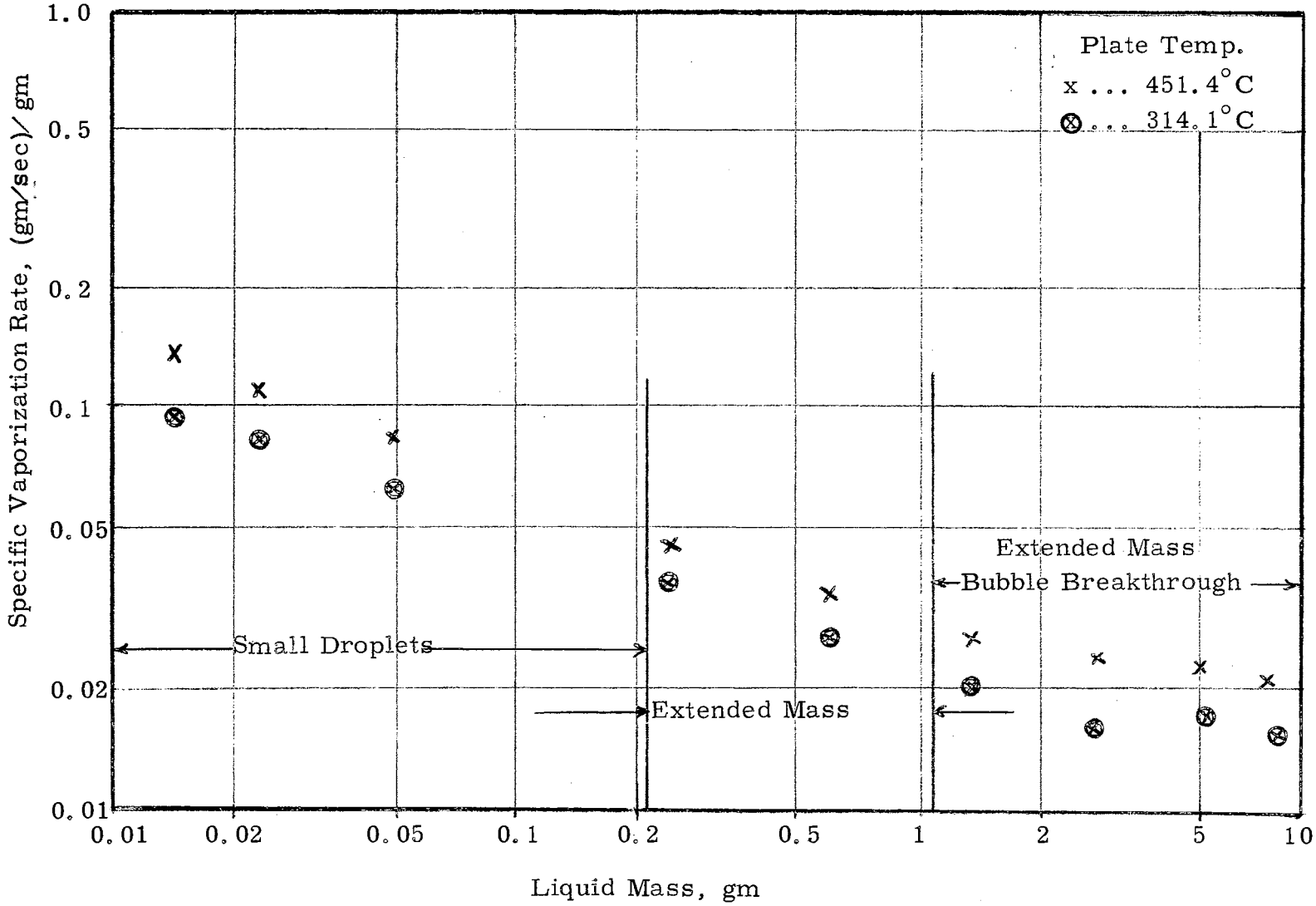

Figure 17. Specific Vaporization Rate Vs Liquid Mass
Ethanol

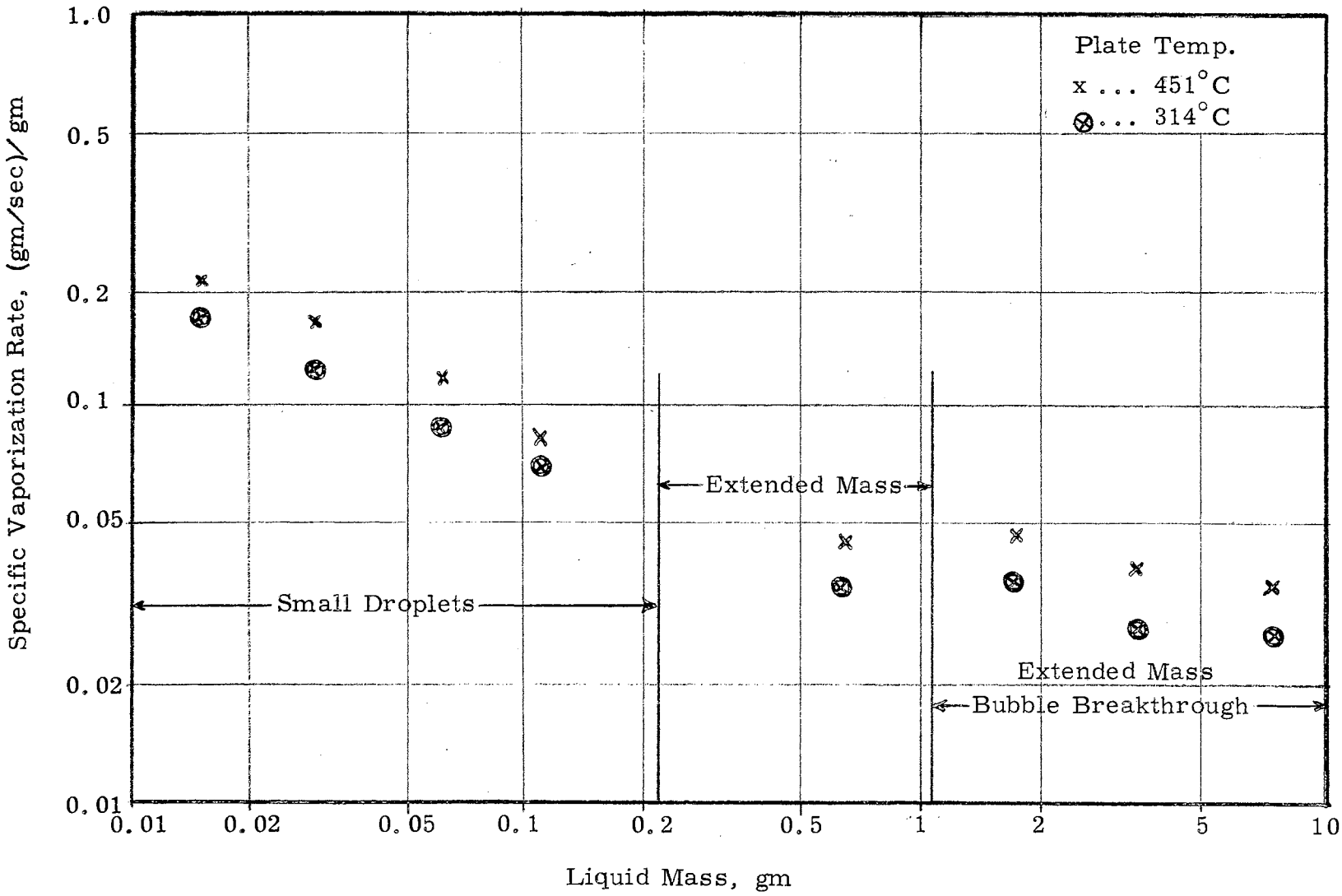

Figure 18. Specific Vaporization Rate Vs Liquid Mass
Benzene

up the relationships among the regimes of small droplets and extended liquid masses. These regimes of liquid masses are marked as shown in Figures 15, 16, 17 and 18. Small droplets of 0.05, 0.1 and 0.15 ml liquid are nearly spherical and there is no sign of bubble formation. For the range of 0.15 to 2 ml of water, the shape changes slowly from almost spherical to elliptical. For the range of 0.15 to 1 ml of organic liquids (ethanol, benzene, and carbon tetrachloride), the shape changes slowly from almost spherical to elliptical. For these ranges (0.15 ml to 1 ml of organic liquids and 0.15 to 2 ml of water), there is no bubble formation in liquid masses. Above 1 ml for organic liquids, and 2 ml for water, the shape changes slowly from elliptical to eventually flat. Bubble break through was observed at about 2.7 ml of water and at about 1.2 ml with ethanol, carbon tetrachloride and benzene.

Sources of Experimental Error in Vaporization Time Study

Errors in vaporization time and/or temperature measurements fall within several categories including human errors and systematic errors. Human errors result from situations where judgement is required in making decisions such as determining total vaporization time or making potentiometer readings. This human error was reduced by making the same run by more than one individual. The agreement between Lee and Patel for total vaporization time was found to be within ± 1 percent of the total vaporization time. Aside from human error, systematic errors may arise from the thermocouples. The calibration results of the thermocouples in absolute units show deviation

from mean less than 0.12 mv (0.13°C) as shown in Appendix A.

For 0.05, 0.1 and 0.15 ml liquid masses, the calibrations of the microliter syringes show a maximum 2 percent mean deviation from mean values as shown in Appendix B. For larger masses (1 to 10 ml), the pipette calibrations shown about 2 or 3 percent deviation from mean values as shown in Appendix B. The delivery time of extended masses from pipette or microliter syringe on hot plate was at most 20 seconds and as low as 4 seconds.

CHAPTER IV

EXPERIMENTAL STUDY OF BREAKTHROUGH DYNAMICS

Limitations of vision in the study of bubble breakthrough phenomena established the need for high-speed photography. Seeing a phenomenon stopped or slowed down can be a great aid to understanding it. Because boiling is a dynamic occurrence, motion pictures are preferable to still photographs.

Normal-speed movies (16 or 24 frames per second) are interesting and helpful (12, 14), but such films show blurred action to the analyst. From the knowledge of photographic work of Drew and Mueller (14), Jakob (23, 22) and several early investigators (41, 15, 39, and 18), Westwater and co-workers (34, 43) took motion pictures varying from 2000 to 3000 pictures per second in pool boiling.

Borishansky (6) took a few still photographs of extended masses on a brass plate in film boiling. The still photographs could be considered representative of the extended masses in boiling at one point in time. Still photographs provide no time coordinate to study average bubble growth and frequency. Therefore, it was the purpose of this experimental work to gain quantitative data of bubble growth rate and period from high-speed motion pictures. The experimental apparatus and procedure will be discussed below.

Apparatus

The photographic assembly shown in Figure 19, mainly consists

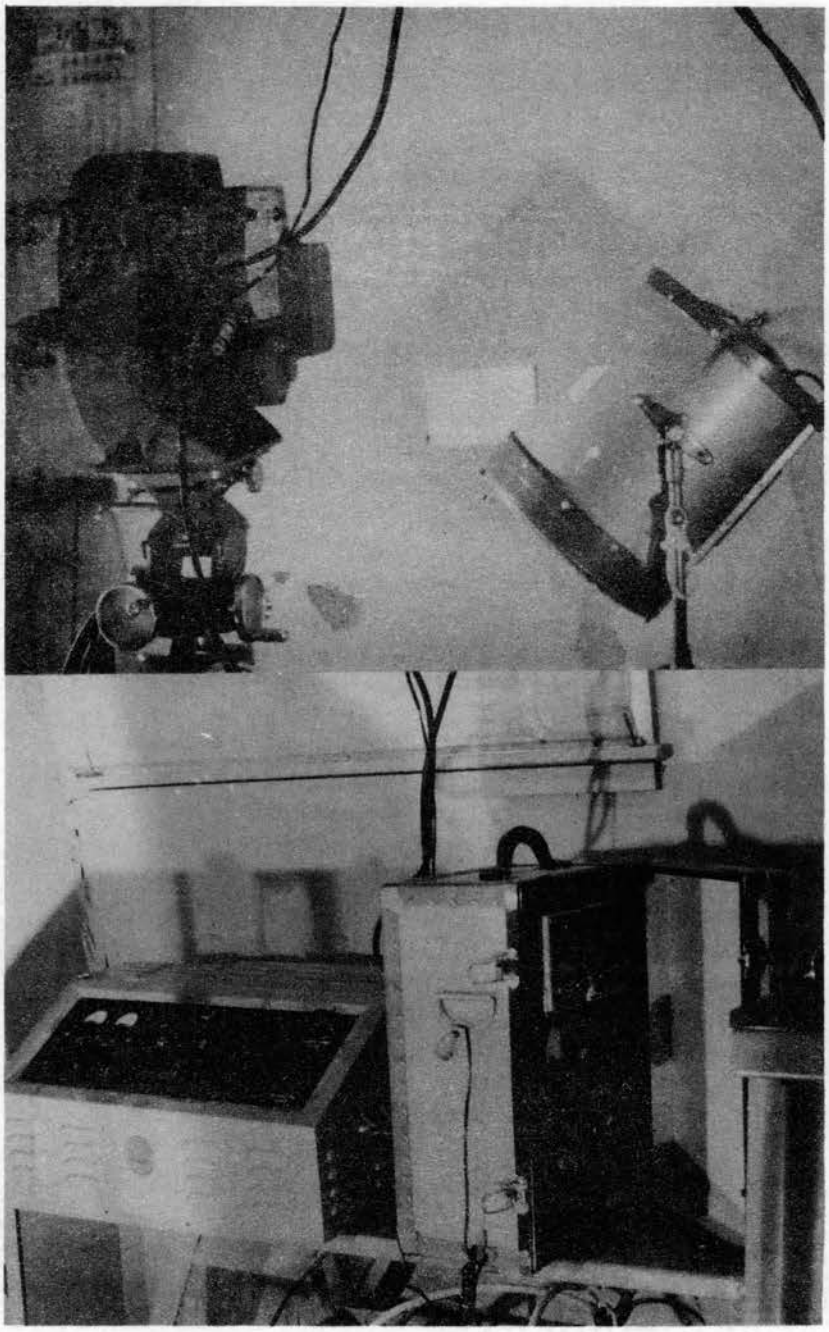

Figure 19. Photographic Apparatus for High-Speed Motion Pictures.

of (top figure from left) camera, xenon lamp, (bottom figure from left) xenon lamp control unit and a Goose control unit for the camera. This apparatus, except the high-intensity xenon lamp, was manufactured by Wollensak Optical Company, Rochester. The high-intensity xenon lamp was manufactured by Mole-Richardson England Ltd. Company and marketed in this country by the Wollensak Optical Company. For a detailed description of the basic principles of photographic apparatus, the reader is referred to the excellent books by Hyzer (21), Chesterman (11) and Jones (24). However, a brief description is included in Appendix E of this dissertation to acquaint the reader with the various photographic components used here.

Photographic Set-up

The arrangement of photographic apparatus is shown in Figure 20. The plate together with heating unit was supported by two asbestos insulating plates which were constructed such that the level of the heating unit was adjustable. This assembly was kept on the floor.

The camera was set on a tripod fastened to the floor. The camera was then set vertically to view the entire surface of the plate. The vertical distance from plate center to lens was about 42 inches.

The xenon lamp head was oriented at 45° to the plane of the plate. The center-to-center distance of plate and front xenon lamp head was about 58 inches. The xenon lamp was connected by insulated cable to the lamp control unit which was connected to the batteries.

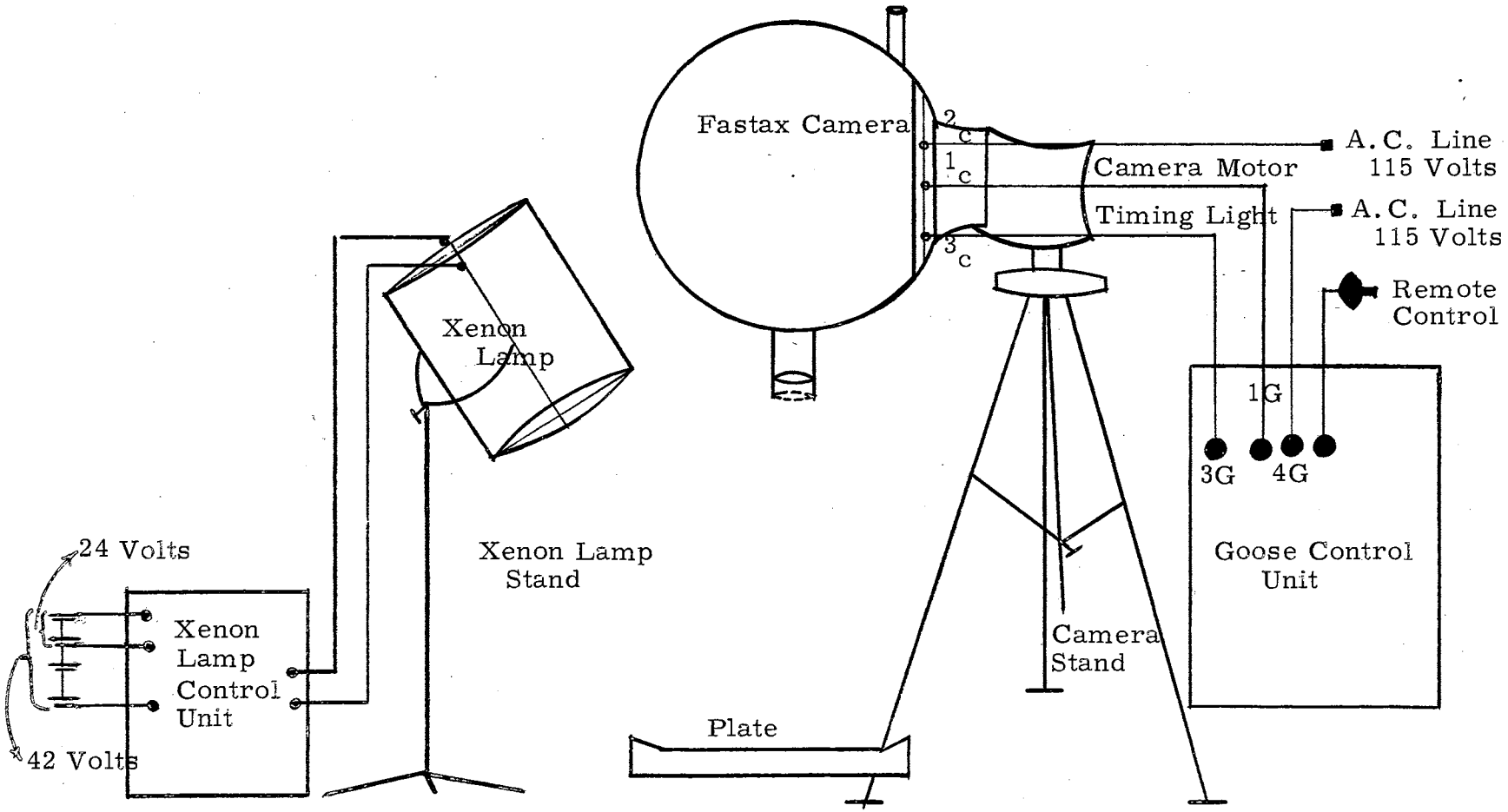

Figure 20. Arrangement of Equipment for High-Speed Motion Photography

Experimental Procedure

Development of experimental technique with the high-speed motion picture camera was a trial and error procedure. The initial problem, in this respect, was the selection of the right speed to arrest the motion of bubble breakthrough. A number of camera speeds were tried before one was selected. Films were taken at 500 and 1000 pictures per second with D.C. current from a Fastax WF-300A rectifier. The WF-300A is a D.C. power supply designated to operate the Fastax camera over the slow speed range. These pictures were blurred. A speed of 2000-2800 pictures per second was found to be satisfactory by using the Goose control unit with camera.

The stainless steel surface was given a surface finish with No. 0 emery paper, cleaned with distilled water and the horizontal level of the heating plate was adjusted. The Variac was turned on and the plate allowed to warm up, requiring about two hours to reach steady state. While the plate was warming up, the camera was lubricated and adjusted.

The camera was mounted properly on the tripod set so that the optical axis was vertical and centered over the test surface.

The camera was checked after the sprocket index mark was aligned with the plate index mark. The distance between the subject and focal plane was measured and the focal length of the lens adjusted. The camera was loaded with unexposed film and the door was closed.

The xenon lamp was adjusted on its stand. The distance measured from lamp-subject was about 58 inches. All necessary connections

(Appendix E) between xenon lamp and xenon control unit were checked and tested for proper operation. Brightness of 13,000 foot candles on the plate was measured by the Wollensak light meter and final adjustment of aperture opening was done on the camera lens. The aperture opening calculation was done from the light strength in foot candles, ASA speed index number of film and camera speed. The sample calculation is included in Appendix E.

All the necessary connections were made for the Goose control and camera. The Goose control was energized by connecting the 120 volt 60 cycle A.C. line circuit into the Goose line receptacle. When the toggle switch below the Goose line receptacle was thrown to the "ON" position, the neon lamp above the "A.C. LINE" receptacle was energized. This indicated that the unit was receiving power. The master control switch on the camera was turned to "ON" position. The indicator light on the camera went on if all connections were in working order. The master switch of the camera was turned "OFF".

The plate temperatures were recorded. A measured ceramic scale was placed on the edge of the plate as a reference scale for calculations. The dimensions of the scale were 1 15/32 inch in width, 23/32 inch depth and 15/64 inch thick.

The approximate amount of film on the spool was read from the film indicator. The operating voltage for the camera motor was chosen from the speed curve provided by Wollensak (45). Then the desired voltage of the camera motor was set on the Goose unit. With the voltmeter toggle switch in the "CAMERA" position, the camera voltage was read from the voltmeter. Then the desired

running time (calculated from film length and camera speed) was set on the camera timer which was located on the front panel of the Goose unit.

The master switch of camera was set on "ON" position. The cycle switch of camera was set at "START" position and the door of the Goose control unit was checked to make sure that the interlock was closed. The xenon lamps on both camera and the Goose unit were checked to be sure that they were energized. The selector switch of the xenon control unit was set at 5-KW to get pulse light for 5 seconds. The main switch of the xenon control was kept at "ON" position and the "STRIKE" button pressed. Striking of the lamp was indicated by an ammeter reading of 37 amperes. The reset button on the xenon lamp control unit was pressed immediately after pressing the strike button. In the meantime, 10 ml of liquid was placed on the test area of hot plate within 20 seconds.

The flash button of the xenon lamp control unit was pressed. The operation of camera was initiated by a push-button which closed the start circuit electrically. For 100 feet of film, the pictures were taken usually within 2.3 seconds at a nominal 2750 pictures per second. The film was developed by employing a continuous film processor as discussed in Appendix E.

Film Analysis

The projector employed for the analysis of all reels of film was an Eastman Kodak Film Projector and Library Film Reader Model C. The reader consists of a film projector, mirror and

24- by 24-inch viewing screen. In use, the film was loaded into the projector on the translucent screen. The film was transported manually in either forward or in reverse direction by turning the knob.

A standard 16-mm motion picture projector was used to project the film several times at 16 frames per second to acquaint the analyst with the major features of the boiling action. Thus, the preliminary visual observations permitted the analyst to select the sequence of frames to be more carefully analysed. This speed gave a slowdown in the action by a factor of about 140 to 1. The film was then projected one frame at a time, using a stop-action projector. Bubble period was determined by finding, in the motion pictures, a number of instances for which several bubbles in succession appeared at the same position.

The bubble breakoff diameter, projected area and bubble spacing were measured on the film reader. A planimeter was used to measure the projected area. A standard 6 inch metal rule graduated to 1/64 inch was used to measured breakoff diameter of vapor bubble and center-to-center distance of vapor bubbles. Twenty or more measurements were made for each reel of film. The sample calculations are included in Appendix E.

Results and Discussion

High-speed motion pictures were taken at a nominal 2750 pictures per second. This speed was obtained by applying 90 volts to the camera motor. The actual speed was determined from the timer marks which were exposed at the edge of film. The timer

marks showed that about one-third of a reel of film was run during acceleration and that the last two-thirds of the reel ran at constant speed. The constant-speed portions were used for quantitative bubble measurements. The high-speed motion picture (2) is available to interested persons, upon request.

Figures 21 and 22 show some selected frames from the motion pictures of extended masses on a hot plate. Also, a corresponding line sketches are shown with the positions of bubbles indicated.

The photograph marked as "a" in Figure 21 is for water at 307°C plate temperature. One big bubble (dotted) is almost completely grown but has not broken through whereas the second tiny bubble represents the initial growth stage of bubble. The shape of liquid is irregular. The volume (10 ml) of water covers a smaller area than the same volume of other liquids because the surface tension of water is higher than for the other liquids in this work. The picture was taken at 2400 frames per second.

The photograph marked as "b" in Figure 21 is for carbon tetrachloride at 185°C plate temperature. There are about nine or ten bubbles. The mass of liquid is essentially flat. There is no regularity in bubble orientation. The bubble shape is irregular. The picture was taken at 2400 frames per second.

The photograph marked as "a" in Figure 22 is for benzene at 184°C plate temperature. There are five or six bubbles. One of these bubbles has completely broken through the liquid and the steel plate is visible. Again, the bubble spacing and shape of liquid are irregular. The picture was taken at 2160 frames per second.

The photograph marked as "b" in Figure 22 is for ethanol at 183.5°C plate temperature. There are five or

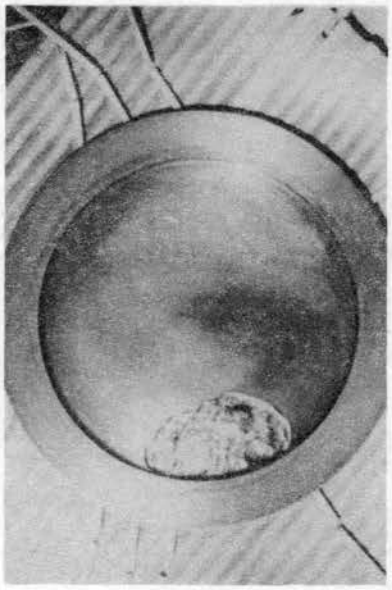

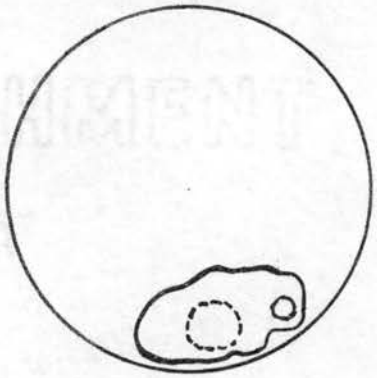

(a) Water
Volume 10 ml
Plate Temperature 307 C
2400 Pictures per second

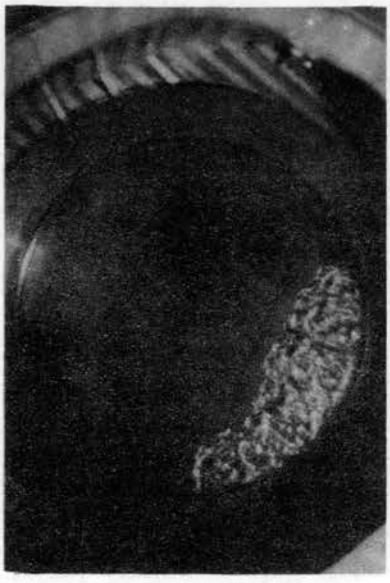

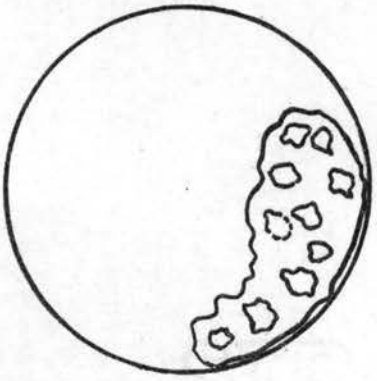

(b) Carbon Tetrachloride
Volume 10 ml
Plate Temperature 185 C
2400 Pictures per second

Figure 21. Photographs of Water and Carbon Tetrachloride as Extended Masses at the Leidenfrost Point.

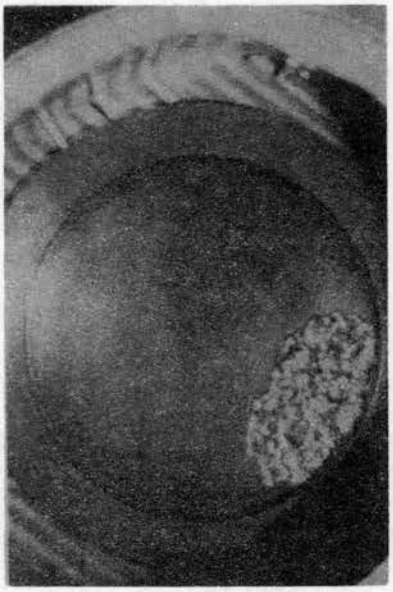

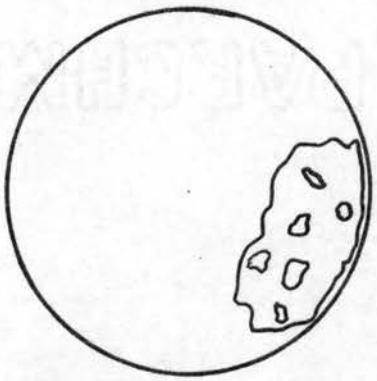

(a) Benzene
Volume 10 ml
Plate Temperature 184 C
2100 Pictures per second

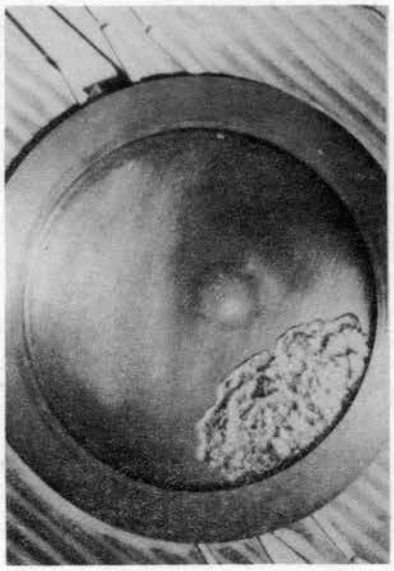

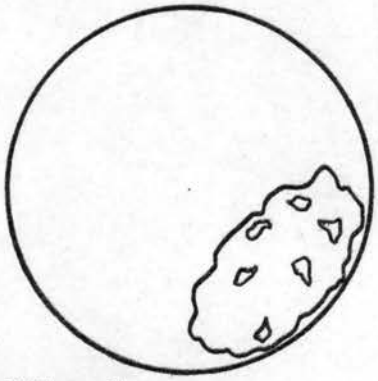

(b) Ethanol
Volume 10 ml
Plate Temperature 183 C
2280 Pictures per second

Figure 22. Photographs of Benzene and Ethanol as Extended Masses at the Leidenfrost Point.

six bubbles. The shape of liquid and the spacing are irregular. The picture was taken at 2280 frames per second The mass of liquid is essentially flat. There is no regularity in bubble orientation.

The quantitative bubble measurements are summarized in Table II and Table III. The center-to-center distance was determined by measuring the distance between adjacent bubbles and then adding this averaged distance to the mean value of the bubble breakoff diameter. The bubble diameter at maximum size is the average of several measurements. Usually, twenty or more measurements were made for each reel of film for each liquid. The bubble diameters at breakoff are in fair agreement with Zuber's predicted values from the most dangerous wavelength as shown in Table II and Table III. Zuber assumed that the bubble diameter at breakoff is equal to a half-wavelength. Berenson's equation predicts low values of the bubble diameter at breakoff. Berenson assumed that the bubble diameter at breakoff is equal to three-fourths of the critical wavelength. Chang's Equation II-8 predicts a very short bubble period and his method does not give realistic values as shown by Tables II and III. Zuber's Equations II-10 to II-13 predict low values of bubble period, but Zuber's Equation II-14 gives rather high predictions for the bubble period as shown in Tables II and III. For Equation II-14, Zuber assumed that the average velocity of the rising bubble is equal to the asymptotic growth rate of the wave amplitude, the wavelength is λ_c, and bubble release is on a close-packed square pattern.

Table III shows the summary of bubble measurements from

TABLE II

SUMMARY OF BUBBLE MEASUREMENTS AT THE LEIDENFROST POINT FOR EXTENDED LIQUID MASSES

	Water	Ethanol	Benzene	Carbon Tetrachloride
Temp. Difference, °C	207	105	104	108
Volume of liquid, ml	10	10	10	10
Measured speed, Pictures per second	2400	2280	2160	2400
Measured liquid projected area, cm^2	22.32	33.91	29.01	38.17
No. of bubbles	1 or 2	6 or 7	6 or 7	9 or 10
Measured projected area of bubble, cm^2				
Maximum	3.11	1.09	0.94	0.89
Average	2.37	0.91	0.90	0.82
Minimum	1.98	0.89	0.87	0.46
Bubble diameter at breakoff, cm				
Maximum	1.59	0.88	0.80	0.79
Average	1.43	0.76	0.73	0.75
Minimum	1.13	0.54	0.49	0.63
Zuber, calculated $0.5\ \lambda_c$	0.79	0.48	0.51	0.38
Zuber, calculated $0.5\ \lambda_d$	1.36	0.83	0.89	0.66
Berenson, calculated $0.75\ \lambda_c$	1.18	0.74	0.77	0.56
Center-to-center distance between two adjacent bubbles, cm				
Maximum	2.69	1.58	1.52	1.49
Average	2.27	1.37	1.38	1.30
Minimum	1.78	1.12	1.11	1.15
Calculated, Eq. II-5	1.57	0.96	1.03	0.76

TABLE II
(Continued)

	Water	Ethanol	Benzene	Carbon Tetrachloride
Calculated, Eq. II-6	2.726	1.65	1.77	1.31
Bubble period, sec				
Maximum	0.26	0.16	0.15	0.14
Average	0.16	0.13	0.12	0.12
Minimum	0.12	0.098	0.086	0.074
Chang, Eq. II-8	4.64×10^{-4}	6.69×10^{-4}	5.09×10^{-4}	5.48×10^{-4}
Zuber, Eq. II-10	0.061	0.040	0.049	0.053
Zuber, Eq. II-11	0.079	0.053	0.064	0.057
Zuber, Eq. II-12	0.065	0.044	0.052	0.047
Zuber, Eq. II-13	0.12	0.077	0.095	0.080
Zuber, Eq. II-14	0.29	0.17	0.21	0.18

TABLE III

SUMMARY OF BUBBLE MEASUREMENTS AT HIGH TEMPERATURE FOR EXTENDED MASSES

	Water	Ethanol	Benzene	Carbon Tetrachloride
Temp. difference, °C	396	415.5	414.5	417.2
Approx. volume of liquid, ml	10	10	10	10
Measured speed, Pictures per second	2040	2280	2280	2160
Measured liquid projected area. cm^2	19.86	28.11	27.68	32.36
No. of bubbles	3 or 4	13 or 14	12 or 13	16 or 17
Measured projected area of bubble, cm^2				
Maximum	2.89	0.98	0.91	0.90
Average	2.31	0.86	0.79	0.81
Minimum	1.85	0.81	0.80	0.54
Bubble diameter at breakoff, cm				
Maximum	1.64	0.85	0.79	0.76
Average	1.50	0.78	0.72	0.69
Minimum	1.17	0.71	0.63	0.62
Zuber, calculated $0.5\lambda_c$	0.79	0.48	0.51	0.38
Zuber, calculated $0.5\lambda_d$	1.36	0.83	0.89	0.66
Berenson, calculated $0.75\lambda_c$	1.18	0.74	0.77	0.56
Center-to-center distance between two adjacent bubbles, cm				
Maximum	2.33	1.38	1.32	1.17
Average	2.08	1.29	1.25	1.02
Minimum	1.97	1.03	0.98	0.84

TABLE III
(Continued)

	Water	Ethanol	Benzene	Carbon Tetrachloride
Calculated, Eq. II-5	1.57	0.96	1.03	0.76
Calculated, Eq. II-6	2.73	1.65	1.77	1.31
Bubble period, sec				
Maximum	0.24	0.14	0.12	0.11
Average	0.17	0.12	0.10	0.097
Minimum	0.10	0.098	0.072	0.063
Chang, Eq. II-8	3.75×10^{-4}	4.08×10^{-4}	3.11×10^{-4}	3.14×10^{-4}
Zuber, Eq. II-10	0.061	0.040	0.048	0.051
Zuber, Eq. II-11	0.077	0.052	0.063	0.055
Zuber, Eq. II-12	0.065	0.042	0.051	0.046
Zuber, Eq. II-13	0.12	0.075	0.092	0.078
Zuber, Eq. II-14	0.27	0.16	0.19	0.15

high-speed motion pictures at high plate temperature. The number of bubbles increases as shown in Tables II and III. The bubble diameter at breakoff and bubble projected area remain practically constant. From Table II and III, the bubble periods are shorter at high temperature than the bubble period at the Leidenfrost point.

Table IV shows the comparison of bubble diameter at breakoff, center-to-center spacing and bubble period of water which were obtained by Hosler and Westwater for a completely submerged surface in film boiling and for extended (water) masses in this work. The agreement between the average values of bubble measurements in both experimental studies is reasonably good. Hosler and Westwater used a 5.3 cm depth of water, whereas in this work, the depth of water was about 0.5 cm, the mass of water was moving freely on the test area, and some vapor was escaping from the edge of masses.

Figures 23, 24, 25 and 26 compare film boiling coefficients. The experimental heat transfer coefficient over the size range 8-10 ml only was calculated from Equation IV-1 (with radiation) and Equation IV-2 (without radiation). Equation IV-1 (with radiation), and Equation IV-2 (without radiation) are shown below.

$$h = \frac{(V_{10} - V_8)(\rho_\ell)(\frac{1}{2} C_v \Delta T + L)}{A_\rho \Delta T (\tau_{10} - \tau_8)} \qquad \text{IV-1}$$

and

$$h = \frac{(V_{10} - V_8)(\rho_\ell)(\frac{1}{2} C_v \Delta T + L)}{A_\rho \Delta T (\tau_{10} - \tau_8)} - \frac{\sigma_c (T_{\rho k}^4 - T_{\rho s}^4)}{(\frac{1}{\epsilon} + \frac{1}{\alpha} - 1)(T_\rho - T_s)} \qquad \text{IV-2}$$

TABLE IV

COMPARISON OF WATER VAPOR BUBBLE MEASUREMENTS OF EXTENDED MASSES AND SUBMERGED SURFACES

	Experimental Data (Hosler & Westwater)	Experimental Data (10 ml of Liquid) (Author)
Temp. difference, °C	148	207
Camera speed, p.p.s.	2000	2400
Diameter at breakoff, cm		
Maximum	2.36	1.59
Average	1.68	1.43
Minimum	1.49	1.13
Center-to-center spacing, cm		
Maximum	4.19	2.69
Average	2.46	2.28
Minimum	1.53	1.78
Bubble period, sec		
Maximum	0.31	0.264
Average	0.20	0.162
Minimum	0.11	0.122

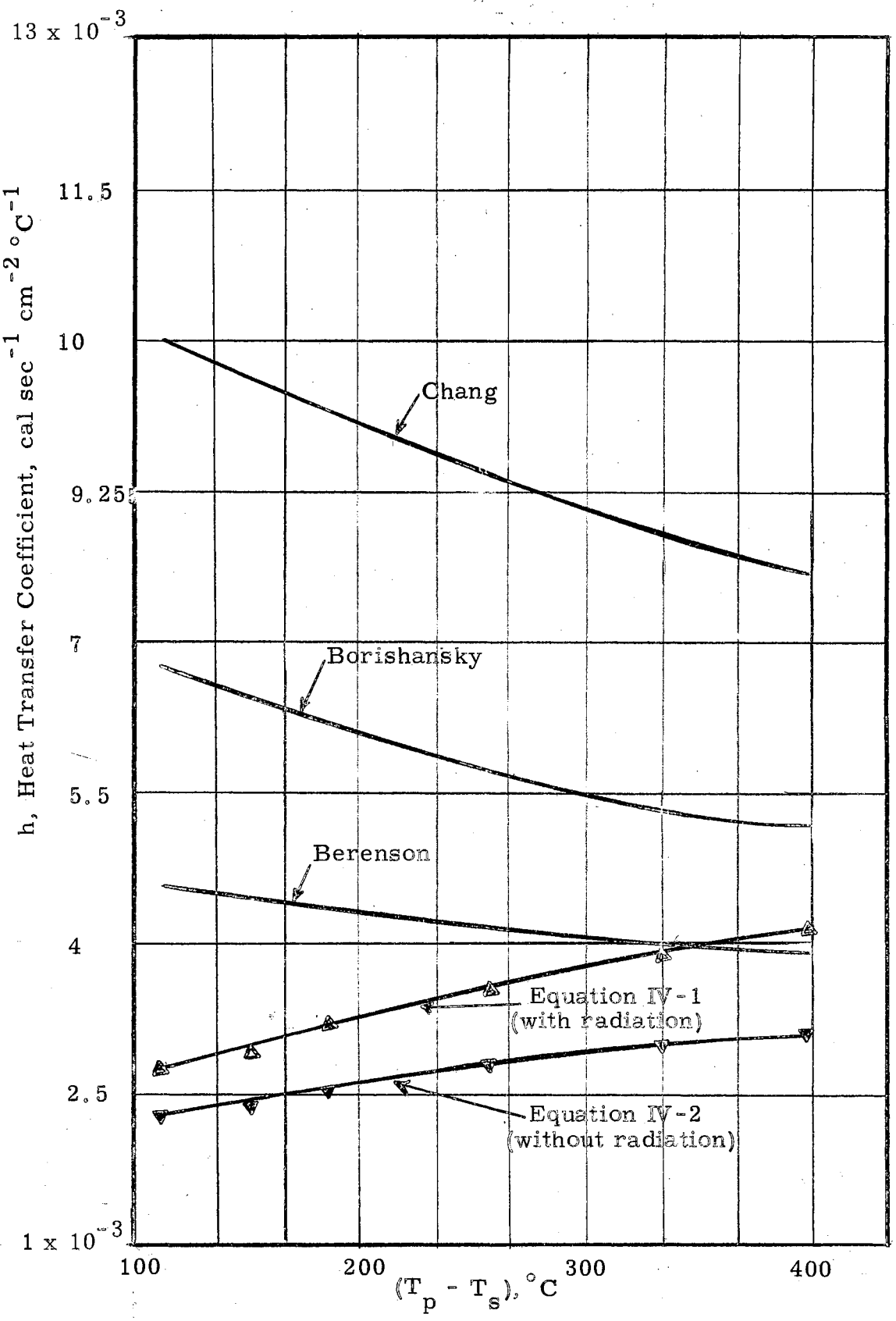

Figure 23. Heat Transfer Coefficient of Water Vs Temp. Difference

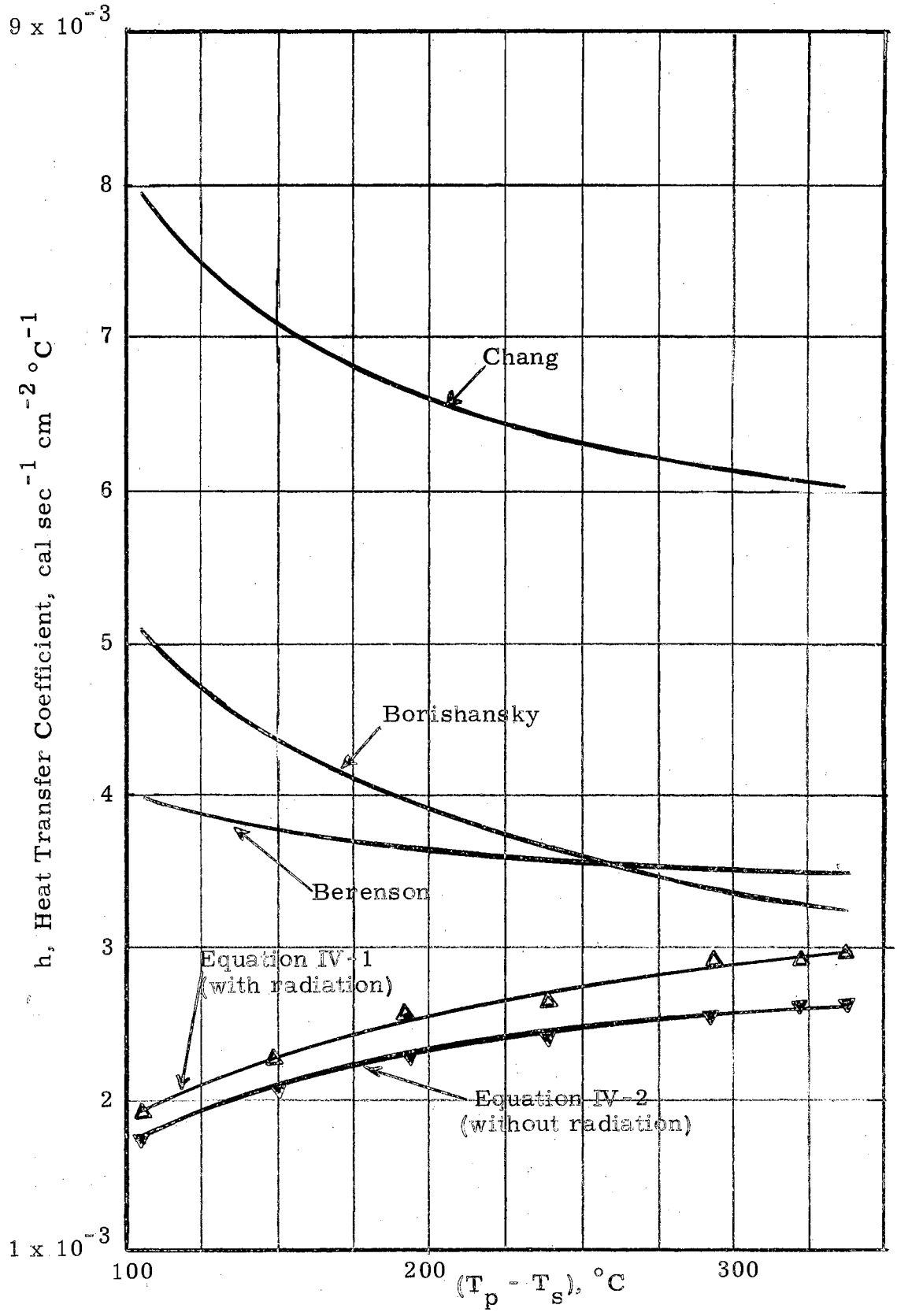

Figure 24. Heat Transfer Coefficient of Ethanol Vs Temp. Difference

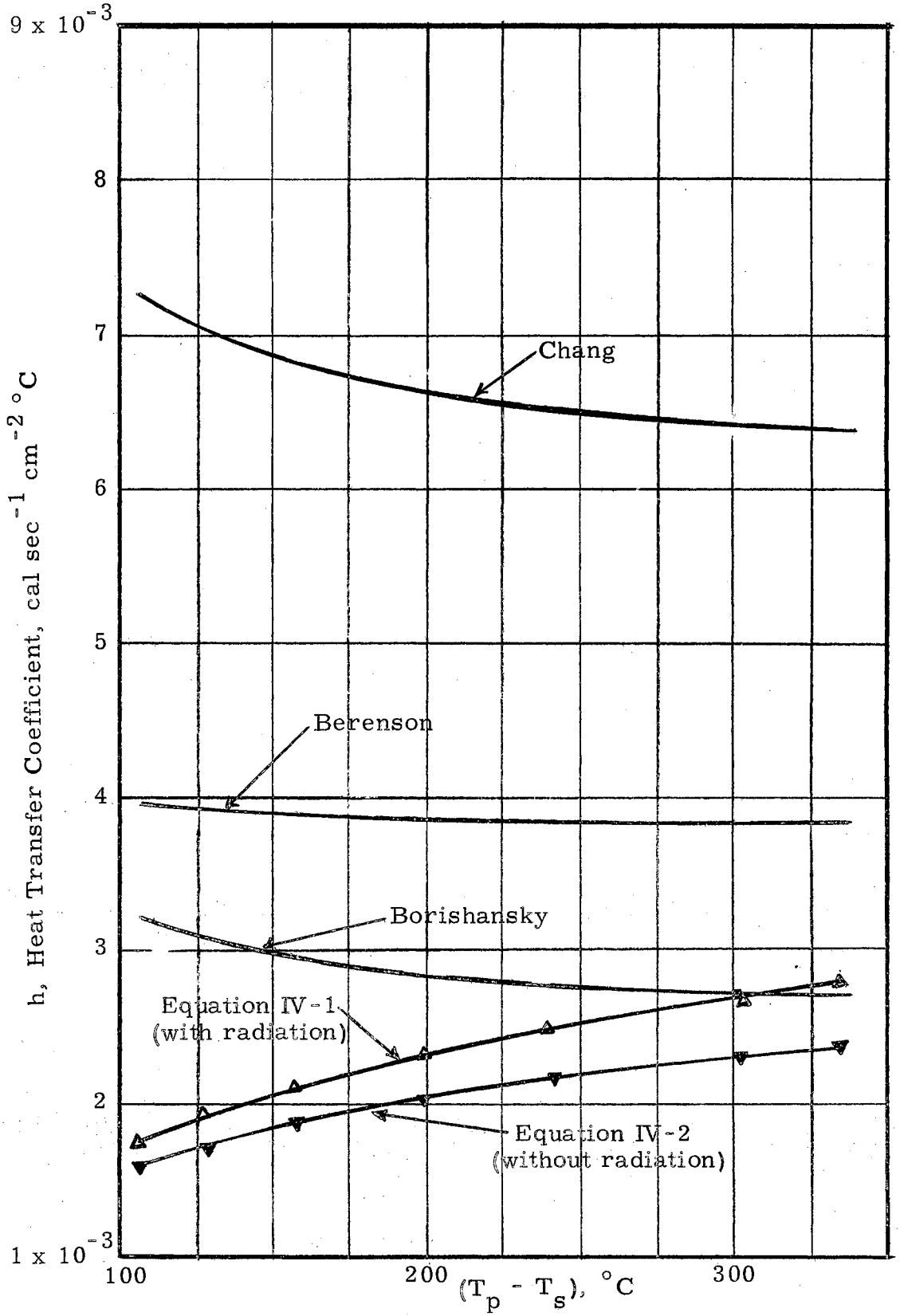

Figure 25. Heat Transfer Coefficient of Benzene Vs Temp. Difference

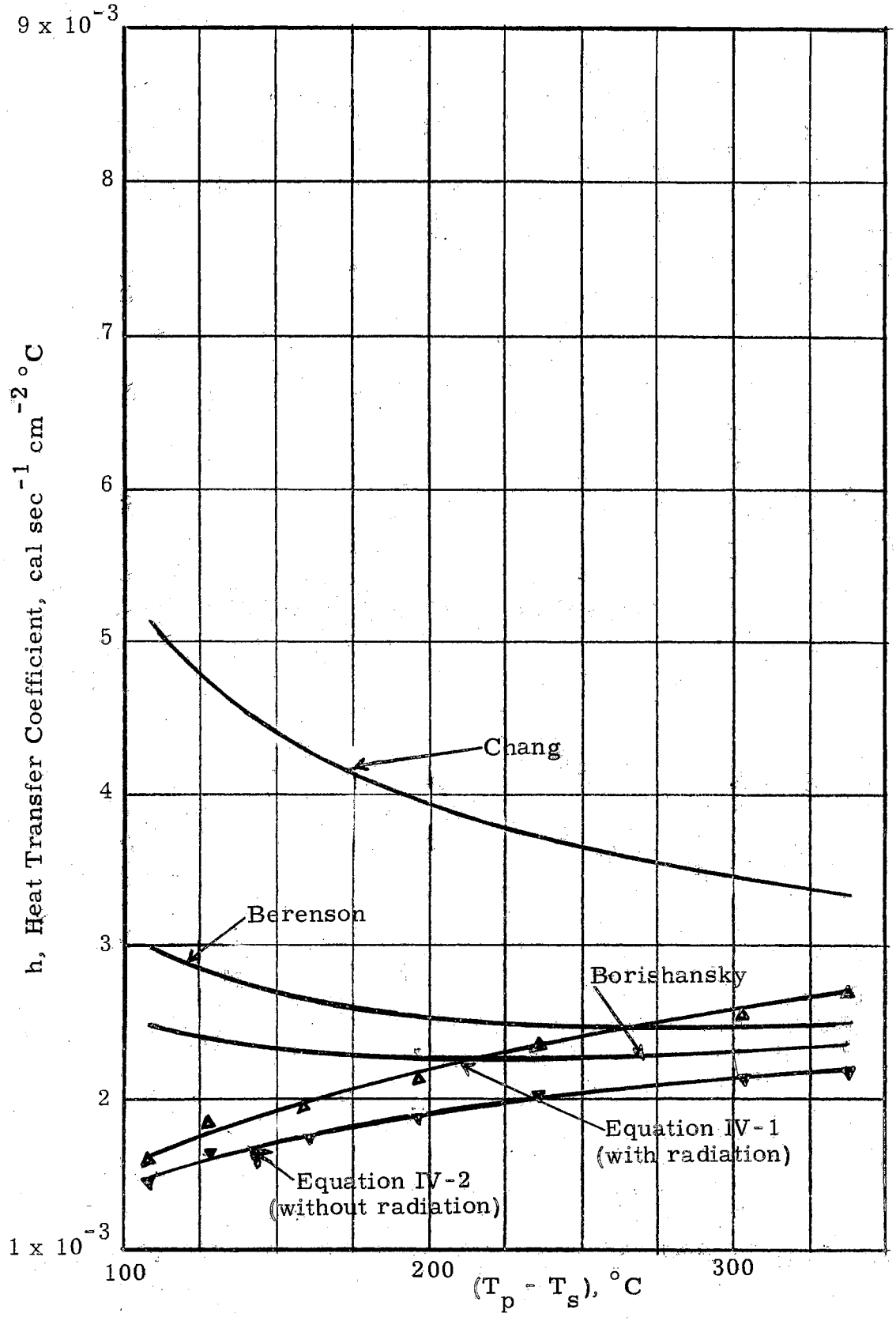

Figure 26. Heat Transfer Coefficient of CCl_4 Vs Temp. Difference

where

$V_{10} - V_8$ is the difference between volumes at 10 and 8 ml liquid.

$\tau_{10} - \tau_8$ is the difference between total vaporization times for 10 and 8 ml liquid.

A_p is the average liquid projected areas for 10 and 8 ml liquid masses and calculated from Figures 13 through 15.

$\Delta T = T_p - T_s$ is the temperature difference between plate and saturated liquid, ^oC.

T_{pk} is the plate temperature, ^oK.

T_{ps} is the saturated liquid temperature, ^oK.

σ_c is the Stefan-Boltzmann constant (1.352×10^{-12} cal/sec cm^2 $^oK^4$

ϵ is the emissivity of the hot plate (steel = 0.73 (13)).

α is the absorptivity of the cold liquid (usually unity).

L is the heat of vaporization of liquid, cal/gm.

It is important to note the $\frac{1}{2}C_v \Delta T + L = C_v(\frac{T_p - T_s}{2} - T_s) + L =$ $\frac{C_v}{2}(T_p - T_s) + L$ in Equations IV-1 and IV-2 represents the superheat, L'. It is assumed that the vapor temperature, T_v is equal to the average value of plate temperature and saturated temperature of liquid.

The sample calculations of heat transfer coefficients for extended liquid masses are included in Appendix F. Chang's prediction, Equation II-7, is not good. His equation gives heat transfer coefficients a factor of three higher than that of liquids in this work. Also, the curve predicted by Chang's equation is about 50 percent higher than the curves predicted by Borishansky's equation. In Figures 23

to 26, the experimental curves (with radiation) of heat transfer coefficients show a slight increase as the temperature difference increases and cross the curves (except of Figures 23 and 24) of heat transfer coefficients predicted by Borishansky's equation. At high temperature, Equation IV-2 (without radiation) gives heat transfer coefficients about 25 percent lower than that of Equation IV-1 (with radiation).

None of the correlations is in agreement with the curve of experimental heat transfer coefficients. As a matter of fact, Borishansky's correlation should show agreement with the present experimental curve of heat transfer coefficients of liquids since Borishansky's correlation was obtained from the measurements of change of volume of extended masses. The reason for the discrepancy may be that he employed a volume change and range of volume different from the values of this work; hence the relative loss of vapor from the edges of the masses is different. The second reason could be that Borishansky used a greater liquid thickness and hence smaller heat transfer area in his calculations compared to the results of this work. Borishansky used 34 ml as initial volume, about 23 ml as final volume and about 0.75 cm as thickness of liquid for the purpose of deriving the dimensional correlation to predict heat transfer coefficients. In this work, the change of volume was from 10 to 8 ml of liquid and the thicknesses of extended masses are shown in Figures 12 through 14.

A calculation of the heat transfer coefficient using only the bubble measurements of Tables II and Table III can be carried out (Equation IV-3):

$$h = V_B f n_d \rho_v (L + \frac{1}{2} C_v \Delta T)_{/\Delta T} \quad \text{IV-3}$$

where

V_B = Bubble volume (the bubbles are assumed to be spheres).

f = Frequency of bubbles, $^{1}/_{sec}$

$n_d = \frac{n_B}{A\rho}$ Total number of bubbles per unit projected area.

ρ_v = Mean vapor density, $^{gm}/_{cm^3}$

Equation IV-3 can be approximately corrected to include vapor loss from the outer periphery by multiplying the h given by Equation IV-3 by a factor $(U_o + U_i)/U_i$

where $U_i = \sum_{\text{bubbles}} (\pi)$ (bubble diameter)

U_o = Outer perimeter of the liquid mass

Table V shows the comparison between heat transfer coefficients by Equation IV-1, Equation IV-2, Equation IV-3 and h corrected from Equation IV-3. The heat transfer coefficients from bubble measurements are calculated by assuming that the bubbles are spheres. The agreement with the values of heat transfer coefficients of Table V is quite good considering the gross assumptions made.

Table VI shows the comparison between experimental and calculated values of the Leidenfrost temperature of small droplets, extended masses and a submerged surface. Berenson derived Equation II-16 to predict the minimum temperature difference (Leidenfrost point) in pool film boiling. Berenson's equation predicts low values of the minimum temperature difference and his prediction is seriously in error for the present case as shown in Table VI. From Table VI, note the experimental Leidenfrost points of water and carbon tetrachloride for submerged surfaces are lower than the experimental Leidenfrost points of either extended masses or small droplets. A possible

TABLE V

COMPARISON BETWEEN HEAT TRANSFER COEFFICIENTS FROM EQUATIONS IV-1, IV-2, IV-3 AND h CORRECTED FROM EQ. IV-3

Liquids	$(\Delta T)^{\circ}C$	$h \times 10^{-3}$, $cal/sec\text{-}cm^2\text{-}^{\circ}C$		$h \times 10^{-3}$, $cal/sec\text{-}cm^2\text{-}^{\circ}C$	
		Eq. IV-1 with radiation	Eq. IV-2 without radiation	Eq. IV-3	Corrected from Eq. IV-3 for entire mass
Water	207	2.77	2.32	1.16	4.47
	396	4.18	3.28	1.79	3.94
Ethanol	105	2.39	2.11	1.57	5.33
	415	3.84	3.06	2.31	4.78
Benzene	104	2.08	1.72	1.06	3.31
	415	3.98	3.19	2.54	5.27
Carbon Tetrachloride	108	1.86	1.58	1.39	3.96
	416	3.75	2.97	1.93	4.14

TABLE VI

COMPARISON OF EXPERIMENTAL AND CALCULATED LEIDENFROST POINTS

	Water	Benzene	Ethanol	Carbon Tetrachloride
Small Droplets				
Experimental****	180	105	100	95
Calculated, Eq. II-16	76.7	85.6	79.8	88.7
Extended Liquid Masses				
Experimental***	200	104	105	108
Calculated, Eq. II-16	76.7	85.6	79.8	88.7
A Pool of Liquid				
Experimental	158**	. . .	. . .	80.6*
Calculated, Eq. II-16	76.7	. . .	. . .	88.7

**** Lee (28)

*** Patel

** Hosler and Westwater (20)

* Berenson (4)

explanation for this is given in the discussion of Borishansky's results in Chapter III.

Sources of Experimental Error in Bubble Dynamics Study

The greatest source of variations between experiments and between experiment and theory is that boiling phenomena are very variable for reasons not completely understood and hence uncontrolable. There were several experimental shortcomings in the present study. The first was uncertainty in the volume of liquid on the plate at the time the camera started. The second class of experimental errors was in the measurement of the bubble breakoff diameters and bubble spacings, due to the irregular shape and lack of a sharp boundary. From the above errors, the accuracy of the analysis of bubble measurements from either still photographic work or high-speed motion pictures is very hard to assess. However, the data have been analysed statistically to estimate the 95 percent confidence levels on the mean.

A measure of the degree of spread of individual measurements about the mean is the standard deviation σ_k, defined by

$$\sigma_k = \sum_{i=1}^{i=N} \frac{(\bar{E} - E_i)^2}{N - 1} \quad \ldots\ldots\ldots\ldots \quad \text{IV-4}$$

where $\bar{E}$ = average value of observation

E_i = individual observation

N = number of observations.

The error of the mean σ_e, is given by

$$\sigma_e^2 = \frac{\sigma_k^2}{N} \quad \text{. . . . . IV-5}$$

The 95 percent confidence limit on the mean σ_ℓ is defined by

$$\sigma_\ell = \left[\begin{array}{l}\text{The value of Student's t 95 percent} \\ \text{probability for (N - 1) degrees of freedom}\end{array}\right] \sigma_e \quad \text{IV-6}$$

Table VII shows the summary of the values of Equations IV-4, IV-5 and IV-6 in the measurements of bubble breakoff diameter and bubble period of the extended masses at the Leidenfrost point. For example, the average value $\bar{E}$ of the 20 measurements of bubble breakoff diameter for water (Table F1 of Appendix F) is 1434×10^{-3} cm. The standard deviation (Equation IV-4) is $\pm 134 \times 10^{-3}$ cm and the error of the mean (Equation IV-5) is $\pm 30 \times 10^{-3}$ cm. The 95 percent confidence limits (Equation IV-6) are $\pm 63 \times 10^{-3}$ cm. The true value of the mean lies within the interval $(1434 \pm 63)\ 10^{-3}$ cm with 95 percent confidence.

TABLE VII

SUMMARY OF ERROR OF MEAN IN THE MEASUREMENTS OF THE BUBBLE BREAKOFF DIAMETER AND BUBBLE PERIOD AT THE LEIDENFROST POINT

Liquid	Average Value of Breakoff Diameter $\bar{E}$, cm	Standard Deviation of Mean σ_k, cm	Error of Mean σ_e, cm	95% Confidence Limits on Mean σ_ℓ, cm
Water	1434×10^{-3}	134×10^{-3}	30×10^{-3}	$\pm 63 \times 10^{-3}$
Ethanol	763×10^{-3}	127×10^{-3}	28×10^{-3}	$\pm 59 \times 10^{-3}$
Benzene	727×10^{-3}	113×10^{-3}	25×10^{-3}	$\pm 52 \times 10^{-3}$
Carbon Tetrachloride	746×10^{-3}	119×10^{-3}	28×10^{-3}	$\pm 58 \times 10^{-3}$

Liquid	Average Value of Bubble Period $\bar{E}$, cm	Standard Deviation of Mean σ_k, sec	Error of Mean σ_e, sec	95% Confidence Limits on Mean σ_ℓ, sec
Water	162×10^{-3}	41×10^{-3}	9.1×10^{-3}	$\pm 19 \times 10^{-3}$
Ethanol	132×10^{-3}	38×10^{-3}	8.5×10^{-3}	$\pm 17 \times 10^{-3}$
Benzene	127×10^{-3}	32×10^{-3}	7.2×10^{-3}	$\pm 15 \times 10^{-3}$
Carbon Tetrachloride	123×10^{-3}	30×10^{-3}	6.8×10^{-3}	$\pm 14 \times 10^{-3}$

CHAPTER V

THEORETICAL ANALYSIS OF VAPORIZATION TIME

One difficulty which arose when attempting to analyse vaporization time of extended masses in film boiling from a flat plate was the fact that the geometrical shape of extended masses was not exactly describable. Gottfried's or Lee's postulated analytical model for vaporization times of small droplets is based on several assumptions, including that the droplet is spherical. The volume of spherical droplets is equal to $(4/3)\pi r^3$, where r is the radius of droplet. This assumption made straightforward analytical work for the determination of the final evaporation rate equation for small droplets. Also, for small droplets, all vapor escapes from the edge of a droplet on a hot surface. Data of Table VIII (page 97) indicated that the analytical vaporization model of small droplets cannot apply to vaporization times of extended liquid masses.

For extended masses in film boiling, the vapor flow pattern on a flat plate was not so obvious. The geometrical shape for extended masses changes from a flat surface with constant height, to ellipsoidal and finally to spheroidal during the course of vaporization. It is practically impossible to define a specific zone for a given shape in extended masses. It was observed during vaporization of large masses that the vapor departs by two processes: 1) breakthrough of vapor bubbles and 2) vapor escape from the edge of liquid masses.

For this situation, the Taylor instability model seems quite promising. The basis for this approach is that film boiling from a flat plate facing up must result in a thin layer of vapor, underneath the liquid; as heat continues to flow, the vapor film over the horizontal surface will grow thicker until, at a certain thickness, instability will set in due to disturbances in the vapor-liquid interface and the interface will start to breakup, allowing the vapor to escape as bubbles.

The actual shape of the extended masses, and the physical model used in the analysis are shown in Figure 27. In the latter part of the analysis of the problem (after Equation V-10), the assumptions pertaining to the applicability of the Navier-Stokes equations for the bubble surrounded by a liquid mass as shown in diagram (page 83), are discussed in detail.

The part marked "a" in Figure 27 shows an extended liquid mass during and after breakthrough of bubbles at the liquid-vapor interface. One bubble grows as shown by "ag" of Figure 27a. The condition of a few milliseconds after bubble breakthrough is shown by "ab" of Figure 27a. Surfaces of extended masses are irregular in detail but flat in general. Figure 27b shows an idealized extended liquid mass supported by a layer of vapor with thickness δ on a hot plate. Part of the vapor forms a bubble of height H, and radius r_i. The radius of liquid mass is r_o. It is also shown in the extreme left part of Figure 27b that the vapor also escapes from the edge of the mass.

Analysis

By applying a mass balance, the following equation results

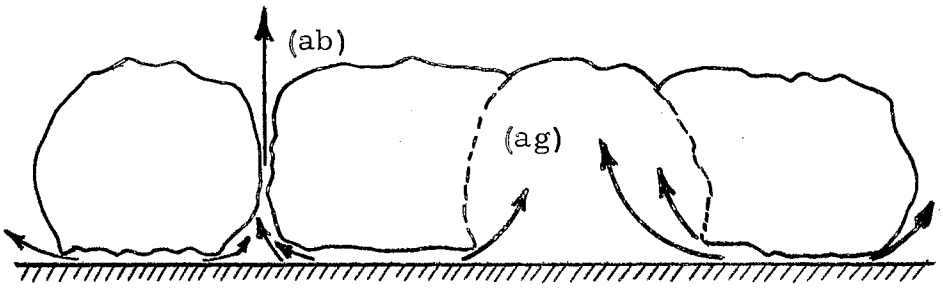

(a)

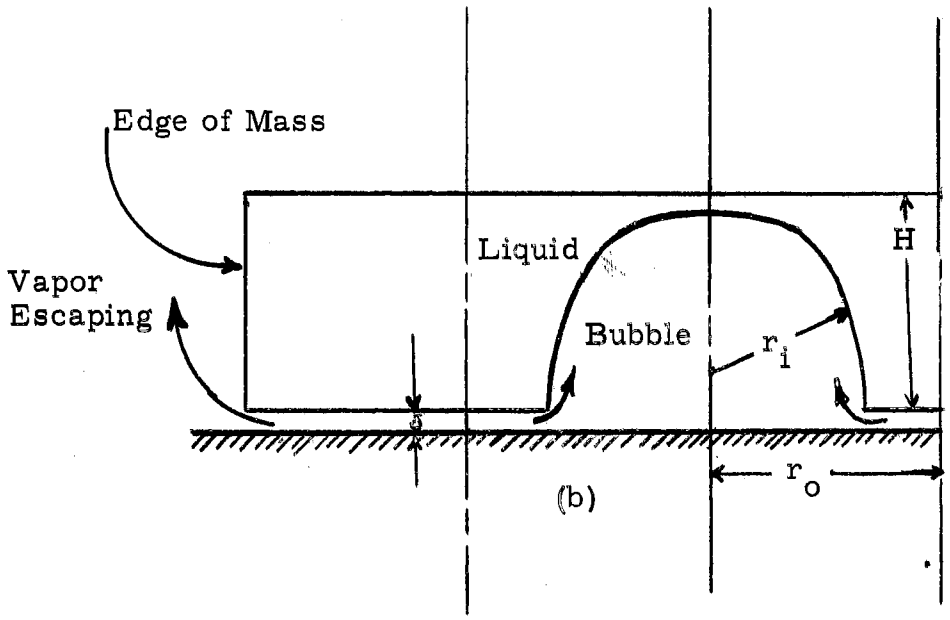

Figure 27. Physical and Idealized Models of Extended Masses in Film Boiling from a Horizontal Surface.

for extended liquid mass:

$$\rho_\ell \frac{dV}{dt} = -w A_p \quad \ldots\ldots\ldots\ldots\ldots\ldots \quad V\text{-}1$$

where w designates the average rate per unit projected area (in gm $cm^{-2}\ sec^{-1}$) at which vapor leaves the mass.

For extended masses, a heat balance yields,

$$Q = w A_p \left[L + C_v (T_v - T_s) \right]. \quad \ldots\ldots\ldots\ldots \quad V\text{-}2$$

Let $$L' = L + C_v (T_v - T_s) = L + \frac{1}{2} C_v \Delta T \quad \ldots\ldots \quad V\text{-}3$$

$$\left(\frac{Q}{A_p}\right)_T = wL' \quad \ldots\ldots\ldots\ldots\ldots\ldots \quad V\text{-}4$$

Assume that the heat is transferred only by conduction and radiation (7). The expression for total heat transferred is

$$\left(\frac{Q}{A_p}\right)_T = \left(\frac{Q}{A_p}\right)_C + \left(\frac{Q}{A_p}\right)_R \quad \ldots\ldots\ldots\ldots \quad V\text{-}5$$

But, $$\left(\frac{Q}{A_p}\right)_C = \frac{k_v \Delta T}{\delta} \quad \ldots\ldots\ldots\ldots\ldots\ldots \quad V\text{-}6$$

Where δ is the mean vapor thickness beneath the liquid mass on a hot plate. The radiation term for two parallel gray plates is given by Equation V-7:

$$\left(\frac{Q}{A_p}\right)_R = \frac{\sigma_c (T_{pk}^4 - T_{ps}^4)}{\frac{1}{\epsilon} + \frac{1}{\alpha} - 1} \quad \ldots\ldots\ldots\ldots \quad V\text{-}7$$

Combining Equations V-6 and V-7 in Equation V-5 yields

$$\left(\frac{Q}{A_p}\right)_T = \frac{k_v \Delta T}{\delta} + \frac{\sigma_c (T_{pk}^4 - T_{ps}^4)}{\frac{1}{\epsilon} + \frac{1}{\alpha} - 1} \quad \ldots\ldots\ldots \quad V\text{-}8$$

Substituting Equation V-8 in Equation V-4, we get

$$wL' = \frac{k_v \Delta T}{\delta} + \frac{\sigma_c (T_{pk}^4 - T_{ps}^4)}{\frac{1}{\epsilon} + \frac{1}{\alpha} - 1} \quad \ldots\ldots\ldots \quad V\text{-}9$$

Solving Equation V-9 for $\frac{1}{\delta}$ yields

$$\frac{1}{\delta} = \frac{wL' - \frac{\sigma}{\frac{1}{\epsilon} + \frac{1}{\alpha} - 1} (T_{pk}^4 - T_{ps}^4)}{k_v \Delta T} \quad \ldots\ldots\ldots \quad V\text{-}10$$

In Equation V-10, the value of mean vapor thickness δ is unknown. Therefore, it is necessary to get an expression for δ. In extended masses there occur numerous bubbles. The idealized situation is shown below:

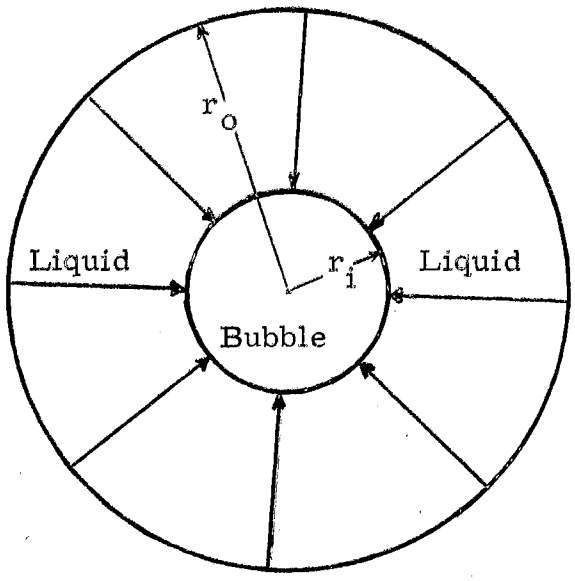

The bubble is assumed to be at the center of a liquid mass. It is assumed that the cross sectional shape of liquid mass and the bubble are circular. The radius of the bubble is denoted by r_i and the radius of the surrounding liquid which supplies vapor to the bubble is r_o. The arrows in the above figure indicate that vapor flow is radially inward to the bubble. The direction z is perpendicular to the plane of the page.

From the Navier-Stokes equations, a simplified equation can be obtained for the vapor flow with several assumptions including: 1) steady state, 2) laminar, viscous flow, 3) incompressible and isothermal fluid, 4) circular symmetry and 5) negligible velocity normal to the plate:

$$0 = -\frac{\partial p}{\partial r} + \mu\left[\frac{\partial}{\partial r}\left(\frac{1}{r}\frac{\partial}{\partial r}(rv_r)\right) + \frac{\partial^2 v_r}{\partial z^2}\right] \quad \text{V-11}$$

Assume that δ is constant. Then a mass balance across a toroidal element of the vapor layer gives

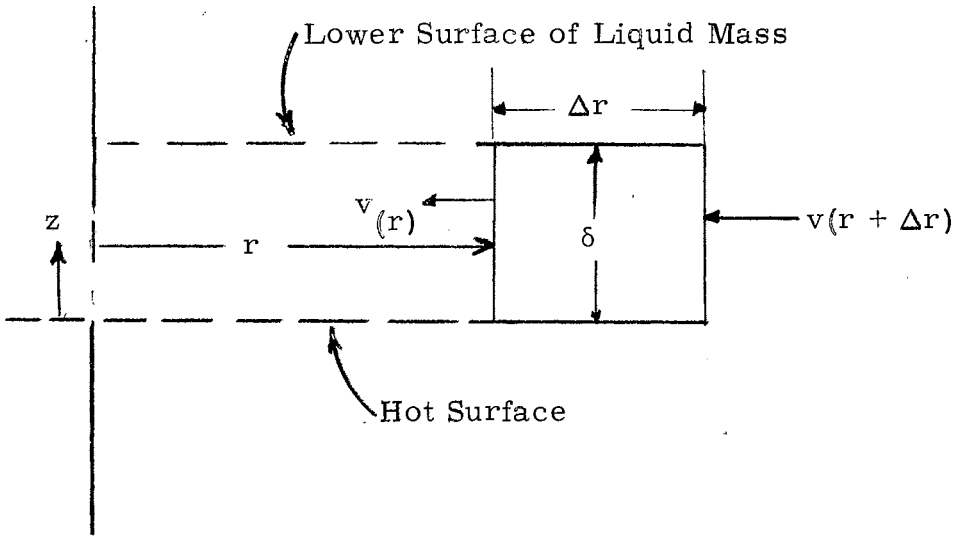

$$2\pi(r + \Delta r)\,\delta(v_r + \Delta v_r) = 2\pi r\,\delta v_r$$

or $$r v_r + r\,\Delta v_r + \Delta r\, v_r + \Delta r\,\Delta v_r = r\, v_r$$

or $$r\,\Delta v_r + v_r\,\Delta r = 0$$

If $\Delta r \rightarrow 0$

$\Delta v \rightarrow 0$

then $$r\frac{\partial v_r}{\partial r} + v_r = 0$$

Then $$\frac{\partial}{\partial r}\left[\frac{\partial v_r}{\partial r} + \frac{v_r}{r}\right] = \frac{\partial}{\partial r}\left[\frac{1}{r}\frac{\partial}{\partial r}(r v_r)\right] = 0$$

Hence, Equation V-11 yields

$$\frac{\partial p}{\partial r} = \mu\,\frac{\partial^2 v_r}{\partial z^2} \quad \ldots\ldots\ldots\ldots\ldots\ldots \quad \text{V-12}$$

Boundary conditions

$v_r = 0$ at $z = 0$ (no slip at solid boundary)

$\frac{dv_r}{dz} = 0$ at $z = \delta/2$ (symmetry about central plane, implying no slip at liquid-vapor interface)

Let $$\mu\,\frac{d^2 v_r}{dz^2} = -c_1$$

then $$\mu\,\frac{dv_r}{dz} = -c_1 z + c_2$$

$$0 = -c_1 \frac{\delta}{2} + c_2$$

$$c_2 = c_1 \frac{\delta}{2}$$

Also $$\mu \frac{dv_r}{dz} = -c_1 (z - \frac{\delta}{2})$$

$$\mu v_r = -c_1 (\frac{z^2}{2} - \frac{\delta z}{2}) + c_3$$

But $c_3 = 0$ ($v_r = 0$ at $z = 0$)

$$-c_1 = \frac{2\mu \bar{v}_r}{z^2 - \delta_z}$$

Average velocity at r is given by

$$\bar{v}_{(r)} = \frac{1}{\delta} \int_0^{\delta} v_r dz = \frac{1}{\delta} \int_0^{\delta} \frac{-c_1 (z^2 - \delta z)}{2\mu} dz = -\frac{c_1}{2\delta\mu} \left[\frac{\delta^3}{3} - \frac{\delta^3}{2}\right] = \frac{c_1 \delta^3}{12 \delta\mu}$$

Thus, Equation V-12 with the above boundary conditions yields the local value of the pressure gradient:

$$-\frac{dp}{dr} = \frac{12 \delta \mu \bar{v}_z}{\delta^3} = \frac{12 \mu \bar{v}_{(z)}}{\delta^2} \quad \ldots\ldots\ldots\ldots \quad \text{V-13}$$

Let the total vapor weight flow rate at radius r be $W_{(r)}$

$$\int_0^{W_{(r)}} dW_{(r)} = -\int_{r_o}^{r} 2 \pi r w dr \quad \ldots\ldots\ldots \quad \text{V-14}$$

Then $$W_{(r)} = w \pi (r_o^2 - r^2) \quad \ldots\ldots\ldots\ldots\ldots \quad \text{V-15}$$

The average vapor velocity at r is

$$\bar{v}_{(r)} = \frac{W_{(r)}}{2\pi r \delta \rho_v} \quad \text{V-16}$$

Combining Equations V-16 and V-15, the expression yields

$$\bar{v}_{(r)} = \frac{w(r_o^2 - r^2)}{2 r \delta \rho_v} \quad \text{V-17}$$

Combining Equations V-13 and V-17, the pressure gradient, $\frac{dp}{dr}$ becomes

$$\frac{dp}{dr} = \frac{12 \mu w (r_o^2 - r^2)}{2 \delta^3 r \rho_v} \quad \text{V-18}$$

or

$$\int_0^p dp = \int_{r_i}^{r} \frac{6 \mu w (r_o^2 - r^2)}{\delta^3 r \rho_v} dr \quad \text{V-19}$$

Solving Equation V-19 for p (above atmospheric pressure), the expression yields

$$p = \frac{6 \mu w}{\delta^3 \rho_v} \left[r_o^2 \ell n \frac{r}{r_i} - \frac{1}{2} (r^2 - r_i^2) \right] \quad \text{V-20}$$

For a unit cell (one bubble and the circle of liquid surrounding it), we get the force balance expression

$$g \rho_\ell H \pi (r_o^2 - r_i^2) = \int_{r_o}^{r_i} p (2 \pi r) dr \quad \text{V-21}$$

where H is the thickness of the liquid mass

r_o is the radius of liquid

r_i is the radius of bubble

Combining Equation V-20 and V-21, the Equation V-22 becomes,

$$g\rho_\ell H\pi(r_o^2 - r_i^2) = -\frac{12\mu w\pi}{\delta^3\rho_v}\int_{r_o}^{r_i}\left[r r_o^2 \ell n\frac{r}{r_i} - \frac{r}{2}(r^2 - r_i^2)\right]dr. \quad \text{V-22}$$

Integration of Equation V-22 gives

$$g\rho_\ell H\pi(r_o^2 - r_i^2) = \frac{12\pi\mu w}{\delta^3\rho_v}\left(\frac{r_o^4}{2}\ell n\frac{r_o}{r_i} + \frac{r_o^2 r_i^2}{2} + \frac{3r_o^4}{8} - \frac{r_i^4}{8}\right). \quad \text{V-23}$$

Now substituting the value of δ (Equation V-10) in Equation V-23, and solving for w, we get Equation V-24

$$w^{1/3}\left[wL' - \frac{\sigma_c}{\frac{1}{\alpha}+\frac{1}{\epsilon}-1}(T_{pk}^4 - T_{ps}^4)\right] =$$

$$\left[\frac{\rho_v k_v^3 \Delta T^3 g\rho_\ell H\pi(r_o^2 - r_i^2)}{12\pi\mu\left(\frac{r_o^4}{2}\ell n\frac{r_o}{r_i} + \frac{r_o^2 r_i^2}{2} - \frac{3r_o^4}{8} - \frac{r_i^4}{8}\right)}\right]^{1/3} \quad \text{V-24}$$

Equation V-24 may be used to calculate heat transfer coefficients for masses by first calculating w and then multiplying the value of w by $L'/\Delta T$. The values of heat transfer coefficient (cal sec^{-1} cm^{-2} $°C^{-1}$) of 10 ml extended masses thus calculated are included in Table VIII. All physical properties are taken from Appendix C. The radius r_o for the liquid mass surrounding one bubble was obtained from the projected area of the mass (Tables II and III) by

$$r_o = \sqrt{\frac{A_p}{\pi N_{bubbles}}}$$

The radius of the bubble r_i was taken from Tables II and III.

TABLE VIII

PREDICTED HEAT TRANSFER COEFFICIENTS FOR
10 ml MASSES FROM EQUATION V-24

Liquid	$(T_p - T_s)$, °C	h, cal sec^{-1} cm^{-2} $°C^{-1}$	
		Predicted Eq. V-24	Experimental Eq. IV-1
Water	207	4.31×10^{-3}	$2,77 \times 10^{-3}$
	396	5.18×10^{-3}	4.18×10^{-3}
Ethanol	105	4.29×10^{-3}	2.39×10^{-3}
	415	6.39×10^{-3}	3.84×10^{-3}
Benzene	104	4.78×10^{-3}	2.08×10^{-3}
	415	7.45×10^{-3}	$3,98 \times 10^{-3}$
Carbon Tetrachloride	108	2.75×10^{-3}	1.86×10^{-3}
	416	3.74×10^{-3}	3.75×10^{-3}

Table VIII shows the comparison of predicted heat transfer coefficient (Equation V-24) and the values of heat transfer coefficient (Equation IV-1, with radiation) for the extended liquid masses. The predicted values of heat transfer coefficients for 10 ml liquid masses from Equation V-24 are generally high compared to the calculated values. Probably the main reason for the prediction of high values of h from Equation V-24 is the assumption pertaining to the vapor thickness. The vapor thickness beneath the liquid mass was assumed to be constant, when in fact, the vapor thickness, likely varies inversely with radial position.

Combining Equations V-1 and V-24, we get,

$$\left(-\frac{\rho_\ell \, dV}{A_p \, dt}\right)^{1/3} \left[-\frac{L' \rho_\ell \, dV}{A_p \, dt} - \frac{\sigma_c (T_{pk}^4 - T_{ps}^4)}{\frac{1}{\alpha} + \frac{1}{\epsilon} - 1}\right] =$$

$$\left[\frac{\rho_v k_v^3 \Delta T^3 \rho_\ell g H (r_o^2 - r_i^2)}{12\mu\left(\frac{r_o^4}{2} \ell n \frac{r_o}{r_i} + \frac{r_o^2 r_i^2}{2} - \frac{3r_o^4}{8} - \frac{r_i^4}{8}\right)}\right]^{1/3} \quad \text{. . . . . V-25}$$

The vaporization time of extended liquid masses can be obtained by integrating Equation V-25. However, Equation V-25 is difficult to integrate analytically. Therefore, numerical computation for the instantaneous evaporation rate and integration over the lifetime of the mass must be employed. Numerical

computation of the evaporation time curves for the extended liquid masses would require a large computer for long periods of time (estimated several hours or an IBM 7090) which precluded further effort along this line. Lee's model as later modified for ellipsoids for the evaporation rate of small droplets would be used for masses below 1.2 ml of benzene, ethanol, and carbon tetrachloride, and below 2.7 ml for water.

Dimensionless Correlation

Dimensional analysis is particularly valuable where the exact mathematical relations are unknown such as in the Leidenfrost phenomenon for extended liquid masses. The useful aspect of dimensional analysis is its ability to provide a relation among the variables for computation within the experimental range covered.

It is assumed that the total vaporization time τ is a function of the following physical properties of extended liquid masses:

$$\tau = a_1 (k_v)^{a_2} (\Delta T)^{a_3} (C_v)^{a_4} (\rho_\ell)^{a_5} (\rho_v)^{a_6} (\sigma_s)^{a_7} (\mu_v)^{a_8} (L)^{a_9} (g)^{a_{10}} (g_c)^{a_{11}} \quad \text{V-26}$$

By employing the method of dimensional analysis, having the fundamental variables by

M = Mass	F = Force
T = Temperature	H = Heat
θ = Time	0 = Length,

the following dimensionless correlation is obtained:

$$\tau \frac{g}{g_c} \frac{\mu_v}{\sigma_s} = C_1 \left(\frac{C_v \mu_v}{k_v}\right)^{C_2} \left(\frac{\rho_\ell}{\rho_v}\right)^{C_3} \left(\frac{L}{C_v \Delta T}\right)^{C_4} \left(\frac{1}{\sigma_s g_c} \sqrt[3]{\frac{\mu_v^4 g}{\rho_\ell}}\right) \quad \ldots \quad \text{V-27}$$

Let $Y = \tau \frac{g}{g_c} \frac{\mu_v}{\sigma_s}$

$$X_1 = \frac{C_v \mu_v}{k_v}$$

$$X_2 = \frac{\rho_\ell}{\rho_v}$$

$$X_3 = \frac{L}{C_v \Delta T}$$

$$X_4 = \frac{1}{\sigma_s g_c} \sqrt[3]{\frac{\mu_v^4 g}{\rho_\ell}}$$

Substituting the above expressions in Equation V-27, we get

$$Y = C_1 (X_1)^{C_2} (X_2)^{C_3} (X_3)^{C_4} (X_4)^{C_5} \quad \ldots \quad \text{V-28}$$

Equation V-28 is solved to evaluate the constant C_1 and the exponents C_2 through C_5 by using the linearized least square method.

In Equation V-28, by taking logarithms of both sides, we get

$$\log Y = \log C_1 + C_2 \log X_1 + C_3 \log X_2 + C_4 \log X_3 + C_5 \log X_4 \quad \ldots \quad \text{V-29}$$

Apply least squares fitting to Equation V-29, the following set of

simultaneous linear algebraic equations may be obtained:

$$n \log C_1 + C_2 \Sigma \log X_1 + C_3 \Sigma \log X_2 + C_4 \Sigma \log X_3 + C_5 \Sigma \log X_4 = \Sigma \log Y \quad \text{V-30}$$

where Σ indicates summation over 100 data points which were obtained from the curves of experimental vaporization times v_s temperature difference for extended liquid masses (Figures 5 through 8).

$$\log C_1 \Sigma \log X_1 + C_2 \Sigma \log (X_1)^2 + C_3 \Sigma \log X_2 \log X_1 + C_4 \Sigma \log X_3 \log X_1 + C_5 \Sigma \log X_4 \log X_1 = \Sigma \log X_1 \log Y \quad \text{V-31}$$

$$\log C_1 \Sigma \log X_2 + C_2 \Sigma \log X_1 \log X_2 + C_3 \Sigma \log (X_2)^2 + C_4 \Sigma \log X_3 \log X_2 + C_5 \Sigma \log X_4 \log X_2 = \Sigma \log X_2 \log Y \quad \text{V-32}$$

$$\log C_1 \Sigma \log X_3 + C_2 \Sigma \log X_1 \log X_3 + C_3 \Sigma \log X_2 \log X_3 + C_4 \Sigma \log (X_3)^2 + C_5 \Sigma \log X_4 \log X_3 = \Sigma \log X_3 \log Y \quad \text{V-33}$$

$$\log C_1 \Sigma \log X_4 + C_2 \Sigma \log X_1 \log X_4 + C_3 \Sigma \log X_2 \log X_4 + C_4 \Sigma \log X_3 \log X_4 + C_5 \Sigma \log (X_4)^2 = \Sigma \log X_4 \log Y \quad \text{V-34}$$

The vaporization times were read at regular temperature intervals from curves which were fitted through the data points in Figures 5 through 8. The solution of Equations V-30 through V-34 gives values for the five constants. The results of the dimensionless correlation will be discussed in the next section.

Results and Discussion

The experimental data were successfully correlated by Equation V-27. The constants were determined by the previously described least squares technique, giving the following values:

$$C_1 = +0.67 \times 10^{-2}$$

$$C_2 = +1.21$$

$$C_3 = -0.95$$

$$C_4 = +0.58$$

$$C_5 = -0.89$$

The final correlation is

$$\tau\left(\frac{g}{g_c}\frac{\mu_v}{\sigma_s}\right) = 0.67 \times 10^{-2}\left(\frac{C_v\mu_v}{k_v}\right)^{1.21}\left(\frac{\rho_\ell}{\rho_v}\right)^{-0.95}\left(\frac{L}{C_v\Delta T}\right)^{0.58}\left(\frac{1}{\sigma_s g_c}\sqrt[3]{\frac{\mu_v^4 g}{\rho_\ell}}\right)^{-0.89} \quad \text{V-35}$$

Figure 28 compares experimental vaporization time (ordinate) to the prediction of Equation V-35 (abcissa). The physical properties L, ρ_ℓ and σ_s are evaluated at saturation temperature and the remaining physical properties C_v, μ_v, k_v and ρ_v were evaluated at mean vapor temperature. The vaporization times were read (from Figures 5 to 8) at regular temperature intervals. From Figure 28 it may be seen that the maximum error is ± 10 percent.

The ranges of the dimensionless groups are listed below:

$$0.57 \leq \frac{C_v\mu_v}{k_v} \leq 1.12$$

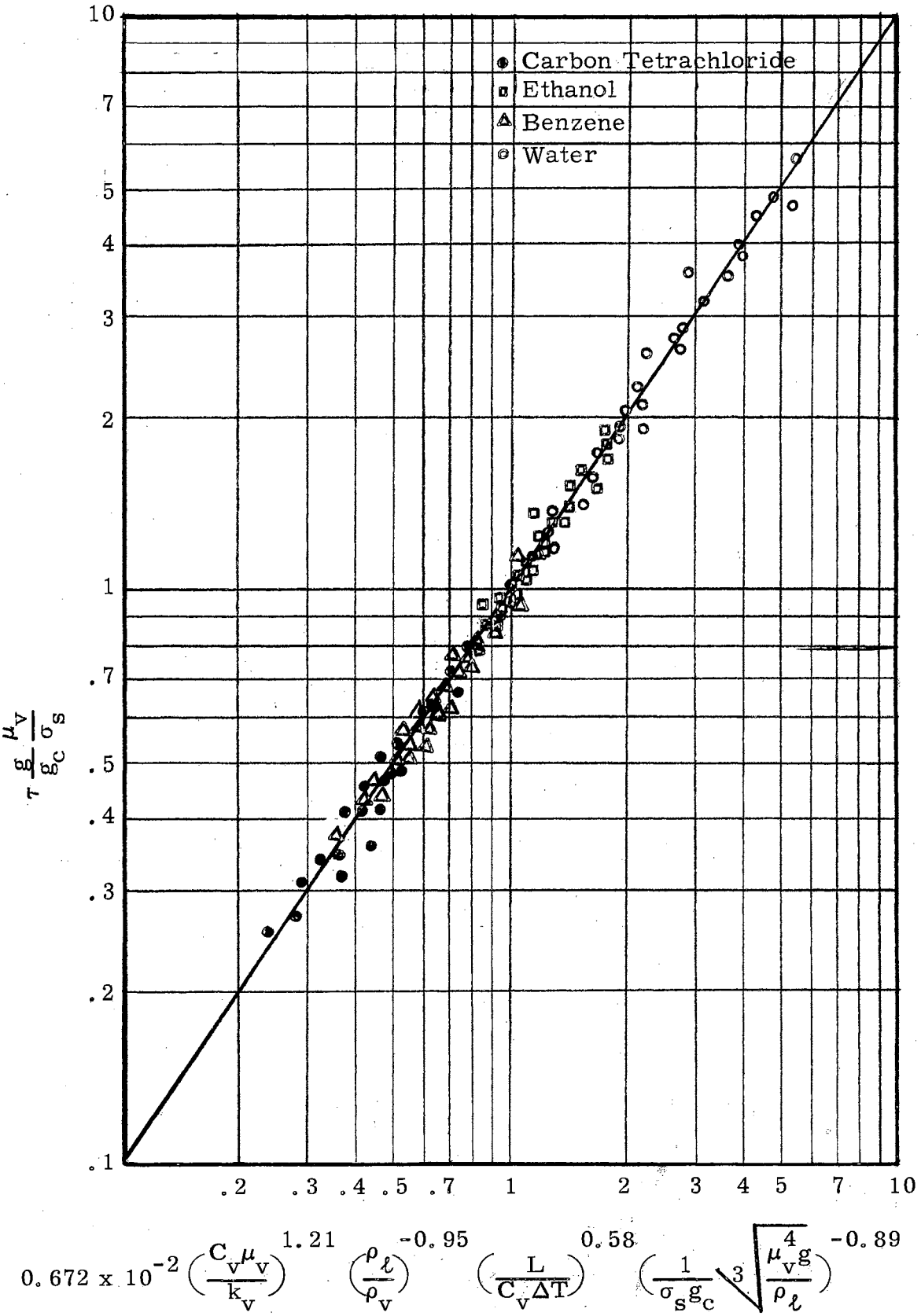

Figure 28. Correlation of Experimental Data

$$0.31 \times 10^{3} \leq \frac{\rho_{\ell}}{\rho_{v}} \leq 2.49 \times 10^{3}$$

$$0.79 \leq \frac{L}{C_{v}\Delta T} \leq 5.68$$

$$0.61 \times 10^{-5} \leq \frac{1}{\sigma_{s} g_{c}} \sqrt[3]{\frac{\mu_{v}^{4} g}{\rho_{\ell}}} \leq 2.74 \times 10^{-5}$$

The validity of the dimensionless correlation has not been ascertained outside of the range indicated. Hence, one must proceed cautiously in uses involving such fluids as cryogenics or liquid metals.

Table IX shows the comparison of the experimental and calculated vaporization data of extended masses from Gottfried's model and Lee's model. Table IX shows that the agreement between experimental and calculated vaporization time is poor. Therefore, neither Lee's Model or Gottfried's Model for small droplets can be applied to predict vaporization times of extended masses.

TABLE IX

EXPERIMENTAL AND CALCULATED VAPORIZATION TIMES OF EXTENDED MASSES FROM GOTTFRIED MODEL AND LEE MODEL

Liquid (1 ml each)	Plate Temperature °C	Experimental Vap. Time sec	Calculated* Vap. Time sec	Calculated** Vap. Time sec
Water	539	243	654	690
Benzene	190	132	392	370
Benzene	490	54.3	115	103
Carbon Tetrachloride	192	147	331	343
Ethanol	480	83.7	252	291

* Lee

** Gottfried (parameter x = 0.25)

CHAPTER VI

CONCLUSION AND RECOMMENDATIONS

The study reported in this thesis includes (a) a review of the literature of the bubble dynamics and heat transfer coefficients of liquids in film boiling, (b) the determination of the total vaporization times for extended masses of water, benzene, ethanol and carbon tetrachloride, (c) the determination of the Leidenfrost point for extended liquid masses, (d) evaluation of the stability characteristics with regard to vapor break through for extended liquid masses, and (e) a correlation of the experimental vaporization data for extended liquid masses.

The major conclusions from the study may be summarized as:

1. The bubble period may be estimated well by a method of Zuber, Equation II-14.
2. The correlations of heat transfer coefficient by Chang, Berenson and Borishansky and the results of this work are not in agreement. These correlations do not apply to extended masses.
3. The vaporization data of Borishansky and this work are in agreement for the extended masses at plate temperature 350°C. For a plate temperature of 275°C, the water vaporization time of Borishansky is about 60 percent higher than the vaporization time of this work.

4. The Leidenfrost point for extended liquid masses occur at about $\Delta T = 105^{\circ}C$ for benzene, $\Delta T = 107^{\circ}C$ for carbon tetrachloride, $\Delta T = 104^{\circ}C$ for ethanol, and $\Delta T = 207^{\circ}C$ for water.
5. As a rule, vapor bubbles appear in masses above 2.7 ml of water and above about 1.2 ml of organic liquids (benzene, carbon tetrachloride, and ethanol).
6. No regular geometric pattern of bubble release is evident.
7. Bubble breakoff diameters are essentially constant and do not vary with plate temperature.
8. Bubble measurements such as bubble breakoff diameters, bubble period, and bubble spacing of extended water masses in film boiling are smaller than the corresponding measurements for water by Hosler and Westwater for submerged surfaces in film boiling.
9. For water, the bubble breakoff diameters are about 54 percent of the most dangerous wavelength. For ethanol and carbon tetrachloride, the bubble breakoff diameters are about 60 percent of the most dangerous wavelength. For benzene, the bubble breakoff diameters are about 42 percent of the most dangerous wavelength.
10. The liquid thickness measurements data of Borishansky and this work are not in agreement for water masses. The liquid thickness found in this work is about 75 percent of Borishansky's result.
11. The analytical model for small droplets by Lee or Gottfried

is not applicable to vaporization data of extended liquid masses.

12. The dimensionless correlation of vaporization time for extended liquid masses shows a maximum error of 10 percent. It cannot apply for any other regimes except the Leidenfrost state for extended masses.

From the information gained in this study, the following recommendations concerning further work may be made.

1. Extend and/or modify analytical model of this work for the vaporization rate of extended masses.
2. Construct two identical plates of brass and steel to determine the effect of thermal diffusivity of metal for liquid vaporization times at the Leidenfrost point.
3. Make runs for the total vaporization times of liquids such as n-octane and cryogenic liquids.
4. Use a Vanguard motion analyzer (21) for data reduction since the Vanguard motion analyzer has many advantages compared to the Kodak film reader.

A SELECTED BIBLIOGRAPHY

1. Asch, V., "A Survey of Liquid Boiling Phenomena: Their Prediction and Analysis." IEEE Trans. Component Parts, March, pp. 12-13 (1963).

2. Bell, K. J. and B. M. Patel, "The Leidenfrost Phenomenon for Extended Masses," Motion Picture, School of Chemical Engineering, Oklahoma State University, Stillwater (1964).

3. Bellman, R. and R. H. Pennington, "Effects of Surface Tension and Viscosity on Taylor Instability," Quar. Appl. Math., 12, 151 (1954).

4. Berenson, P. J., "Film-Boiling Heat Transfer from a Horizontal Surface," Trans. ASME, 83, 351 (1961).

5. Birkhoff, G., "Hydrodynamics," Princeton University Press, Princeton, New Jersey (1960).

6. Borishansky, V. M., "Heat Transfer to a Liquid Freely Flowing over a Surface Heated to a Temperature above the Boiling Point," AEC-tr-3405, Problems of Heat Transfer During a Change of State: A Collection of Articles, ed. by S. S. Kutateladze pp. 109-144 (1953).

7. Bromley, L. A., "Heat Transfer in Stable Film Boiling," Chem. Engr. Prog., 46, 221 (1950).

8. Castles, J. T., M. S. Thesis in Chemical Engineering, Massachusetts Institute of Technology, Cambridge, 1947.

9. Chang, Yan Po, "A Theoretical Analysis of Heat Transfer in Natural Convection and in Boiling," Trans. ASME, 79, 1501 (1957).

10. Chang, Yan Po, "Wave Theory of Heat Transfer in Film Boiling," Journal of Heat Transfer, Series C, 81, 1 (1959).

11. Chesterman, W. D., "The Photographic Study of Rapid Events," Clarendon Press, Oxford (1951).

12. Corty, Claude, and A. S. Foust, "Surface Variables in Boiling," Motion Picture, Univ. of Mich., Ann Arbor, Michigan (1953).

13. Drew, T. B., and J. G. Santangelo, "Photographic Study of Boiling," Trans. Am. Inst. Chem. Engr. 33, 449 (1937).

14. Drew, T. B., and A. C. Mueller, "Boiling," Motion Picture, E. I. duPont de Nemours & Co., Wilmington, Del. (1937).

15. Farber, E. A. and R. L. Scorah, "Heat Transfer to Water Boiling," Trans. ASME, 70, 369 (1948).

16. Gottfried, B. S., "The Evaporation of Small Drops on a Flat Plate in the Film Boiling Regime," Ph. D. Thesis, Case Institute of Technology, Cleveland, Ohio, (1962).

17. Gross-Gronomski, "Drop Evaporation Problems of Nitric Acid and Aniline, Combustion and Flame," 7, 217 (1963).

18. Gunther, F. C., "Photographic Study of Surface-Boiling Heat Transfer to Water with Forced Convection," Trans. ASME, 73, 115 (1951).

19. Hodgman, C. D., Ed., "Handbook of Chemistry and Physics," 39th ed., Chemical Rubber Publishing Co., Cleveland, Ohio (1958).

20. Hosler E. R. and J. W. Westwater, "Film Boiling on a Horizontal Plate," ARS Journal, 32, 553 (1962).

21. Hyzer, W. G., "Engineering and Scientific High-Speed Photography," The MacMillan Co., New York (1962).

22. Jakob, Max, "Heat Transfer in Evaporation," Mech. Engr. 58, 643 (1936).

23. Jakob, Max, "Heat Transfer," Vol. 1 Chapter 29. Wiley, New York (1949).

24. Jones, G. A., "High-Speed Photography, Its Principles and Applications," John Wiley, New York (1952).

25. Kern, D. Q., "Process Heat Transfer," McGraw-Hill Book Co. Inc., New York (1950).

26. Kristensen, K. S., Tids. Physik og Chemie 9, 161 (1888).

27. Lamb, H. "Hydrodynamics," Dover Publ., New York (1957).

28. Lee, C. J., "The Leidenfrost Phenomenon for Small Droplets," Ph. D. Thesis, Oklahoma State University, Stillwater, Oklahoma (1965).

29. Leidenfrost, J. G., "De aquae communis nonullis qualitatibus tractatus," Duisburg, 1756; "Treatise on Several Properties of Ordinary Water," Translated into English by Mrs. Carolyn Wares, University of Oklahoma, Norman, Oklahoma (1964).

30. Lewis, D. J., "The Instability of Liquid Surfaces When Accelerated in a Direction Perpendicular to Their Plane II," Proc. Roy. Soc., London, A-202, 81 (1950).

31. McAdams, W. H., "Heat Transmission" 3rd ed., Chapter 14 McGraw-Hill, New York (1954).

32. Milne-Thompson, L. M., "Theoretical Hydrodynamics," MacMillan Co., New York (1950).

33. Nukiyama, S., "The Maximum and Minimum Values of the Heat Q Transmitted from Metal to Boiling Water," Soc. Mech. Engr., Japan 37, 367 (1934).

34. Perkins, A. S. and J. W. Westwater, "Measurements of Bubbles Formed in Boiling Methanol," AICHE Journal 2, 471 (1956).

35. Perry, J. H. (ed.), "Chemical Engineers' Handbook," 3rd ed., McGraw-Hill Book Co., Inc., New York (1950).

36. Pleteneva, N. A., and P. A. Rebinder, "Certain Facts Concerning Evaporation of Liquid in the Spheroidal State," Phys. Chem., pp. 961-973 (1946); Bull USSR Acad. Sci., Div. Tech. Sci., 12, (1946).

37. Reid, R. C. and T. K. Sherwood, "The Properties of Gases and Liquids," McGraw-Hill Book Co., Inc., New York (1958).

38. Rohsenow, W. M., "Heat Transfer and Fluid Mechanics Institute," pp. 1930196, Stanford Univ. Press, Palo Alto, California (1953).

39. Sauer, E. T., "Heat Transfer to Liquids," M. S. Thesis in Chem. Engr., Mass. Inst. Technology (1937).

40. Scott, H., "Heat Transfer," Trans. Am. Soc. Metals, 22, 557 (1934).

41. Siegel, R. and C. Usiskin, "A Photographic Study of Boiling in the Absence of Gravity," Trans. ASME, 81, 230 (1959).

42. Taylor, G. I., "The Instability of Liquid Surfaces When Accelerated in a Direction Perpendicular to Their Plane," Proc. Roy. Soc. London, A-201, 192 (1950).

43. Westwater, J. W. and J. G. Santangelo, "Photographic Study of Boiling," Ind. Engr. Chem. 47, 1605 (1955).

44. Wollensak Optical Co., "Fastax Instruction Book" Wollensak Optical Co., Rochester, New York (1962).

45. Wollensak Optical Co., Instruction Manuals on WF-4ST, WF-367, WF-301 and WF-360., Wollensak Optical Co., Rochester, New York (1962).

46. Zmola, P., "Investigation of the Mechanism of Boiling in Liquids," Ph. D. Thesis, Purdue University, Lafayette, Ind. (1950).

47. Zuber, Novak, "Hydrodynamic Aspects of Boiling Heat Transfer," Ph. D. Thesis, Dept. of Engr., Univ. of California, Los Angeles (1959).

48. Zuber, N. and M. Tribus, "Further Remarks on the Stability of Boiling Heat Transfer," Report 58-5. University of California, Los Angeles, California; AECU-3631 (1958).

49. Zuber, Novak, "On the Stability of Boiling Heat Transfer," Trans. ASME, 80, 711 (1958).

APPENDIX A

THERMOCOUPLE CALIBRATION

Chromel-alumel thermocouples were used for temperature measurements. These particular metals were selected for their high thermal emf output per degree of temperature difference and stability over the temperature range anticipated.

The thermocouples were calibrated in the Heat Transfer Laboratory at Stillwater, utilizing boiling water at atmospheric pressure. Data were taken with the same potentiometer which was used to take the test data, with the temperature of melting ice as reference point.

The emf values are expressed in absolute electrical volts. The calibration measurements are tabulated below. Each thermocouple used was individually calibrated as an added precaution.

Boiling Water
Temperature = 99.82°C
Standard mv = 4.093

Thermocouple No.	Millivolts observed	Deviation (Standard mv minus mv observed)	Deviation from Standard mv
	mv	mv	Percent
1	4.078	0.015	0.366
2	4.081	0.012	0.293
3	4.081	0.012	0.293
4	4.080	0.013	0.317
5	4.083	0.010	0.244
6	4.082	0.011	0.286

Thermocouple No.	Millivolts observed	Deviation (Standard mv minus mv observed)	Deviation from Standard mv
	mv	mv	Percent
7	4.080	0.013	0.317
8	4.083	0.010	0.244
9	4.084	0.009	0.219
10	4.079	0.014	0.342
11	4.083	0.010	0.244
12	4.082	0.011	0.286
13	4.083	0.010	0.244

Average deviation, mv = $0.0115 \pm 0.279\%$

APPENDIX B

PIPETTE CALIBRATION

TABLE B1. CALIBRATION OF 1 ml PIPETTE

Liquid	Liquid Mass, gm	Deviation From Mean, percent	Liquid	Liquid Mass, gm	Deviation From Mean, percent
Water	0.9981	+0.0200	Ethanol	0.7284	+1.1266
27°C	0.9989	+0.0601	27°C	0.7403	-0.4882
	0.9978	-0.0501		0.7382	-0.2036
	1.0005	+0.2203		0.7411	-0.5972
	0.9993	+0.0100		0.7392	-0.3393
	0.9988	+0.0602		0.7368	-0.0135
	0.9997	+0.1402		0.7328	+0.5294
	0.9923	-0.6010		0.7383	-0.2172
	1.0021	+0.3806		0.7442	-1.-181
	0.9958	-0.2504		0.7278	+1.2081
Avg.	0.9983	±0.1792	Avg.	0.7367	±0.4741
Benzene	0.8261	-1.0398	Carbon	1.3843	+0.3419
27°C	0.7993	+0.9909	Tetra-	1.4032	+0.2093
	0.8214	-0.4893	chloride	1.4861	-0.3698
	0.8235	-0.7462	27°C	1.4421	-0.0628
	0.8194	-0.2446		1.3982	+0.2441
	0.7987	+2.2877		1.4233	+0.0698
	0.8242	-0.8319		1.4891	-0.3907
	0.8246	-0.8808		1.4241	+0.0628
	0.8164	+0.1223		1.4464	-0.0907
	0.8208	-0.4155		1.4382	+0.0348
Avg.	0.8174	±0.8029	Avg.	1.4330	±0.1876

TABLE B2. CALIBRATION OF 3 ml PIPETTE

Liquid	Liquid Mass, gm	Deviation From Mean, Percent	Liquid	Liquid Mass, gm	Deviation From Mean, Percent
Water	2.7346	+2.5977	Ethanol	2.1882	+4.8071
27°C	2.9383	-6.1647	27°C	2.3698	-3.0932
	2.8135	+0.8283		2.4121	-4.9332
	2.9147	-2.7351		2.2163	+3.5846
	2.9696	-4.6702		2.0257	+3.1757
	2.7371	+3.5247		2.3124	-0.5959
	2.8480	-0.3842		2.4165	-5.1246
	2.6148	+7.8601		2.2964	+0.1001
	2.8392	-0.0740		2.3623	-2.7667
	2.9319	-3.3414		2.3876	-3.8674
Avg.	2.8371	±3.2181	Avg.	2.2987	±3.2048
Benzene	2.3985	+1.6524	Carbon	4.3633	-0.3611
27°C	2.3642	+3.0588	Tetra-	4.3189	+0.6601
	2.5314	-3.7969	chloride	4.1284	+5.0418
	2.5486	-4.5022	27°C	4.4237	-1.7503
	2.4976	-2.4110		4.2318	+2.6635
	2.3181	+4.9409		4.3683	-0.4761
	2.6172	-7.3437		4.5016	-3.5421
	2.3181	+4.9245		4.3574	-0.2254
	2.5087	-2.8621		4.4365	-2.0448
	2.3843	+2.2347		4.3462	+0.0322
Avg.	2.4388	±3.7727	Avg.	4.3476	±1.6797

TABLE B3. CALIBRATION OF 5 ml PIPETTE

Liquid	Liquid Mass, gm	Deviation From Mean, Percent	Liquid	Liquid Mass, gm	Deviation From Mean, Percent
Water	4.8644	-2.6352	Ethanol	3.6395	+0.5899
27°C	4.4383	+6.3551	27°C	3.4846	+4.8209
	4.8498	-2.3272		3.5153	+3.5334
	4.9117	-3.6332		3.8436	-4.9848
	4.8616	-2.5804		3.6127	+1.3220
	4.3415	+8.3975		3.7343	-1.9993
	4.6319	+2.2702		3.6082	+1.3339
	4.7223	+0.3439		3.7983	-3.7475
	4.8691	-2.7344		3.6258	+0.9642
	4.9038	-3.4666		3.7327	-1.9556
Avg.	4.7395	±3.4743	Avg.	3.6611	±2.4143
Benzene	3.9436	+6.5938	Carbon	7.3267	-1.9083
27°C	4.3487	-2.9985	Tetra-	7.4872	-4.1407
	4.1821	+0.9473	chloride	7.5011	-4.3341
	4.0033	+5.1822	27°C	7.4356	-3.5621
	4.3324	-2.6124		6.8265	+5.0490
	4.5014	-6.6152		7.2338	-0.4771
	4.4395	-5.1491		7.2877	-1.3658
	4.3186	-4.6541		7.3425	-1.8499
	3.8257	+9.3887		7.2286	-0.5438
	4.3264	-2.4703		6.9812	+2.8972
Avg.	4.2221	±4.6611	Avg.	7.1895	±2.6127

TABLE B4. CALIBRATION OF 8 ml PIPETTE

Liquid	Liquid Mass, gm	Deviation From Mean, Percent	Liquid	Liquid Mass, gm	Deviation From Mean, Percent
Water	7.7812	-3.3266	Ethanol	5.6228	+2.6982
27°C	7.2389	+2.6231	27°C	5.9343	-0.8977
	7.6147	-2.4321		6.2727	-6.6513
	7.3898	+0.5932		6.3234	-7.5133
	7.5327	-1.3290		5.7326	+2.7526
	6.8663	+7.6352		5.6191	+2.5316
	7.6125	-2.4025		6.3222	-7.4929
	7.9314	-6.6923		5.3819	+8.4944
	6.9383	+6.6667		5.6238	+4.3815
	7.4341	-0.0026		5.9825	-1.7172
Avg.	7.4339	±3.3703	Avg.	5.8815	±4.4131
Benzene	6.8188	-3.9181	Carbon	10.8647	+4.1194
27°C	6.3774	+2.9611	Tetra-	11.3183	+0.1164
	6.4682	+1.4249	chloride	10.9396	+3.3702
	6.3776	-2.5283	27°C	10.8365	+4.3683
	6.5982	-0.5562		11.3848	-0.4703
	6.6535	-1.3990		11.8122	-4.2422
	6.9236	-5.5153		11.5639	-2.0509
	6.2842	+4.2290		11.6385	-2.7092
	6.3327	+3.4899		11.5756	-2.1453
	6.4236	+2.1046		11.3974	-0.5815
Avg.	6.5617	±2.8126	Avg.	11.3315	±2.4193

TABLE B5. CALIBRATION OF 10 ml PIPETTE

Liquid	Liquid Mass, gm	Deviation From Mean, Percent	Liquid	Liquid Mass, gm	Deviation From Mean, Percent
Water	9.6324	-1.1572	Ethanol	7.2585	+0.7262
27°C	9.4183	+1.0911	27°C	7.4613	-0.6797
	9.5948	-0.7624		7.6348	-4.4190
	9.6107	-0.9294		7.5188	-2.8338
	9.3227	+2.0951		7.1522	+2.1801
	9.4765	+0.4799		7.3233	-0.1600
	9.5172	+0.0525		7.1682	+1.9612
	0.6323	-1.1562		7.3376	-0.3555
	9.4194	+1.0795		6.9865	+4.4463
	9.5986	-0.8023		7.2757	+0.4910
Avg.	9.5222	±0.9611	Avg.	7.3116	±2.4961
Benzene	8.0536	+0.8702	Carbon	14.0127	+1.3001
27°C	8.2621	-1.6964	Tetra-	14.0836	+0.8712
	8.3762	-3.1018	chloride	14.3495	-1.0001
	7.8649	+2.8429	27°C	14.7383	-3.7367
	8.2412	-1.4388		14.2134	-0.0422
	8.0374	+1.0696		13.7641	+5.2247
	8.4386	-3.8686		13.9459	+1.8405
	7.7697	+4.3646		14.6426	-3.0631
	8.1073	+0.2092		13.8878	-4.7891
	8.0925	+0.3912		14.4362	-1.6104
Avg.	8.1243	±1.9853	Avg.	14.2074	±2.3478

TABLE B6. CALIBRATION OF 0.05 ml MICROLITER SYRINGE

Liquid	Liquid Mass, gm	Deviation From Mean, Percent	Liquid	Liquid Mass, gm	Deviation From Mean, Percent
Water	0.05379	-2.1644	Ethanol	0.04075	+1.1445
27°C	0.05560	+2.9465	27°C	0.04080	+1.7497
	0.05553	+1.0004		0.04058	+0.9679
	0.05344	-2.8011		0.04017	-0.2978
	0.05654	+2.8374		0.03998	+0.7694
	0.05596	+1.7825		0.03904	+2.1097
	0.05288	-3.8196		0.04173	-3.5740
	0.05465	-0.6002		0.03987	+0.7942
	0.05595	+0.6646		0.04028	+0.0248
	0.05455	-0.7821		0.03958	+1.7870
Avg.	0.05498	±1.8616	Avg.	0.04029	±1.2890
Benzene	0.04248	-2.6358	Carbon	0.08021	+0.6933
27°C	0.04447	+1.9253	Tetra-	0.08027	+0.6190
	0.04400	+0.6188	chloride	0.08590	-0.2229
	0.04317	-1.0543	27°C	0.08179	-1.2628
	0.04359	-0.0916		0.08173	-1.1886
	0.04313	-1.1460		0.07951	+1.5599
	0.04455	+2.1086		0.08036	+0.5070
	0.04348	-0.3438		0.08136	-0.7552
	0.04399	+0.5959		0.08050	+0.3343
	0.04349	-0.3208		0.08411	-0.4581
Avg.	0.04363	±1.0841		0.08077	±0.7601

TABLE B7. CALIBRATION OF 0.10 ml MICROLITER SYRINGE

Liquid	Liquid Mass, gm	Deviation From Mean Percent	Liquid	Liquid Mass, gm	Deviation From Mean, Percent
Water	0.1071	+0.7050	Ethanol	0.08280	-0.4492
27°C	0.1067	+0.3008	27°C	0.08257	-0.2428
	0.1068	+0.3007		0.08186	+0.6191
	0.1047	-1.4571		0.08268	+0.3764
	0.1055	-0.8272		0.08277	+0.4856
	0.1070	+0.6016		0.08201	-0.4492
	0.1063	-0.1316		0.08203	-0.4127
	0.1065	+0.0188		0.08264	+0.3035
	0.1071	+0.6580		0.08205	-0.3885
	0.1056	-0.8364		0.08234	-0.0364
Avg.	0.1064	±0.4108	Avg.	0.08237	±0.3768
A					
Benzene	0.09139	+0.3403	Carbon	0.1676	+0.9216
27°C	0.09162	+0.5929	Tetra-	0.1665	+0.2891
	0.09132	+0.2635	chloride	0.1673	+0.7891
	0.09101	-0.0878	27°C	0.1660	-0.0121
	0.09169	-0.4382		0.1671	+0.6385
	0.09156	+0.5201		0.1653	-0.4336
	0.09113	+0.0549		0.1644	-0.9577
	0.09070	-0.4172		0.1659	-0.5421
	0.09064	-0.4831		0.1663	+0.2108
	0.09077	-0.3404		0.1638	-1.3492
Avg.	0.09108	±0.3538	Avg.	0.1661	±0.6143

TABLE B8. CALIBRATION OF 0.15 ml MICROLITER SYRINGE

Liquid	Liquid Mass, gm	Deviation From Mean, Percent	Liquid	Liquid Mass, gm	Deviation From Mean, Percent
Water	0.1551	+0.5901	Ethanol	0.1190	-1.5882
27°C	0.1529	-0.7783	27°C	0.1198	-0.9016
	0.1532	-0.6423		0.1211	+0.1737
	0.1543	+0.0454		0.1217	+0.7196
	0.1534	-0.4993		0.1221	+1.0339
	0.1545	+0.2399		0.1214	+0.4549
	0.1548	+0.3697		0.1209	+0.0413
	0.1551	+0.5448		0.1214	+0.4384
	0.1549	+0.5443		0.1206	-0.1654
	0.1542	+0.0324		0.1207	-0.1323
Avg.	0.1541	±0.4287	Avg.	0.1208	±0.5649
Benzene	0.1336	-0.1569	Carbon	0.2435	-0.0984
27°C	0.1342	+0.3064	Tetra-	0.2446	+0.3404
	0.1343	+0.3961	chloride	0.2435	-0.1189
	0.1341	+0.2242	27°C	0.2424	-0.5789
	0.1340	+0.2541		0.2444	+0.2772
	0.1341	+0.2242		0.2436	-0.0492
	0.1336	-0.1494		0.2438	+0.0164
	0.1325	-0.9714		0.2439	+0.0492
	0.1333	-0.3961		0.2439	+0.0007
	0.1342	+0.2015		0.2449	+0.4759
Avg.	0.1338	±0.3295	Avg.	0.2437	±0.2006

APPENDIX C

PHYSICAL PROPERTIES

TABLE C1. PHYSICAL PROPERTIES OF SATURATED LIQUIDS

Physical Properties	Water	Benzene	Ethanol	Carbon Tetrachloride	Reference
Boiling point, °C	100	80.1	78.5	76.9	19
Molecular weight	18	78	46.1	153.8	19
Density, gm/cm^3	0.958	0.817	0.737	1.433	6
Heat of vaporization, cal/gm	559	94.1	204.3	46.8	35
Emissivity	0.96	0.96	0.96	0.96	31
Surface tension, gm-force/cm	0.06	0.0216	0.0171	0.0206	6

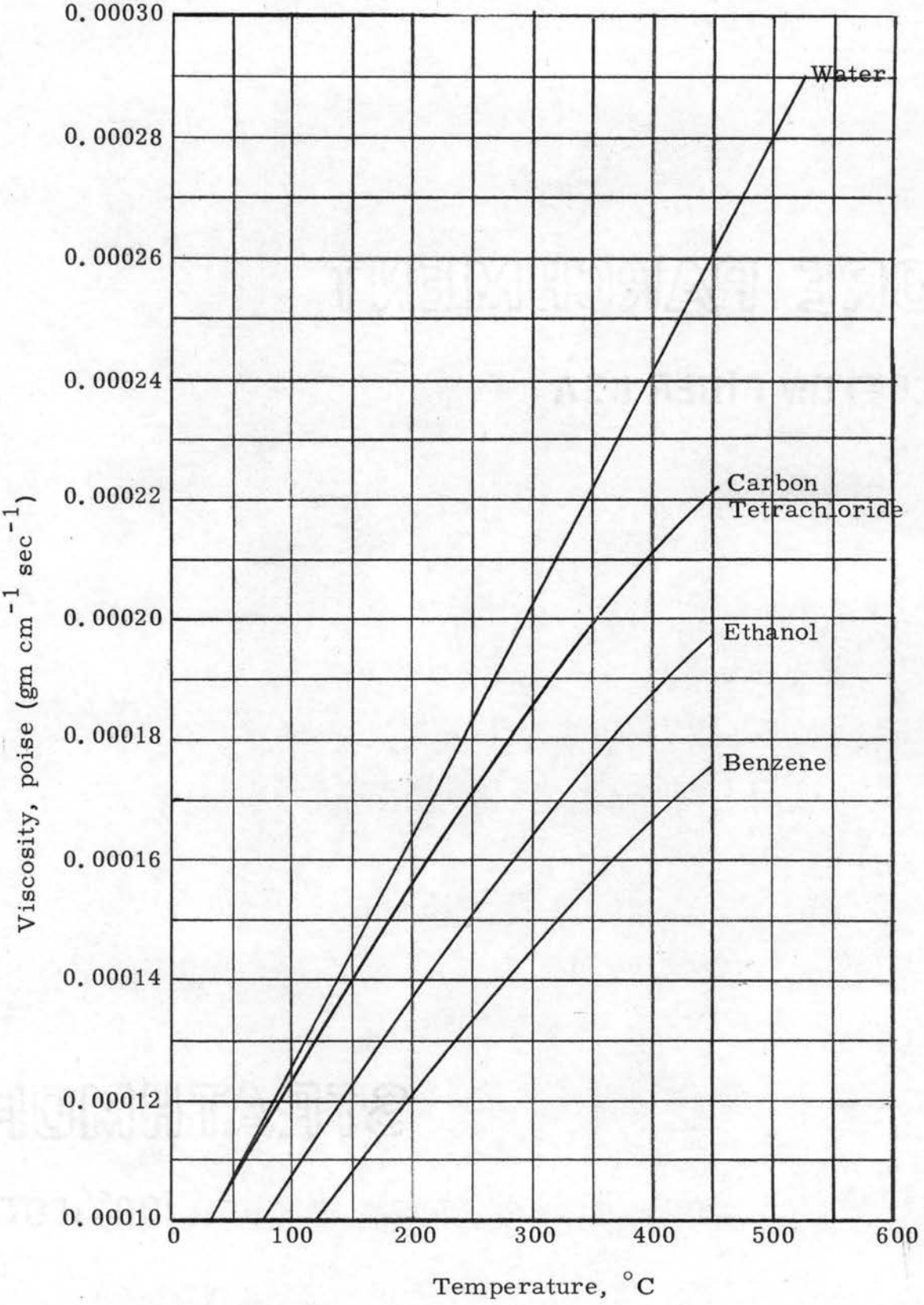

Figure C1. Viscosity of Gases

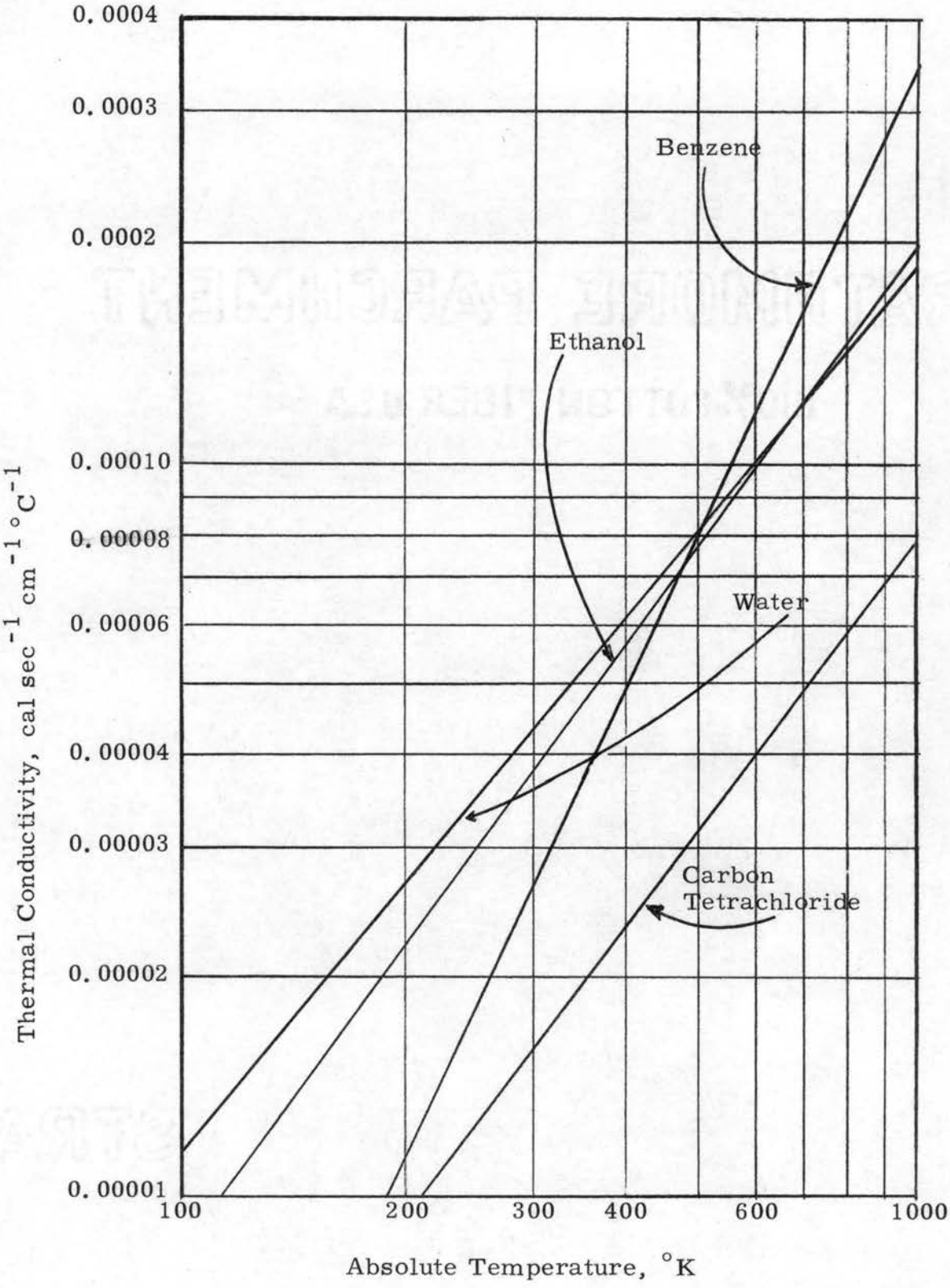

Figure C2. Thermal Conductivity of Gases

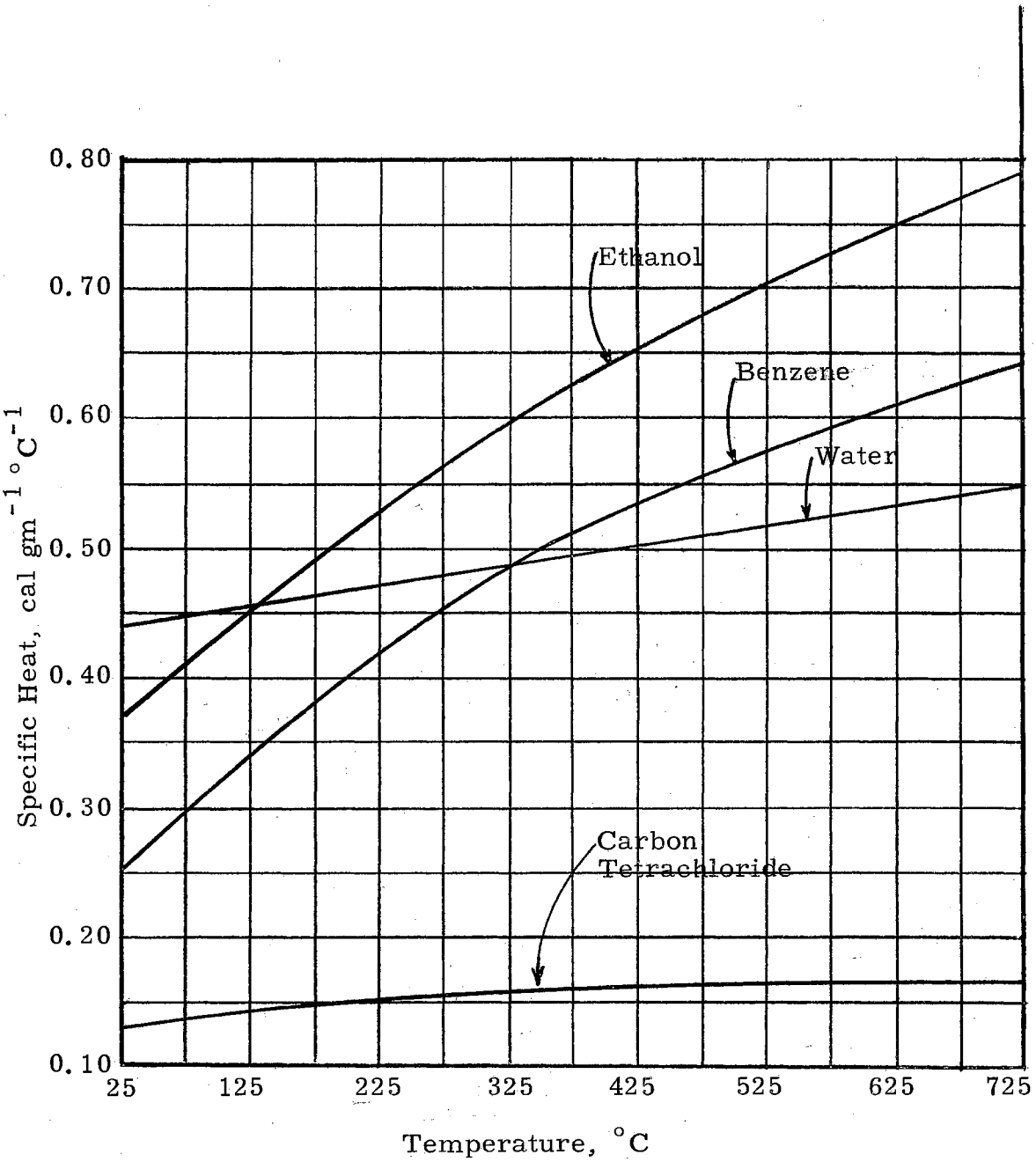

C3. Specific Heat of Gases

APPENDIX D

EXPERIMENTAL VAPORIZATION DATA OF EXTENDED LIQUID MASSES

TABLE D1. VAPORIZATION DATA OF WATER

Liquid Volume, ml	Temperature Difference $(T_p - T_s)$, °C	Average Vaporization Time, sec	Liquid Volume, ml	Temperature Difference $(T_p - T_s)$, °C	Average Vaporization Time, sec
0.05	50.8	12.7	0.10	57.3	10.2
	98.5	1.4		89.5	1.25
	158.3	89.2		122.3	6.42
	206.8	118.15		160.8	99.3
	258.5	103.9		206.9	154.6
	292.0	97.3		259.0	129.9
	321.8	88.7		323.0	117.7
	367.3	78.5		365.8	104.1
	438.6	61.8		435.2	86.4
0.15	27.5	56.5	1.0	98.6	18.9
	59.8	12.56		124.3	88.8
	97.5	4.84		198.6	286.0
	162.0	90.8		206.7	418.0
	190.0	178.6		218.1	398.0
	207.0	191.8		230.6	351.0
	259.0	176.5		258.4	323.0
	300.1	149.8		294.5	286.3
	332.0	142.1		328.6	277.8
	387.0	101.7		371.4	249.2
	428.3	93.3		418.1	221.1
				438.7	212.4

TABLE D2. VAPORIZATION DATA OF WATER

Liquid Volume, ml	Temperature Difference $(T_p - T_s)$, °C	Average Vaporization Time, sec	Liquid Volume, ml	Temperature Difference $(T_p - T_s)$, °C	Average Vaporization Time, sec
3.0	118	33.5	5.0	104	22.8
	160	178		174	203
	197	503		197	586
	207	660		206.8	745
	220	646		215	732
	247	543		264	618
	285	464		331	501
	327	388		375	418
	373	351		298	552
	416	332		421	391
	437	321		438	353
8.0	109	44	10.0	108	54
	174	486		158	348
	185	652		196	945
	207	882		206	1006
	224	823		227	934
	249	762		266	819
	288	661		299	743
	337	560		347	651
	394	516		400	549
	436	451		437	532

TABLE D3. VAPORIZATION DATA OF CARBON TETRACHLORIDE

Liquid Volume, ml	Temperature Difference $(T_p - T_s)$, °C	Average Vaporization Time, sec	Liquid Volume, ml	Temperature Difference $(T_p - T_s)$, °C	Average Vaporization Time, sec
0.05	71.2	1.5	0.1	64.0	2.06
	82.2	6.94		89.2	57.74
	88.5	41.65		106.5	62.22
	107.7	45.1		121.5	59.12
	120.2	43.51		145.5	54.09
	144.2	41.19		183.8	50.85
	182.0	39.27		208.0	47.17
	209.7	35.44		239.0	44.18
	237.0	30.85		283.8	40.42
	281.2	28.97		309.0	38.04
	310.5	27.5		348.2	35.05
	345.0	26.2		388.7	32.12
	387.7	24.45		434.6	30.3
	436.8	22.8			
0.15	46.7	4.6	1.0	84.7	48.1
	82.5	4.0		107.2	145.0
	106.7	73.7		139.45	134.8
	122.2	69.84		179.45	115.6
	138.2	66.91		211.0	104.9
	147.2	64.04		286.2	91.0
	187.5	59.46		362.1	74.8
	207.0	54.87		407.2	68.3
	244.8	52.42		435.2	62.1
	284.5	45.62			
	309.5	42.17			
	435.6	33.41			

TABLE D4. VAPORIZATION DATA OF CARBON TETRACHLORIDE

Liquid Volume, ml	Temperature Difference $(T_p - T_s)$, °C	Average Vaporization Time, sec	Liquid Volume, ml	Temperature Difference $(T_p - T_s)$, °C	Average Vaporization Time, sec
3.0	85.0	95.53	5.0	84.0	114.4
	106.6	209.61		105.8	227.6
	139.4	194.3		140.0	215.0
	178.45	155.0		178.7	84.6
	210.2	137.33		210.5	168.0
	286.2	124.66		275.2	140.6
	360.3	101.2		348.0	118.2
	408.7	90.93		407.0	101.7
	433.5	77.85		436.5	95.6
8.0	84.7	58.76	10.0	82.0	66.13
	106.7	260.3		107.2	274.7
	140.0	247.0		141.4	255.6
	178.7	210.33		179.2	224.1
	212.7	187.0		217.1	202.0
	273.6	160.3		273.8	167.0
	350.2	135.8		355.0	145.8
	408.2	114.25		407.2	122.4
	438.2	109.72		436.2	120.3

TABLE D5. VAPORIZATION DATA OF ETHANOL

Liquid Volume, ml	Temperature Difference $(T_p - T_s)$, °C	Average Vaporization Time, sec	Liquid Volume, ml	Temperature Difference $(T_p - T_s)$, °C	Average Vaporization Time, sec
0.05	68.8	2.2	0.10	60.9	4.15
	80.5	1.85		79.0	2.94
	84.3	7.1		84.5	9.3
	104.8	64.2		105.0	86.26
	129.0	60.1		135.8	75.4
	180.3	48.20		181.5	64.65
	309.1	34.87		239.0	53.18
	343.5	31.32		306.3	40.09
	386.3	26.38		345.5	38.46
	431.0	19.75		386.5	35.6
				436.0	26.25
0.15	40.0	10.1	1.0	83.5	9.8
	79.8	3.48		104.75	194.8
	84.3	12.08		119.81	188.3
	105.2	96.1		132.5	174.0
	136.5	86.82		189.75	152.3
	184.8	73.39		217.75	126.1
	239.5	62.08		282.0	100.66
	310.3	49.42		360.4	83.7
	351.0	45.28		398.5	75.9
	389.0	32.96		421.1	76.8
	438.0	31.42		436.6	74.1

TABLE D6. VAPORIZATION DATA OF ETHANOL

Liquid Volume, ml	Temperature Difference $(T_p - T_s)$, °C	Average Vaporization Time, sec	Liquid Volume, ml	Temperature Difference $(T_p - T_s)$, °C	Average Vaporization Time, sec
3.0	82.8	20.9	5.0	82.3	26.43
	105.3	324.0		105.8	36454
	132.2	249.0		128.3	290.66
	163.0	219.0		135.5	288.0
	217.3	172.0		163.5	246.66
	273.4	144.8		216.5	203.0
	350.75	115.9		272.3	165.33
	395.5	108.1		349.5	137.38
	412.0	100.2		397.3	123.3
	437.6	92.8		412.8	115.0
				436.7	109.6
8.0	80.0	33.2	10.0	77.0	39.53
	105.3	404.5		104.8	442.2
	126.5	341.33		117.0	399.86
	133.75	330.00		128.0	369.3
	166.00	271.21		131.0	358.0
	215.75	228.60		165.5	306.0
	277.0	189.66		218.3	247.66
	350.75	148.63		271.9	203.5
	396.6	141.10		252.5	160.2
	412.8	129.80		395.5	147.0
	437.0	124.32		414.8	134.55
				438.6	129.8

TABLE D7. VAPORIZATION DATA OF BENZENE

Liquid Volume, ml	Temperature Difference $(T_p - T_s)$, °C	Average Vaporization Time, sec	Liquid Volume, ml	Temperature Difference $(T_p - T_s)$, °C	Average Vaporization Time, sec
0.15	78.9	1.91	0.10	59.9	3.55
	85.4	29.0		76.8	2.03
	104.1	65.2		84.9	25.4
	117.7	63.8		103.7	54.42
	135.5	57.6		132.7	49.3
	175.9	49.39		179.9	42.23
	204.4	44.43		205.9	38.20
	238.9	40.15		237.2	35.17
	281.7	37.60		282.4	30.65
	307.2	35.01		305.6	29.41
	350.2	32.51		345.2	26.35
	380.7	28.36		384.2	24.30
	426.1	25.22		430.0	21.20
0.05	60.4	1.5	1.0	79.2	4.66
	78.9	1.31		104.9	134.7
	87.4	18.8		132.4	114.3
	104.4	39.68		175.15	102.4
	132.7	36.98		220.7	85.03
	178.7	33.19		277.7	74.66
	205.9	29.32		326.2	62.8
	234.4	27.08		403.2	53.5
	279.5	24.14		410.4	51.4
	305.2	23.2			
	343.4	19.98			
	387.9	18.35			
	430.1	15.70			

TABLE D8. VAPORIZATION DATA OF BENZENE

Liquid Volume, ml	Temperature Difference $(T_p - T_s)$, °C	Average Vaporization Time, sec	Liquid Volume, ml	Temperature Difference $(T_p - T_s)$, °C	Average Vaporization Time, sec
3.0	79.2	13.06	5.0	67.9	11.8
	104.3	211.41		104.7	237.5
	131.9	187.6		126.9	220.3
	172.9	148.1		171.15	167.66
	219.7	132.7		222.15	151.7
	280.7	106.3		280.7	122.3
	278.6	86.2		335.1	102.8
	401.9	75.1		401.2	86.8
	408.8	74.9		411.4	81.3
8.0	76.4	18.23	10.0	76.2	21.63
	104.4	279.15		104.5	310.8
	132.9	247.0		132.15	262.6
	170.4	188.1		169.4	202.3
	223.9	162.2		219.3	186.5
	279.7	136.56		278.9	146.7
	336.6	120.2		347.1	125.8
	389.9	97.1		401.2	104.3
	410.4	94.65		409.2	103.75

APPENDIX E

HIGH-SPEED PHOTOGRAPHIC TECHNIQUES

WF-4ST Fastax Camera: This camera consists of a main housing and the six component assemblies. Internal component assemblies are the drive assembly which is the principal operating part, the film take-up spindle and the timer assembly. The drive assembly consists of the direct-drive film sprocket and the lens aperture plate, which concentrates the light and directs it to the prism. The hold-down roller and a film stripper are associated with the sprocket to maintain even film feeding and to insure proper operation.

Externally mounted on the camera housing are the lens and protective cap, the drive and take-up motors, the camera carrying handle, and the electrical connector. The camera is driven by two $\frac{1}{4}$ hp, 120-volt universal motors. One motor drives the take-up spindle and the other drives the sprocket and rotating prism assembly. The electrical connector of the timer assembly is located on the housing below the drive motors. The telescopic view finder and an internal take-up spool film guard are mounted on the door.

The camera is capable of a maximum of 6,000 pictures per second.

WF-360 Xenon Lamp System: The lighting assembly consisted of a control unit, xenon lamp, lamp housing, telescopic stand and connecting cables. The xenon lamp was operated on a portable battery supply of 36 to 42 volts to fire the mercury-cadmium arc. The xenon

lamp flashes 12,000 foot candles for 5 seconds at the 5 KW setting of the selector switch on the xenon control unit. Similarly, the xenon lamp flashes nearly 20,000 foot candles for 2 seconds at $7\frac{1}{2}$ KW setting of the selector switch on the xenon control unit.

The Fastax Control Unit Model J-515 (Goose): The Goose control unit consists of a variable transformer of 20-ampere capacity for varying the camera voltage from 0 to 300 volts, a voltmeter for measuring the camera and the line voltages to select the desired camera speed from a speed characteristic curve of WF-4ST, a preset electric timer which operates at camera voltages above 130 volts, and two externally adjustable timers for controlling electric power to the camera and the event.

WF-327 Exposure Meter: The Fastax illumination meter is designed specifically for high-speed motion-picture work. The instrument comprises a photoelectric cell and meter. The meter has three scales having the ranges of 0 to 3000, 0 to 30,000 and 0 to 300,000 foot candles.

WF-367 16-mm Continuous Processor: This machine is composed of take-up arm assembly, sump pump, two electric motors, dry box, 16 tanks and dark cover. The dark cover permits the use of the machine in normal daylight. With this machine the film is unreeled and pulled continuously through the various processing and wash solutions and finally air-dried at the output side of the machine. This machine operates in normal light to process two feet of film per minute. The machine has a maximum capacity of 400 ft. of film for one processing run.

A very brief description of the photographic apparatus is given in manuals of the Wollensak Optical Company (44).

Focusing and Composing

The 16-mm camera is provided with an integral reflex-type view finder which projected the image formed at the film plane through an optical system mounted on the camera door to an eyepiece located at the rear of the view finder housing. The viewing prism is mounted through the camera door and fits within the sprocket on the optical axis of the camera. The sprocket has holes to allow viewing when properly aligned with the lens aperture. The image formed at the film plane by the camera objective was focused by the eyepiece at the rear of the view finder housing. The view finder was provided with a light trap operated by a lever on top and at the front of the finder housing. The light trap was opened when the lever was turned parallel to the plane of the camera door. After placing the left eye at the eyepiece, the knurled part was rotated until the small circular reticle was in sharp focus. Also, in order to achieve critical focusing, parallax was artificially introduced by mvoing the position of the left eye slowly from side to side before the view finder eyepiece. After observing the image of the relative movements which was produced from the reticle and the subject, the focus ring of the objective lens was slowly adjusted until relative movements disappeared.

Film

Kodak Tri-X reversal 16-mm film was used for high-speed motion pictures. The film was black and white, two edges perforated,

and with an ASA speed index of 200.

Film-Processing Technique

After taking the high-speed motion pictures, the loaded aluminum spool was removed from camera take-up assembly in the darkroom. The undeveloped film was transferred to another spool which had about 100 feet of exposed film. Thus, the spool was loaded with extra exposed film at the bottom and undeveloped film at the top. This step was necessary to develop film continuously at constant speed in the Cramer Processor.

Processing solutions were prepared with distilled water from chemical kits and kept with their proper contents in the individual tanks of the machine. All of the wash tanks were filled with distilled water at 68° F. The switch of the sump pump was put in "ON" position and the needle valves were opened to obtain the degree of agitation desired in each solution tank.

The spool of undeveloped film was placed on the spool shaft in the dark side of the machine and the front end of the film was attached to the rear end of a clear leader. About 80 feet of clear leader was wound previously through various rollers and tanks in the machine. The main switch was put in "ON" position and the film proceeded through the various solution tanks, the dryer box, and onto the take-up spool. When the front end of the developed film exited from the dryer box, the developed film was separated immediately from the clear leader. The front end of the developed film was inserted into a plastic spool which was placed on the machine. The time required for processing 100 feet of film at a rate of 4 fpm took about 52 minutes.

Processing Chemicals

The processing chemicals employed were in kits (S-9020) from Milsco Manufacturing Company, Milwaukee, Wisconsin. The machine employed was the Cramer Continuous 16-mm Processor, Model 60, manufactured by Milsco. Processing solutions were prepared and kept in specific tanks in machine as suggested in the instruction book (45). The chemicals are listed below:

1. First Developer S-9021
2. Bleach S-9023
3. Clear S-9024
4. Second Developer S-9022
5. Fixer Hypo S-9025
6. Hypo Clearing S-9026
7. Wetting Agent S-9027

Camera Speed

Camera operating speed was calculated from timing marks exposed on the film edge. The timing-lamp assembly consisted of a neon glow lamp enclosed in a cylindrical housing mounted under the drive sprocket. The lamp was energized by 115-volt 60-cycle line current. The light emitted from neon lamp was focused on the edge of the film by a small lens in the top of the housing. 120 timing marks per second were produced from 60 cycle current. Camera speed was determined by multiplying the number of frames between timing marks exposed on the film by 120; e. g. 19 x 20 = 2280 pictures per second.

APPENDIX F

Sample Calculations

A sample calculation is presented to show the steps used in the calculation of the heat transfer coefficients and the statistical error analysis for the breakoff diameter of extended masses.

The liquid that was used for this sample calculation was water and the physical properties of extended masses were used from Appendix C.

(1) Chang's Equation II-7

$$h = \left[\frac{k_v^3(\rho_\ell - \rho_v)g}{8\pi^2\mu_v\left(\frac{k_v\Delta T}{2L\rho_v}\right)}\right]^{\frac{1}{3}}$$

At $\Delta T = 207^\circ C$

$$h = \left[\frac{(0.72 \times 10^{-4})^3(0.958 - 0.467 \times 10^{-3}(980)}{8(3.142)^2(0.165 \times 10^{-3})\left[\frac{0.72 \times 10^{-3}(307 - 100)}{2(539)(0.467 \times 10^{-3})}\right]}\right]^{\frac{1}{3}}$$

$$h = 10.81 \times 10^{-3} \text{ cal sec}^{-1} \text{ cm}^{-2} {}^\circ C^{-1}$$

At $\Delta T = 420^\circ C$

$$h = \left[\frac{(0.94 \times 10^{-4})^3(0.958 - 0.375 \times 10^{-3})(980)}{8(3.142)^2(0.205 \times 10^{-3})\left[\frac{0.94 \times 10^{-3}(520 - 100)}{2(539)(0.375 \times 10^{-3})}\right]}\right]^{\frac{1}{3}}$$

$$h = 8.69 \times 10^{-3} \text{ cal sec}^{-1} \text{ cm}^{-2} {}^{\circ}\text{C}^{-1} ,$$

(2) Berenson's Equation II-15

$$h = \left[\frac{k_v^3 \rho_v (\rho_\ell - \rho_v) L' g}{\mu_v \Delta T \left(\frac{g_c \sigma_s}{g(\rho_\ell - \rho_v)} \right)^{\frac{1}{2}}} \right]^{\frac{1}{4}}$$

At $\Delta T = 207^{\circ}C$

$$h = \left[\frac{(0.72 \times 10^{-4})^3 (0.467 \times 10^{-3})(0.958 - 0.467 \times 10^{-3})(586.6)(980)}{0.165 \times 10^{-3}(307 - 100)\left(\frac{980.6(0.06)}{908(0.958 - 0.467 \times 10^{-3})} \right)^{\frac{1}{2}}} \right]^{\frac{1}{4}}$$

$$h = 4.44 \times 10^{-3} \text{ cal sec}^{-1} \text{ cm}^{-2} {}^{\circ}\text{C}^{-1} ,$$

At $\Delta T = 420^{\circ}C$

$$h = \left[\frac{(0.94 \times 10^{-4})^3 (0.375 \times 10^{-3})(0.958 - 0.375 \times 10^{-3})(638.9)(980)}{(0.205 \times 10^{-3})(520 - 100)\left(\frac{980.6(0.06)}{980(0.958 - 0.375 \times 10^{-3})} \right)^{\frac{1}{2}}} \right]^{\frac{1}{4}}$$

$$h = 4.06 \text{ cal sec}^{-1} \text{ cm}^{-2} {}^{\circ}\text{C}^{-1} ,$$

(3) Borishansky's Equation II-15

$$h = \frac{7.9 \left(\frac{L'}{C_v \Delta T} \right)^{0.6}}{\left(\frac{g_c}{g} \frac{\sigma_s}{(\rho_\ell - \rho_v)} \right)^{0.5}}$$

At $\Delta T = 207^{\circ}C$

$$h = \frac{7.9\left(\frac{586.6}{0.4606(207)}\right)^{0.6}}{\left(\frac{980.6\,(0.06)}{980(0.958 - 0.467 \times 10^{-3})}\right)^{0.5}}$$

$$h = 6.48 \times 10^{-3} \text{ cal sec}^{-1} \text{ cm}^{-2} {}^{\circ}C^{-1},$$

At $\Delta T = 420^{\circ}C$

$$h = \frac{7.9\left(\frac{638.9}{0.481(420)}\right)^{0.6}}{\left(\frac{980.6(0.06)}{980(0.958 - 0.375 \times 10^{-3})}\right)^{0.5}}$$

$$h = 5.34 \times 10^{-3} \text{ cal sec}^{-1} \text{ cm}^{-2} {}^{\circ}C^{-1},$$

(4) Bubble dynamics, Equation IV-3

$$h = V_B f n_d \rho_v (L + \tfrac{1}{2} C_v \Delta T) / \Delta T$$

Let $L' = L + \frac{1}{2} C_v \Delta T$

$$V_B = \pi/_b \text{ (bubble breakoff diameter)}^3$$

At $\Delta T = 207^{\circ}C$

$$h = \frac{0.5236(1.43)^3(1/0.16)(\frac{2}{22.32})(0.462 \times 10^{-3})(586.6)}{207}$$

$$h = 1.14 \times 10^{-3} \text{ cal sec}^{-1} \text{ cm}^{-2} {}^{\circ}C^{-1},$$

At $\Delta T = 396^{\circ}C$

$$h = \frac{0.5236(1.5)^3\left(\frac{1}{0.17}\right)\left(\frac{4}{19.38}\right)(0.386 \times 10^{-3})(634.4)}{396}$$

$$h = 1.79 \times 10^{-3} \text{ cal sec}^{-1} \text{ cm}^{-2} {}^{\circ}C^{-1},$$

(5) Equation IV-2

$$h = \frac{(V_{10} - V_8)(\rho_\ell)(L')}{A_p \Delta T(\tau_{10} - \tau_8)} - \frac{\sigma_c(T_{pk}^4 - T_{ps}^4)}{\left(\frac{1}{\epsilon} + \frac{1}{\alpha} - 1\right)(T_p - T_s)}$$

At $\Delta T = 207^{\circ}C$

$$h = \frac{(2)(0.958)(586.6)}{19.8(207)(984 - 885)} - \frac{1.352 \times 10^{-12}(580^4 - 373^4)}{\left(\frac{1}{0.73} + \frac{1}{1} - 1\right)(207)}$$

$$h = 2.77 \times 10^{-3} - 0.45 \times 10^{-3}$$

$$h = 2.32 \times 10^{-3} \text{ cal sec}^{-1} \text{ cm}^{-2} {}^{\circ}C^{-1},$$

At $\Delta T = 396^{\circ}C$

$$h = \frac{2(0.958)(634.4)}{18.3(396)(558 - 516)} - \frac{1.352 \times 10^{-12}(769^4 - 373^4)}{\left(\frac{1}{0.73} + \frac{1}{1} - 1\right)(396)}$$

$$h = 4.11 \times 10^{-3} - 0.82 \times 10^{-3}$$

$$h = 3.29 \times 10^{-3} \text{ cal sec}^{-1} \text{ cm}^{-2} {}^{\circ}C^{-1},$$

TABLE F1. ERROR ANALYSIS OF BUBBLE BREAKOFF DIAMETER FOR WATER AT $\Delta T = 207^{\circ}C$

Individual Observation E_i, cm	Deviation From Mean $(\bar{E} - E_i)$, cm	Square of Deviation From Mean $(\bar{E} - E_i)^2$, cm^2
1.39	+0.04	0.0016
1.48	-0.05	0.0025
1.56	-0.13	0.0169
1.47	-0.04	0.0016
1.37	+0.06	0.0036
1.13	+0.30	0.0900
1.57	-0.14	0.0196
1.39	+0.04	0.0016
1.44	-0.01	0.0001
1.59	-0.16	0.0256
1.48	-0.05	0.0025
1.15	+0.28	0.0784
1.52	-0.09	0.0081
1.44	-0.01	0.0001
1.24	+0.19	0.0361
1.56	-0.13	0.0169
1.44	-0.01	0.0001
1.38	+0.05	0.0025
1.51	-0.08	0.0064
1.48	-0.05	0.0025

average value, $\bar{E} = \frac{28.68}{20} = 1.43$, cm $\qquad \Sigma(\bar{E} - E_i)^2 = 0.339$, cm^2

$$\sigma_k = \frac{\sum_{i=1}^{i=N} (\bar{E} - E_i)^2}{N - 1} = \frac{0.339}{19} = 1.34 \times 10^{-1}, \text{ cm}$$

$$\sigma_e = \sigma_k / \sqrt{N} = 0.134 / \sqrt{20} = 30 \times 10^{-3}, \text{ cm}$$

$$\sigma_\ell = \pm \left[St_{0.975} \text{ (no. of degrees of freedom)} \right] \sigma_e$$

With reference to Table A. 3, page 433 of the Principles and Procedures of Statistics by G. D. Steel and J. H. Torrie (1960), the value is 2. 093 for 95 percent probability and 19 degrees of freedom.

Then, $\sigma_\ell = \pm 2.093 (30 \times 10^{-3}) = \pm 63 \times 10^{-3}$, cm

NOMENCLATURE

A	total liquid area, cm^{-2}
A_p	Liquid projected area, cm^{-2}
B_i	bubble period, sec (i = 1 ... 6 gives alternate value)
C	constant
C_i	empirical coefficient (i = 1, 2, 3, etc.)
C_p	liquid heat capacity, cal $gm^{-1}\,°C^{-1}$
C_v	vapor heat capacity, cal $gm^{-1}\,°C^{-1}$
D	bubble breakoff diameter, cm
E_i	individual observation
$\bar{E}$	average value of observation
f	frequency of bubble emission at one location, sec^{-1}
g	acceleration of gravity, cm sec^{-2}
g_c	conversion factor, 980.6 gm-mass cm gm-force^{-1} sec^{-2}
H	liquid thickness, cm
h	heat transfer coefficient of liquid, cal $sec^{-1}\,cm^{-2}\,°C^{-1}$
j	wave number 2π/wavelength, cm^{-1}
k_v	vapor thermal conductivity, cal $cm^{-1}\,sec^{-1}\,°C^{-1}$
L	latent heat of vaporization, cal gm^{-1}
L'	latent heat of vaporization plus sensible heat of vapor, cal gm^{-1}
N	number of observations used for error analysis
n	number of data points used in dimensionless correlation
n_d	n_B/A_p, number of bubbles per unit projected area
p	pressure, dyne cm^{-2}

Q	heat transfer rate, cal sec^{-1}
r	radial position
r_i	radius of bubble, cm
r_o	radius of liquid unit cell, cm
s	complex value of wavefrequency, sec^{-1}
t	time, sec
T_p	temperature of plate, °C
T_{pk}	temperature of plate, °K
T_{ps}	temperature of saturated liquid, °K
T_s	temperature of saturated liquid, °C
ΔT	$(T_p - T_s)$, °C
U_i	$\sum_{\text{bubbles}} (\pi)$ (bubble diameter), cm
U_o	outer perimeter of liquid mass, cm
V	volume of liquid, cm^{+3}
V_B	bubble volume, cm^{+3}
$W_{(r)}$	total vapor flow at radius r
w	rate of vaporization per unit area, gm cm^{-2} sec^{-1}
X	distance along horizontal axis
X_1	dimensionless group, $\frac{C_v \mu_v}{k_v}$
X_2	dimensionless group, $\frac{\rho_\ell}{\rho_v}$
X_3	dimensionless group, $\frac{L}{C_v \Delta T}$
X_4	dimensionless group, $\frac{1}{\sigma_s g_c} \sqrt[3]{\frac{\mu_v^4 g}{\rho_\ell}}$
Y	dimensionless group, $\tau \frac{g}{g_c} \frac{\mu_v}{\sigma_s}$
Z	distance along vertical axis

Z_ℓ	value for the larger liquid volume
Z'	value for the smaller liquid volume
α_c	the absorptivity of the liquid
δ	vapor thickness, cm
η	distance perpendicular to mean position of liquid-vapor interface, cm
η_o	initial perturbation at interface, cm
λ	wavelength, cm
λ_c	critical wavelength, cm
λ_d	most dangerous wavelength, cm
λ_o	wavelength greater than critical wavelength, cm
μ_v	vapor viscosity, gm cm^{-1} sec^{-1}
ρ_ℓ	liquid density, gm cm^{-3}
ρ_v	vapor density, gm cm^{-3}
σ_c	Stefan - Boltzmann constant, 1.352×10^{-12} cal sec^{-1} cm^{-2} $^\circ K^4$
$\sigma_{\overline{E}}$	error of the mean
σ_k	standard deviation from mean
σ_ℓ	95 percent confidence limits on the mean
σ_s	surface tension, gm-force cm^{-1}
τ	total vaporization time of liquid mass, sec
ϵ	emissivity of plate

VITA

Bhailalbhai Mathurbhai Patel

Candidate for the degree of

Doctor of Philosophy

Thesis: THE LEIDENFROST PHENOMENON FOR EXTENDED LIQUID MASSES

Major Field: Chemical Engineering

Biographical:

Personal Data: Born in Tarsali, Baroda (India), March 17, 1934, the son of Mathurbhai R. and Ichhaben M. Patel.

Education: Attended grade school in Tarsali, Baroda; graduated from Sarva Vidyalaya High School in 1952; received Bachelor of Science Degree from the Maharaja Sayajirao University of Baroda, with a major in Chemistry and minor in Physics in June 1956; received Bachelor of Science in Technology Degree from the Department of Chemical Technology, University of Bombay, with a major in Oils, Fats and Waxes in 1958; received Bachelor of Science Degree from the University of Michigan, with a major in Chemical Engineering in Spring 1960; received the Master of Science Degree from the School of Mines and Metallurgy, University of Missouri, with a major in Chemical Engineering in May 1961; completed requirements for the Doctor of Philosophy Degree in fall 1964.

Professional Experience: Employed as an Assistant Research Chemist with the Tata Oil Mills Company in Bombay, India, 1956; served eight months as a Research Chemist in the Jello Subsidiary Industrial Company in Bombay, India, 1958-1959.